UNIVERSITÀ DEGLI STUDI DI CATANIA

IN CONVENZIONE CON

UNIVERSITÀ DEGLI STUDI DI PALERMO

DOTTORATO DI RICERCA IN

SCIENZA DEI MATERIALI E NANOTECNOLOGIE - XXXII CICLO

ROSALBA RANDAZZO

CHIRAL INDUCTION IN SUPRAMOLECULAR SYSTEMS: MEMORY AND ENANTIOMERIC RECOGNITION

TUTOR: DOTT.SSA L. D'URSO

COORDINATORE: PROF.SSA M. G. GRIMALDI

TESI PER IL CONSEGUIMENTO DEL TITOLO DI DOTTORE DI RICERCA

TABLE OF CONTENTS

CHIRAL INDUCTION IN SUPRAMOLECULAR SYSTEMS: MEMORY AND ENANTIOMERIC SEPARATION

AIM OF THE WORK

Nature is the main inspiration for scientist in all fields, observing abiotic matter or biological system what man immediately thinks is how it is possible that it works perfectly?

During time the route for the synthesis of materials or the mechanism for the biological processes are always considered the best, and what we can do is just observe that and try to emulate the nature perfection.

In the last 60 years one of the fields in chemistry that as increased in a exponential way is supramolecular chemistry, the branch that study the capability of molecules to interact each other in a non-covalent way. Supramolecular chemistry start from the observation and the knowledge of natural mechanism and try to replicate them using new molecules trying to obtain materials with a high degree of specificity and with features that are not only the sum of that of the molecules that constitute the supramolecule but they are new.

During my PhD, I studied the effect of different experimental condition on aggregation process of species. The right balance between thermodynamic and kinetic governs indeed aggregation in a supramolecular system. Thus the deep knowledge of the mechanism adopted by self- assembled specie allows us to control and to obtain the desired species.

Using a non-covalent approach is possible to gain architecture with very interesting properties electronic, energetic or structural. Among the countless intriguing aspect of supramolecular entities, the one that still today continue to be the more fascinating is asymmetry.

Chirality (the absence of symmetry) is one of the features of molecules that nature chose for the most important systems involved in life evolution; if we think at proteins or DNA the building blocks of these two important complex systems (respectively amino acids and sugars) are chiral.

The processes involved in life evolution are till now partially unknown, studying supramolecular chiral systems can allow us to better understand them. We conjugate the information obtained in the study of self-assembled system adding the variable of the chiral message, and it should help to solve the questions about the origin of homochirality in nature.

A big part of my study was dedicate to the interaction between chiral molecules and achiral poprhyrins, I used polyelectrolyte and also small molecules as amino acids, the importance of this study reside in the possibility to use the obtained aggregates both to study the origin of

chirality at a supramolecular level but also as basis for the synthesis of new complexes that can be used as bio inspired materials.

Among the endless fields where supramolecular chemistry can be used there is sensing, during my PhD we used the capability of porphyrins to bind metals and take the advantage of their spectroscopic variations to develop an easy sensing device for the monitoring of the presence of Zn and Pb ions in water solution.

One of the aspects of technology that nowadays capture great interest is the energy storage, the use of even more performing device but also the sensibility in the use of renewable energies has focused the attention on new materials able to collect energy, store it and preserve it for a long time, supercapacitors are materials with the above mentioned features but unfortunately they are able to work just in non natural conditions as for examples in very low temperatures.

I spent six months at the Trinity College in Dublin; I used the supramolecular approach to enhance the features as supercapacitor of a 2D nanomaterial as the MnO_2. I had studied the interaction between porphyrins and 2D nanomaterials in the past, observing that the interaction occurred between a positive porphyrin and the negatively charged graphene oxide (GO) not only was observable but it was so strong to lead a chirality transfer from the GO to the porphyrin, this means that the communication was very robust. In the same way I studied the system composed by the positive porphyrin H_2T4 and negative transition metal oxide MnO_2, in that case no chirality can be observed but the interaction between the two component is very important and the porphyrin is able to increase the electronic conductivity in MnO_2.

1 INTRODUCTION

1.1 From molecular to supramolecular chemistry

Chemistry is the science of matter; thinking on every material, all is made up of matter, it is part of everything in our lives and in our own bodies. Chemistry is a central science, it is involved in energy, environment, sustainability, materials, biology, and medicine, and it studies the aggregation states and the conversion of matter from the simplest to the more highly organized systems.

One of the more intriguing questions in our daily life is how it is possible that in Nature we can observe elementary particles that mixed together form complex structure up to thinking organism?

In order to answer to the above question, chemists has studied the way to connect atoms using covalent bonds, to obtain new molecules able to form new materials gaining new properties.[1]

Despite the use of covalent bonds to construct big molecules lead to arrays with atoms that are linked in a well defined and controlled manner, it possess some limits. Molecular chemistry requires a high investment of time and manpower; in a covalent synthesis,[2] after every reaction step, where yields could be low, there are purification steps and part of the product can be lost during this phases.

Therefore, for the development of nanoscale structures, molecular chemistry must look to novel hypotheses and new methodologies in the search for efficient procedures of generating compounds with the desired characteristics.

Nature by-pass the limits of molecular chemistry using a specific logic: when the complex reach a particular complexity using the path of the covalent bond, it builds more complex systems using molecules as the building blocks and the non covalent bonds (electrostatic, hydrogen bonding, donor acceptor interactions) as the glue to build the so called supramolecular systems (Figure 1).

Supramolecular-chemistry was defined by J. M. Lehn (who won the Nobel prize for his studies in the filed in the 1987) as the “chemistry of molecular assemblies and of the

intermolecular bond" or more colloquially this may be expressed as "chemistry beyond the molecule".

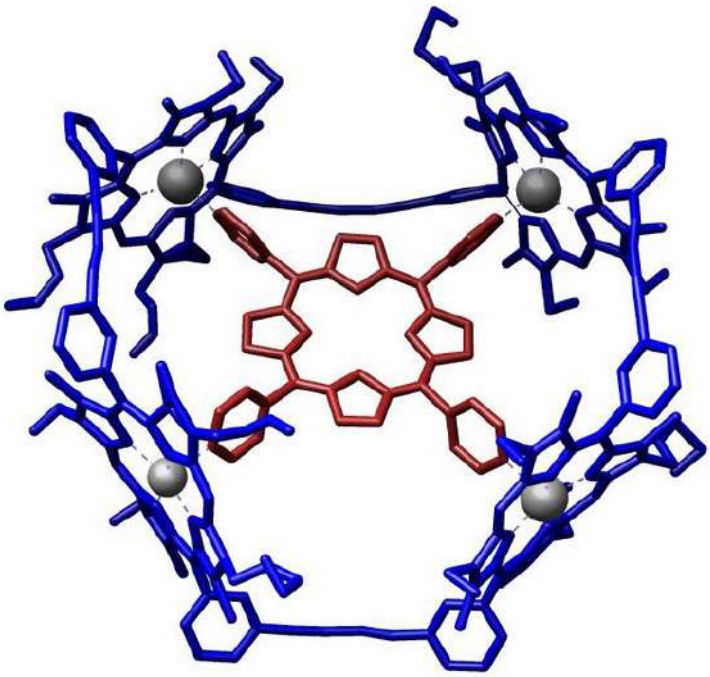

Figure 1: An example of supramolecular system

In the wide field of supramolecular chemistry we can find both *supermolecules* and *molecular assemblies*. The main difference among these two species reside in the actors involved in their formation; more in detail, supermolecules are well-defined oligomolecular species that result from the intermolecular association of a few components (a receptor and its substrate(s)) based on the principles of molecular recognition, while molecular assemblies are polymolecular systems, they result from the spontaneous association of a non defined number of components into a specific phase having more or less well-defined microscopic organization and macroscopic characteristics depending on the nature of the constituent molecules (layers, membranes, vesicles, micelles, mesomorphic phases, etc.~'"]).[3]

Supramolecular assemblies possess their own well-defined structural, conformational such as thermodynamic and kinetic dynamical properties. The properties of a supramolecular species not always coincide with the simple sum of the features of its constituents. Supramolecular entities are characterized by the spatial arrangement of their components, their architecture or superstructure, and by the nature of the intermolecular bonds that hold its components together.

The forces that held together molecules to form supramolecular structures are weaker than covalent bonds, so they are thermodynamically less stable and kinetically more labile and dynamically more flexible than molecules.

Despite already in 1930s the word *supermolecule* was introduced in the scientific field, the difficulty in managing the reactivity in non-covalent assemblies prevented the broadly development of supramolecular chemistry. Only in the last 50 years the supramolecular chemistry has registered an extraordinary growth. The development of high complex systems using non covalent bonds require a deep knowledge of organic chemistry, physical chemistry, coordination chemistry, theoretical study on interactions but also biochemistry and biological processes.

Sometimes supramolecular chemistry is defined as a mix and shake process, but despite this *naïf* classification it is not a simple process. A supramolecular process is a designed series of assembly steps able to build more complex structures following reproducible procedures.[4] The use of weak interactions for the directed assembly of a given structure requires knowledge of their strength and of their dependence on distances and on angles; a strict control of the forces such as the possibility to measure and manage all the necessary parameter is fundamental and has required lot of time to develop the right working method in this field.

Supramolecular complex formation and growth can follows different pathways, obviously depending on the energetic landscape. Based on the free energy of the final assembled state we can distinguish between thermodynamic and kinetic controlled systems (see Figure 2).

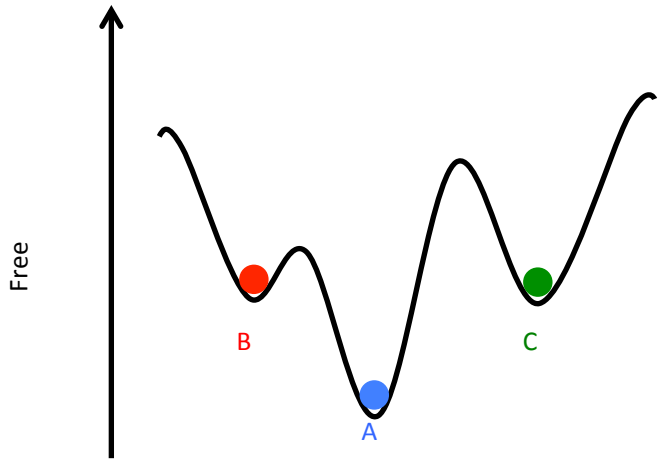

Figure 2: Schematic representation of energy states in A) thermodynamically, B) metastable and C) kinetically controlled supramolecular systems.

In the thermodynamically controlled systems we can find for example supramolecular polymers; in these complexes monomers are held together thanks to non-covalent interactions. The final properties of the polymer (rigidity or flexibility) only depend on their structure and on the interactions between the monomers. The system is in a global free-energy minimum; no changes can be observed during time. Supramolecular assemblies in a thermodynamic minimum are still dynamic, changing the environmental free-energy cause a perturbation in the system that can tend to reach a new energy minimum.

A system under kinetic control also defined as kinetically trapped, is a system in a local minimum of energy. Depending on the energy landscape around the minimum the system can evolves following two pathways: *i)* the energy barrier to reach a thermodynamic minimum is low, the complex can undergo a thermodynamically controlled system (metastable state); *ii)* the energy barrier is high, the system remain "trapped" in the free-energy minimum, the formation of this last system requires well defined experimental conditions.

To reach the desired architecture, a supramolecular complex must respect defined steps, among these *molecular recognition* is the first, is widely used in Nature and plays a pivotal role in supramolecular chemistry.

The *molecular recognition* is the basic energy in a supramolecular process; it involves the storage and the reading of the molecular information (stored by the molecule read at a supramolecular level), it is not just a binding, it is defined as a *"binding with a purpose"*, moreover it is a very selective process. The most complex expression of molecular recognition is represented by the biological molecular recognition, leading to highly selective binding, reaction, transport, regulation etc. It provides inspiration for the unravelling of basic principles and for the design of model systems as well as of abiotic receptors. The molecular recognition that we can find in enzyme-substrate reactions is also at the basis of the separations methods used in pharmaceuticals synthesis.[5]

Another important tool that Nature chose (and that we learned to use) for the opportune supramolecular complexes design is the *hierarchical control*.

The molecular recognition is a thermodynamic process while on the other end the hierarchical control is a kinetic one.

The construction of mesoscopic structures following a hierarchically controlled pathway occur with increasing levels of complexity, in biology among the plethora of hierarchically

controlled processes we can find for example the collagen formation or the tobacco mosaic virus assembly.

Hierarchical self-assembly can be defined as ‘‘the formation of an organized structure through different and distinct levels of self-assembly processes that decrease in strength’’;[6] it is also a time dependent process. Considering the collagen formation, the pathway is as follows:

1. Synthesis of the polypeptidic chain;
2. Three polypeptidic chain fold to form a triple helix;
3. The formed helices assemble to give the collagen fibres.

The collagen fibres formation (step 3) occurs only if the previous two steps take place.

In a hierarchical controlled process the formation of the desired specie can be driven by the parameters choice, modulating the pH, the temperature, the ionic strength or the solvent it is possible to push the aggregation towards the wanted specie.

The aim is to reach the ideal conditions to allow the molecular components to self-assemble in order to obtain the desired supramolecular architecture. If the molecular components have the right information (electronic, energetic and steric) the simple mixing of the various chemical species allow them to recognise each other and to form spontaneously the wanted supramolecular aggregate.

Self-assembly can be defined as the driving force that leads from a mixture of disordered molecules to an ordered complex, it is a process where the organization of single components spontaneously generates well-defined functional supramolecular architectures.[1, 7-16]

If molecules are able moving towards each other (molecular recognition), and they are in the opportune conditions, self-assembly take place leading to a stable supramolecular complex (hierarchical control), one of the necessary condition is that the molecules must contain the necessary information (shape, surface properties, charge, polarizability, magnetic dipole, mass, etc.) that able them to recognize and interact in the opportune way.

The biological world offers countless examples of self-assembled systems, one of the most studied system is the DNA double helix, where the base coupling is a hydrogen bond guided process following the Watson and Crick pairing and the folding of the helix is a mixture of hydrogen bonding and solvophobic interactions.[2] The interest in studying the DNA folding has led to discovery different DNA secondary structure having lot of functionalities, one example is the important role of G quadruplex, they represent promising activity as drugs such as diagnostic tools.[17-20]

The kinetic lability of supramolecular systems, as for example the cited DNA, gives to those complexes systems the ability to undergo annealing and self-healing of defects or mismatch;[1] therefore self-assembly requires that the components either equilibrate between aggregated and non-aggregated states, or adjust their relative positions to one another once in a supramolecular complex.

A typical self-organization process may be considered to involve three main stages: (*i*) molecular recognition, this first stage is very important for the correct specificity and precision of the final specie; the basic components must be choose in a opportune way in order to lead to selective binding; (*ii*) growth through sequential and eventually hierarchical binding of multiple components in the correct relative disposition; it may present cooperativity and nonlinear behaviour, the addition of a component in a reaction mixture is an important step that must be done in the opportune moment, the hierarchical controlled growth of a complex can lead for example to a linear assembly instead of a globular one just depending on the addition order of the components; (*iii*) termination of the process, requiring a built-in feature, a stop signal, that specifies the end point and signifies that the process has reached completion.[7]

Self-assembled system nowadays are widely applied, the deeper knowledge of biological systems has allowed scientist to employ this information in many fields even non biological with the aim to mimic them for the evolution of new systems with new types of functions.

1.2 Supramolecular chirality

Pasteur stated "*L'univers est dissymétrique*", when he pronounced that sentence no one would have imagined how true it was.

After the 1848 Pasteur's discovery of the two types of tartaric acid crystals, he paved the way on the study of the handedness of molecules, on their chirality.[21]

In 1884 in Baltimore lectures Lord Kelvin introduced the property "**chirality**" for objects that were identical in every respect, but proved NOT to be superimposable (from the Greek *kheir*, hand).

In molecules chirality can be classified as punctual, depending on the presence in the molecule of a chiral carbon (an sp^3 carbon having attached four different groups); plane, molecules constitutes by two or more non coplanar rings that are connected not symmetrically, they are also unable to easily rotate around the chemical bond; and axial if the molecule possess an axis and a set of substituents is held in a spatial arrangement not superimposable on its mirror image (figure 3).[22]

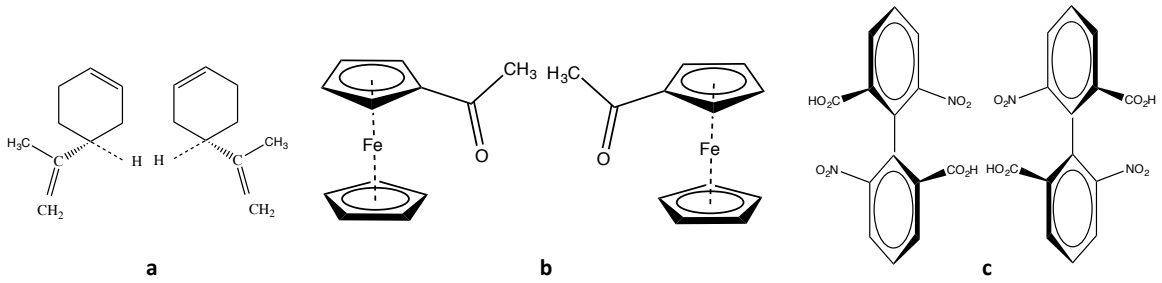

Figure 3: Examples of molecular chirality a) punctual or central in limonene, b) planar in 1-acetylferrocene and c) axial in 6,6'-dinitro-2,2'-diphenolic acid.

Today it is a common wisdom that at all levels, from the subatomic to the macroscopic scale, asymmetry is a basic characteristic of matter (figure 4). We know that at a subatomic level we can find only left handed helical neutrinos; moving to the molecular level the number of chiral molecules is huge, simply thinking at amino acids and sugars and so on. At the macromolecular scale there are many supramolecular systems showing chirality, like proteins, DNA but also more complex systems as viruses and bacteria. On a larger level we are able to observe plants and snails exhibiting helical shapes ending with the galaxy system that is itself chiral.

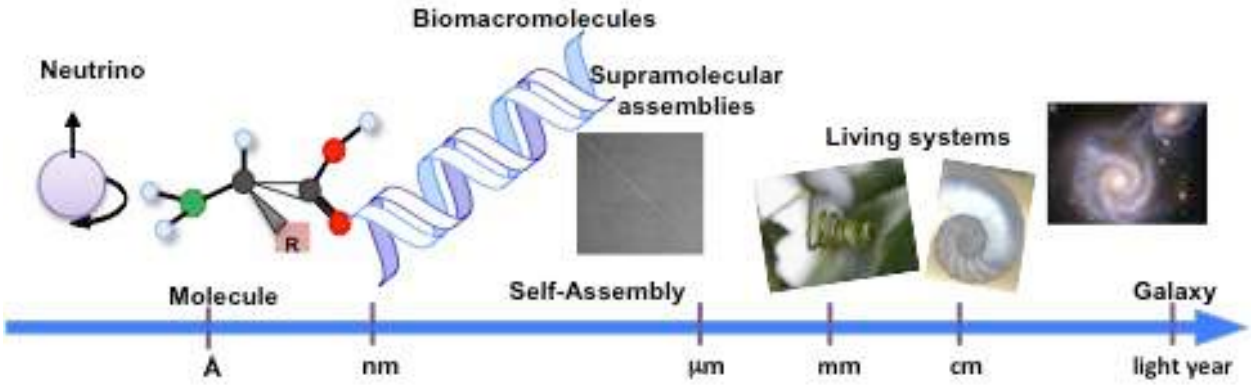

Figure 4: Chiral elements at various level, from subatomic to molecular, macromolecules, living systems and galaxies.

Not only there are examples of asymmetric systems at all scales, the more intriguing aspect is that only one enantiomer is present in Nature. Despite lot of studies there are still open questions on the reason why Nature has chose homochirality for the evolution of life: *i)* how biomolecules with a chiral preference have arisen; *ii)* is homochirality a consequence or the condition for the evolution of life; and *iii)* what is the gap that made possible to have this unbalance.

The production of unequal amounts of L and D amino acids in Nature obtained trough symmetric chemical reaction is a paradox called *spontaneous symmetry breaking*, a mechanism by which a symmetric system naturally goes to an asymmetric state.

Many theories try to attempt the origin of homochirality in nature, and to explain the spontaneous symmetry breaking process. The model designed by Charles Frank in 1953 was a starting point for many researchers who tried to convert its theoretical study in experimental evidences. The Frank model is based on the assumption that chiral symmetry breaking could be a consequence of the law of mass action, the basic law of classical chemical kinetics.[23-25]

At present is well known that the spontaneous symmetry breaking arise only under specific physical conditions, it is a process that occur because of the dissymmetric character of natural forces such as magnetic and electrical forces; their asymmetry can derive from the radiation of the sun, the rotatory motion of the heart or of the entire solar system.[26-30] But the question on the pathway which led to the unbalance toward one enantiomer respect to another is still under study.

Chirality is, not only one of the most fascinating and significant properties of matter, it was initially correlated only to crystallography (thanks to the Pasteur's discovery), but very early its fundamental role in the specific functions of biomolecules was understood.

Trying to synthesize protein chain containing both L and D amino acids the folding led to an incorrect α-helix shape; the correct folding in the secondary structure of proteins is essential for their catalytic function. This is one of the examples confirming homochirality in biological systems is extremely important, it is possible to speculate that without homochirality the complexity of life wouldn't be the same.[21]

As other chemical feature, chirality is one of the properties of matter that can be transferred, both using covalent bonds creating asymmetry, but more interestingly chirality can be transferred in supramolecolar complexes by non-covalent interactions. The fine control of kinetic and thermodynamic parameters allows obtaining the desired results.

If a chiral influencer is introduced in a medium with achiral monomers and they are able to interact the resulting complex will be chiral, this is the principle of templating.

Templating is a synthetic procedure, where "helper" specie is involved in the assembly of molecular or supramolecular complexes. Templating can be considered as a unite step in self-assembly process. A chiral templating agent in an achiral mixture can leads to a chiral supramolecular complex. [31,32]

The templating process is one manifestation of the so-called *sergeant-and-soldiers* principle.[33] The chiral molecule (sergeant) able to interact with the achiral moieties in the solution (soldiers), give a supramolecular chiral complex thanks to the strong established interaction. The absence of the chiral molecule in solution leads to the formation of racemate supramolecular assemblies.

It is important to underline that the chirality transfer from a chiral inducer to supramolecular complex is a process that can be dynamic or static depending on pathway followed during the assembly formation.

If the process in under thermodynamic control the chirality transfers is dynamic. Changing the conditions that allow the communication between the inducer and the achiral molecules, the system easily goes back to the initial condition (see figure 5).

In a process under kinetic control the transfer of chirality is static, this mean that even if the inducer is removed from the supramolecular complex the information is retained from the obtained complex, leading to the memorization of the transferred feature. In the static chirality

transfer process, the final specie is in a kinetic minimum; even if the conditions that allow the supramolecular complex formation are modified the initial state cannot be obtained because of the energetic disfavouring conditions.

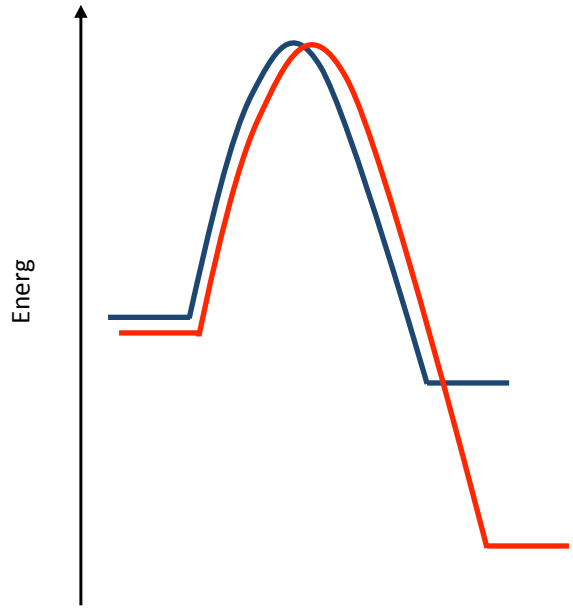

Figure 5: Energy diagram for reactions under thermodynamic (blue curve) and kinetic (red curve) control.

Chirality is a significant phenomenon in chemistry; moreover its importance is even higher in biology, in material science and in physics. The pivotal role of chirality in different field has triggered to a deep study in transfer and amplification of this characteristic. Among the different chirality transmission mechanism, a great interest was addressed toward the induction using weak physical forces as well as circularly polarized light,[34-36] electroweak interaction,[37,38] vortex motion,[39] stirring [40-43] and magnetic fields.[44]

The aim, in all these study is to have a fine control on the formation of supramolecular chiral complexes with the desired properties.

1.3 Porphyrins

1.3.1 Properties of porphyrins

Porphyrins are a class of aromatic compounds consisting of four pyrrole rings connected by four methine bridges.

This class of molecules play different roles in the environment. They are the active centre of many fundamental enzymes involved in photosynthesis, biological oxidation and reduction and oxygen transport; porphyrins are ubiquitous in biological systems they can be found in haemoglobin in vertebrates and chlorophyll in plants, but also in cytochrome P450 an enzyme systems that is present from microbial organisms to the liver of higher complex organisms.

Various side chains, at the peripheral positions, may substitute the tetrapyrrole structure, also called porphine, leading to the wide variety of porphyrins.

If the substituents are on the methinic carbons (positions 5,10,15,20), it is possible to get meso-poprhyrins, while they are called β-substituted porphyrins if the substituents are bonded to the β-pyrrolic position (positions 2, 3, 7, 8, 12, 14, 17 and 18) as showed in figure 6.

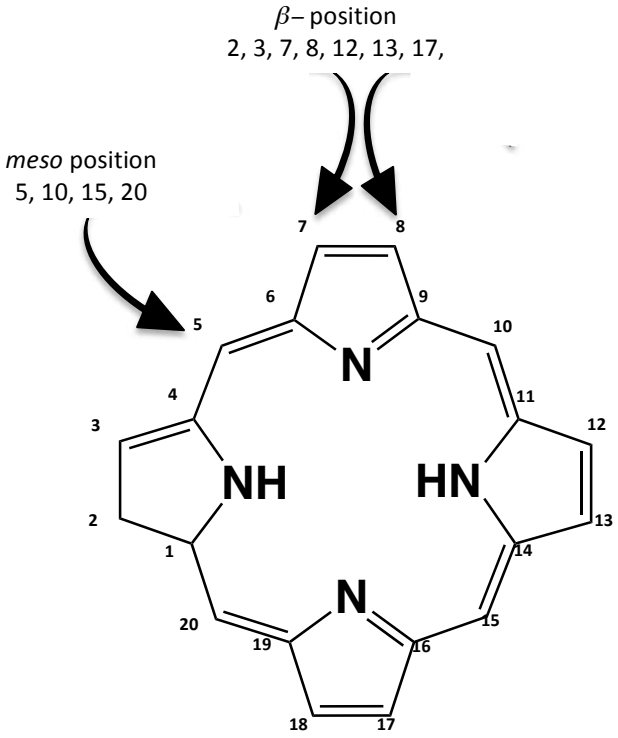

Figure 6: schematic representation of the porphyrin skeleton

The macrocicle contain a total of 22 conjugated π electrons, 18 of which are incorporated into the delocalization pathway, in accordance with the Huckel's rule for aromaticity [4n+2] where n=4; the delocalization pathway for the 18 π-electrons is depicted in figure 7.

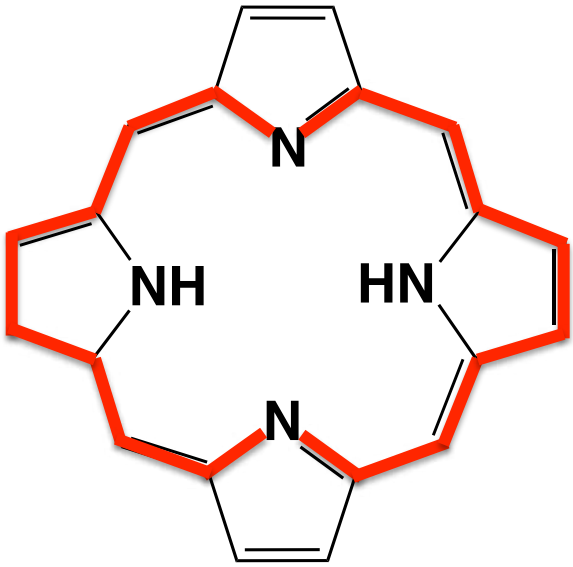

Figure 7: Schematic representation of the delocalization pathway in porphyrin ring.

The chemistry of porphyrins is wide, not only the peripheral position are available to undergo addition, paving the way to an endless list of porphyrins; the core of the macrocycle is also able to coordinate metals to form equatorial complexes. Depending on the nature of the bonded atoms they are also capable to bind additional axial ligands.

1.3.2 Porphyrins UV visible spectra

Porphyrins are deeply coloured; their name derives from the greek word πορφύρα (*porphyra*), meaning *purple*. This aspect is strictly related to their rich light absorption and the emission properties that we can observe in spectroscopy.

The free base porphyrin absorption spectra is characterized by four Q bands in the absorption region between 500 and 750 nm and a stronger band around 395-450 nm called Soret band (in honour to the scientist who discovered); the features of the typical absorption spectra of both, porphyrin free base and metalated complexes can be explained by the four orbital model proposed by Gouterman in 1960's.[45]

The four visible bands are ascribed to π–π transitions, from the higher energy occupied orbital to the lowest energy unoccupied, while the Soret or B band absorption is a consequence of the transition between the last occupied to the higher unoccupied orbital, this is the reason for the higher intensity of the band (figure 8).

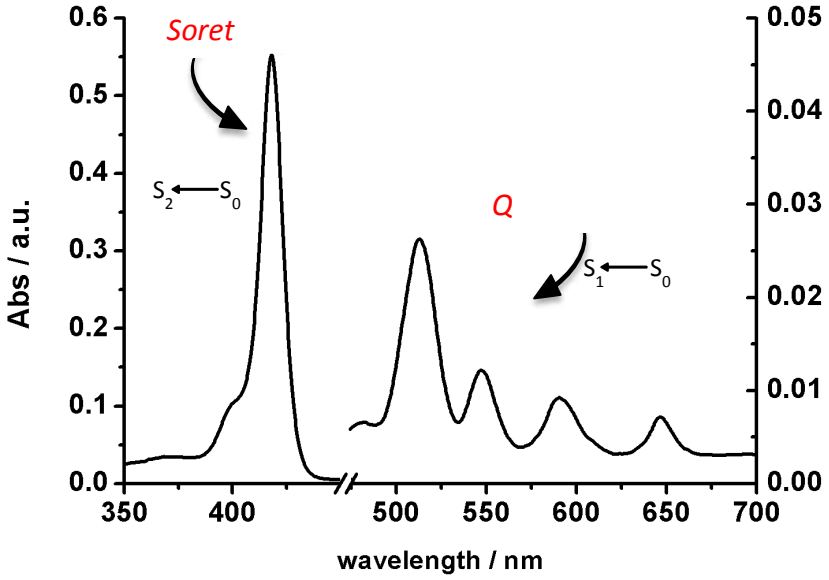

Figure 8: Absorption spectra of Tetraphenil porphyrine H_2TPP 1μM in Toluene

Changing in the conjugation pathway of the central ring can affect the spectroscopic characteristics; the relative intensity of Q bands is related to the kind and the position of substituents on the macrocycle ring. Basing on this latter consideration, porphyrins could be classified as etio, rhodo, oxo-rhodo e phyllo;[46] if the four central nitrogen form a complex with a metal, the number of the Q band pass from 4 to 2 due to the changing in the ring symmetry, also it is possible to observe a red shift of the absorption bands as showed in figure 9.

Since the 1935 when Rothemund published the procedure for the synthesis of tetraphenil porphyrin by reaction between pyrrole and benzaldehyde,[47] the number of porphyrin derivatives has increased enormously. The binding of charged groups to the porphyrin core allows obtaining macrocycle able to dissolve in water. Despite their capability to disperse in water, porphyrin core is still solvophobic, this condition render them good candidates for aggregation studies in water.

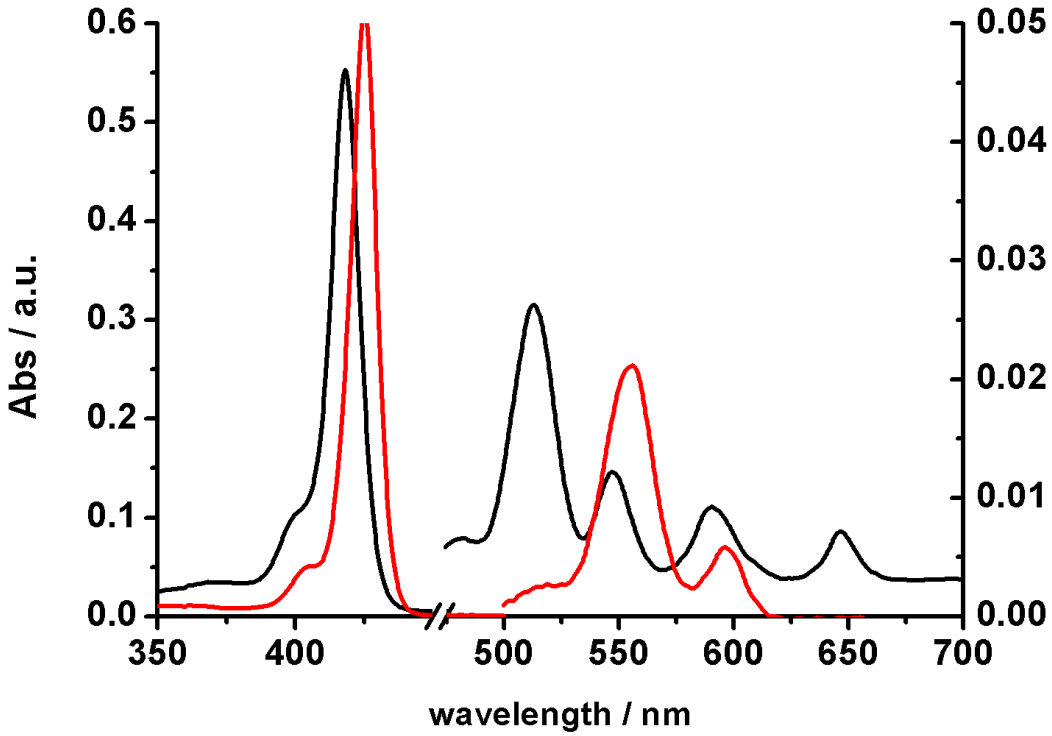

Figure 9: Absorption spectra of Tetraphenil porphyrine H_2TPP 1μM (black curve) and of Zinc Tetraphenil porphyrine ZnTPP 1μM (red curve) in Toluene.

1.3.3 Porphyrins aggregation

Dye aggregates are a significant class of supramolecular complexes, they have been studied because of its application in various fields from medicine to catalysis from sensing to light harvesting or energy storage.

In 1930, Sheibe [48-51] and Jelley [52] independently, observed that the absorption spectra of a pseudoisocyanine chloride in water were different from the spectra observed in organic solvents; in particular the absorption maxima was shifted.

Nowadays dyes aggregates showing a bathochromic shift in the absorption spectra are called J aggregates (because of Jelley), while aggregates with a hypsochromic shift are called H.

Among molecular dyes aggregates the study of the mechanism of porphyrin aggregation has developed an increasing interest. It was extensively demonstrate that porphyrin aggregation is a process strictly dependent on the combination of physical-chemical characteristics,[53,54] such as ionic strength, pH and solvent composition; the opportune management of the above factors can facilitate the processes. [55-59]

The high tendency to undergo aggregation in porphyrins is related to their capability to form π–π interactions among the aromatic macrocycles. Aggregation process depends on the porphyrin substituents, on the presence of a metal, on the pH or the solvent.

The preferential arrangement of porphyrins in aggregates is the one having the pyrrole ring of one porphyrin directly above the cavity at the centre of the other (figure 10); such an organization has the aim to minimizes π–π repulsion and, maximizes attraction between the σ–framework around the inner edge of the π-cavity of one porphyrin with the π-electrons of the pyrrole ring immediately above.

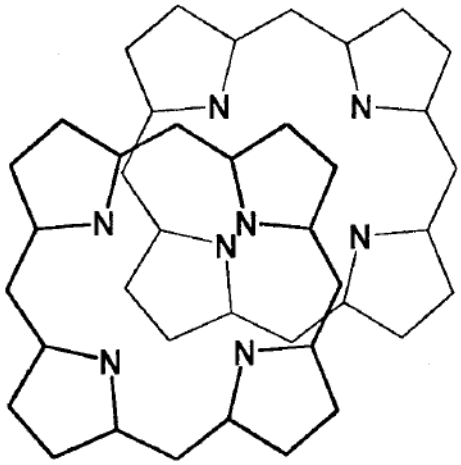

Figure 10: Schemati representation of preferential arrangement of porphyrins in aggregates

Even metalloporphyrins are able to aggregate, the presence of a metal cation in the macrocycle can increase the attraction between the positive charge and the negative electron cloud; it is important to underline that aggregation cannot occurs if the metal ion has an axial coordination, the ligand presence hinder the possibility of porphyrins to move close one to the other because of steric reason.

Porphyrins aggregates show peculiar spectroscopic properties, so the molecular associations of porphyrins were generally investigated using UV–Vis absorption and fluorescence spectroscopy.[60]

The aromatic character of porphyrins causes a strong π-π interaction,[61] enabling the formation of the two structure types: the “J-type” and the “H-type” showed in figure 11.

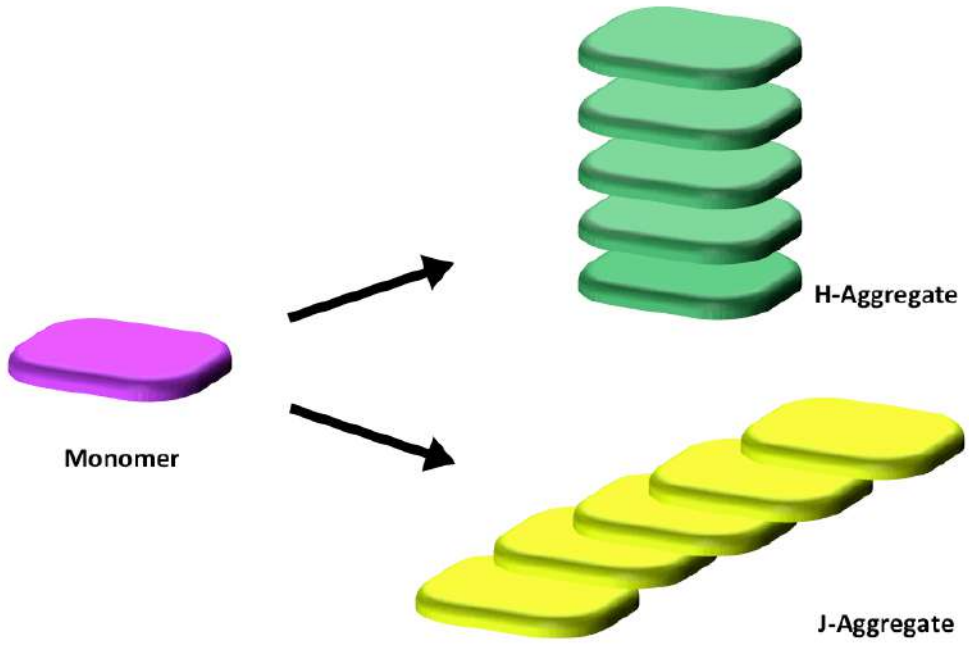

Figure 11: Schematic representation of H and J Aggregates.

In the J type aggregates, monomers are arranged along one dimension, in a side-by-side way; the monomeric molecules organised such that the transition moment of porphyrins are parallel, the angle between the transition moment and the line joining the molecular centres is zero.[62] The strong coupling of monomers results in a coherent excitation with a red shift relative to the monomer band. The nature of J-band has been assigned to a Frenkel exciton-like transition.[64,65]

H-aggregates are again a one-dimensional arrangement of strongly coupled monomers, but the transition moments of the monomers are perpendicular (ideal case) to the line of centre. On the contrary of J-aggregates, the arrangement in H-aggregates is face-to-face. The dipolar coupling between monomers leads to a blue shift of the absorption band.

The spectroscopic variation in the absorption spectra of porphyrins that follow aggregate formations can be explained using the Kasha theory of exitronic splitting. [65] The titled theory can be applied in all the cases where the orbitals overlap is weak, and the molecules that constitute the aggregate can be considered as individual entities; this condition is useful to apply the perturbation theory to the system.

We must therefore consider the wave function that describes the energy states of our aggregate as product of the wave functions, each describing various monomeric units, and the relative Hamiltonian operator as a summation of terms functions to the single molecules

component plus other terms to the intermolecular perturbation potentials. This kind of treatment uses a mathematical formalism similar to that of the theory of molecular orbitals, starting from different physical bases, gives different physical interpretations from the results obtained.

The Kasha theory provides for the aggregate a non-degenerate ground state, with only one value of energy, while a so-called excitonic splitting is expected for the excited state. That is, the excited state can be listed as described by two energy levels arising from the resonant splitting of the excited states of the individual interacting monomer units. However, it should be noted, that this is not the removal of some pre-existing energetic degeneration, since in the single molecules (in their isolate state) there was no degeneration in the energy of excited state. The above can be approximated and visualized through a vector representation, taking into consideration the interactions between the electrostatic dipole moments of the molecules.

Schemes 1 and 2 list two limit cases, related to the interaction between only two molecules, whose dipole moments lie in the molecular plane. In the transition 1 (Scheme 1), the dipole moments of the monomers are additive, the resulting transition moment will therefore be different from zero; in the case of transition 2 (Scheme 1), the dipole moments are non additive and therefore the transition will not take place. The $\Delta E_{transiz}$ of the formed dimer is greater than that of the monomer, since the arrangement of the dipole moments of the monomers within the dimeric specie is energetically disadvantageous.

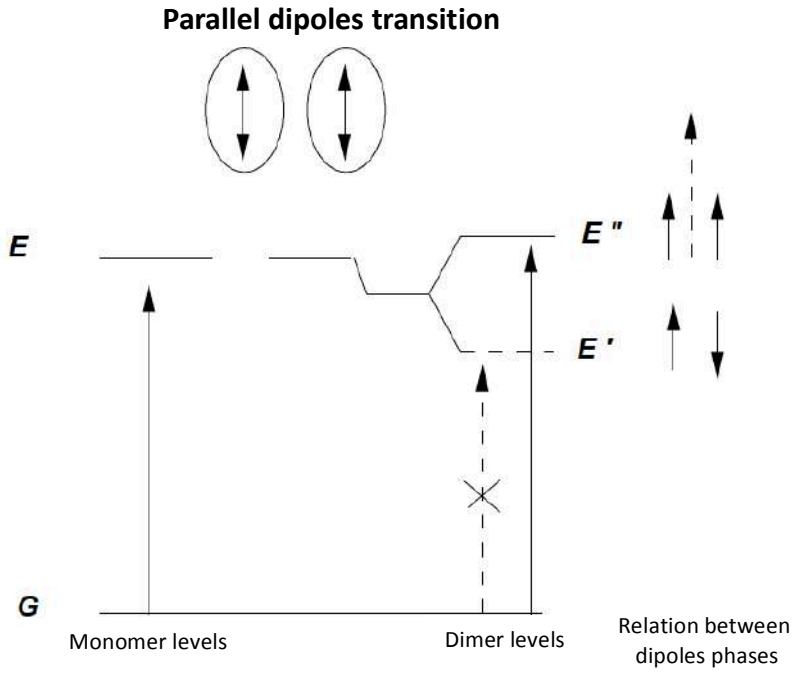

Scheme 1: Limit case designing a blue shift of the absorption band

This involves a shift of the absorption band of the aggregate towards shorter wavelengths (greater energies), which is towards blue, respect to the band of the monomeric unit. This spectroscopic characteristic is typical of "H" type aggregates, to which a "face-to-face" structure is associated. Instead, there is a different situation when the dipole moments are in line. In transition 1 (Scheme 2) the dipole moments of the monomers are additives, therefore the transition will be allowed; in transition 2 (Scheme 2) the dipole moments are non additives and the transition will not take place.

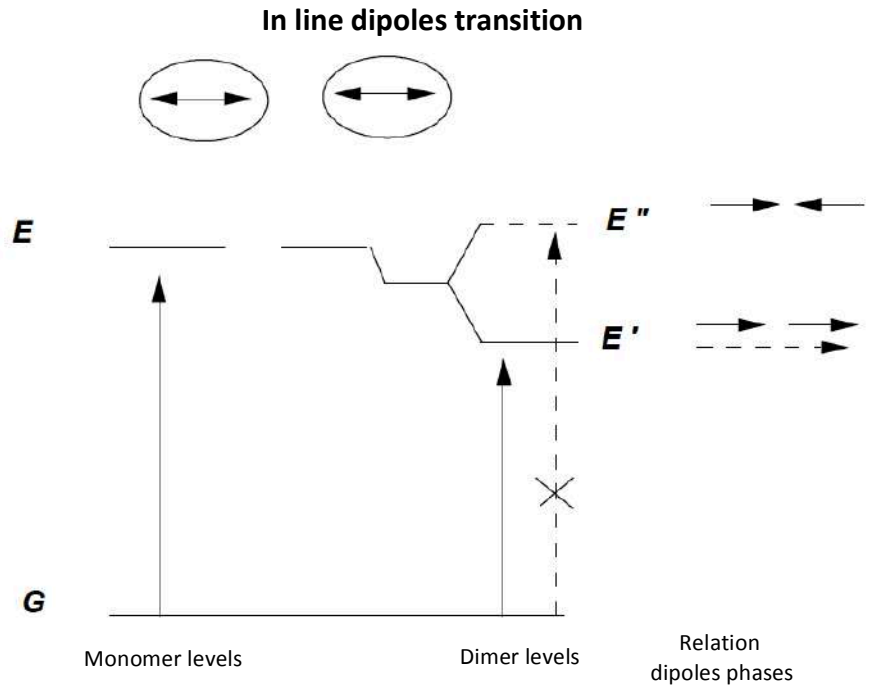

Scheme 2: Limit case designing a red shift of the absorption band

In this case, the $\Delta E_{transiz}$ of the dimer is smaller than that of the monomer, because the arrangement of the dipole moments is energetically favoured. Thus the absorption band of the aggregate is shifted towards longer wavelengths (lower energy), i.e. towards the red, with respect to the monomer band. This spectroscopic characteristic is typical of "J" type aggregates, to which an "edge-to-edge" type structure is associated.

Obviously, for intermediate geometries with respect to those represented in Scheme 1 or 2, both transitions become partially allowed, so the absorption spectrum of these aggregates should

be characterized by the simultaneous presence of two bands, one shifted towards blue and one shifted towards red, with respect to the monomer band.

1.4 Materials and methods

1.4.1 Circular dichroism

The circular dichroism (CD) is a spectroscopic technique widely used in the study of chiral molecules and aggregates.

The theoretical basis of the technique is as follows.

Electromagnetic radiation is a complex waveform that can be considered as two simple wave motions perpendicular each other; one of the components is magnetic (M) and the other is electric (E). To describe the phenomena we consider only the electric component E.

The E-wave can oscillate in any direction perpendicular to the propagation direction; this is the unpolarized light propagation, the light that came from the sun or from a lamp (figure 12).

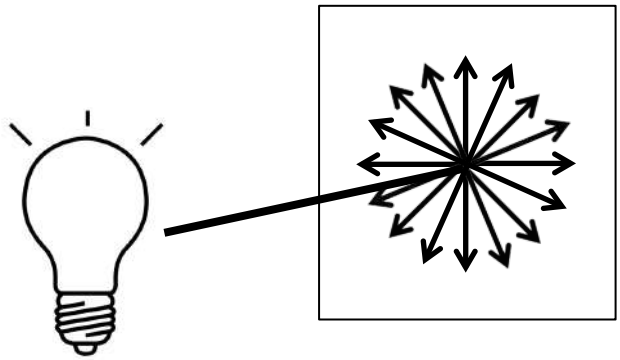

Figure 12: unpolarized light, the electric component can be oriented in every direction orthogonal to the propagation direction.

When the direction of the electric component is restricted to a plane perpendicular to the direction of propagation the light is linearly polarized. The linearly polarized electromagnetic radiation can be resolved in two components, L and R, they are circularly polarized the magnitude of their oscillation is constant but the rotation sense is opposite as showed in figure 13.

The differential absorption of radiation polarized in two directions as function of frequency is called dichroism. When applied to plane polarized light, this is called linear dichroism, for circularly polarized light, circular dichroism.

Figure 13: schematic representation of the two components that give the linearly polarized lighth.

After passing through an optically active sample, circularly polarized light will be changed. The two components are still circularly-polarized, but the magnitudes of the counter-rotating E-components will no longer be equal as the molar extinction coefficients for right ε_R and left ε_L polarized light are unequal. The direction of the electric vector no longer traces a circle - instead it traces an ellipse (actually an elliptical screw if we do not confine ourselves to the projection). There will also be a rotation of the major axis of the ellipse due to differences in refractive indices (figure 14).

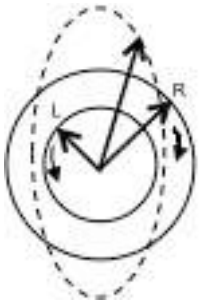

Figure 14: Schematic representation of the two components that give the circularly polarized light.

Inherently asymmetric chromophores or symmetric chromophores in asymmetric environments will interact differently with right- and left-circularly polarized light resulting in two related phenomena. Circularly polarized light rays will travel through an optically active medium with different velocities due to the different indices of refraction for right- and left-circularly polarized light giving the **optical rotation** or **circular birefringence** phenomena. The variation of optical rotation as a function of wavelength is called **optical rotary dispersion (ORD)**. Right- and left-circularly polarized light will also be absorbed to different extents at some wavelengths due to differences in extinction coefficients for the two polarized rays this is the **circular dichroism (CD)**.

The CD signal is a representation of the optical activity produced in the absorption band. To generate a CD signal the transition must be allowed for the electric dipole but also for the magnetic one. A charge transition and a charge rotation must occur contemporary giving an electronic excitation that follow a helix pathway; this is possible if the electric and magnetic vectors are not perpendicular, so it happen only for molecules having rotational symmetry, just in chiral molecules.

1.4.2 UV-Vis

A light beam of proper wavelength passing through a chromophores solution can give the absorbance phenomenon. The Lambert-Beer law demonstrate that there is a linear correlation between the specie absorbance and its concentration:

$$A = \varepsilon \times b \times C \qquad (1)$$

In equation 1 A is the absorbance, C is the concentration of the sample, b is the path length and ε is the molar extinction coefficient; it represent the absorbance of the sample at a given wavelength when b and C are equal to one.

To obtain the Lambert-Beer law we assume that the decreasing intensity of the light coming from the source is proportional to the concentration of the sample multiply by the intensity of the light exit from the cell and the depth of the volume considered

$$-dI = C \times I \times dx \qquad (2).$$

The 2 is valid only for limited concentration values; for higher “C” the estimated “I” than what we can assess and the number of revealed absorption events is no more linear.

The linearity of the Lambert-Beer law is confirmed for samples concentration whose absorbance is in the range 0.1 to 1.

Moreover deviations of the Lambert-Beer law can be observed because of instrumental abnormalities, this is another reason for the necessity to define a validity range. The range of linearity depends on the pendency of the curve; it can’t be defined in function of the concentration of the sample because it could vary depending on the nature of the specie. For the above reason the range is defined in function of the Absorbance from 0.1 to 1.

The interval lower limit is strictly related to instrumental errors, so it severely depends on the type of machine used for the measurement.

During my research activity I used the spectrophotometer Jasco V 530 and V630.

1.4.3 Fluorescence

Molecules can absorb energy following the interaction with the electromagnetic radiation; energy absorption allows molecule's electrons to move from a ground to an exited state.

The following reported Jablonski energy diagram is a schematic representation of the processes that can occur after energy absorption (figure 15).

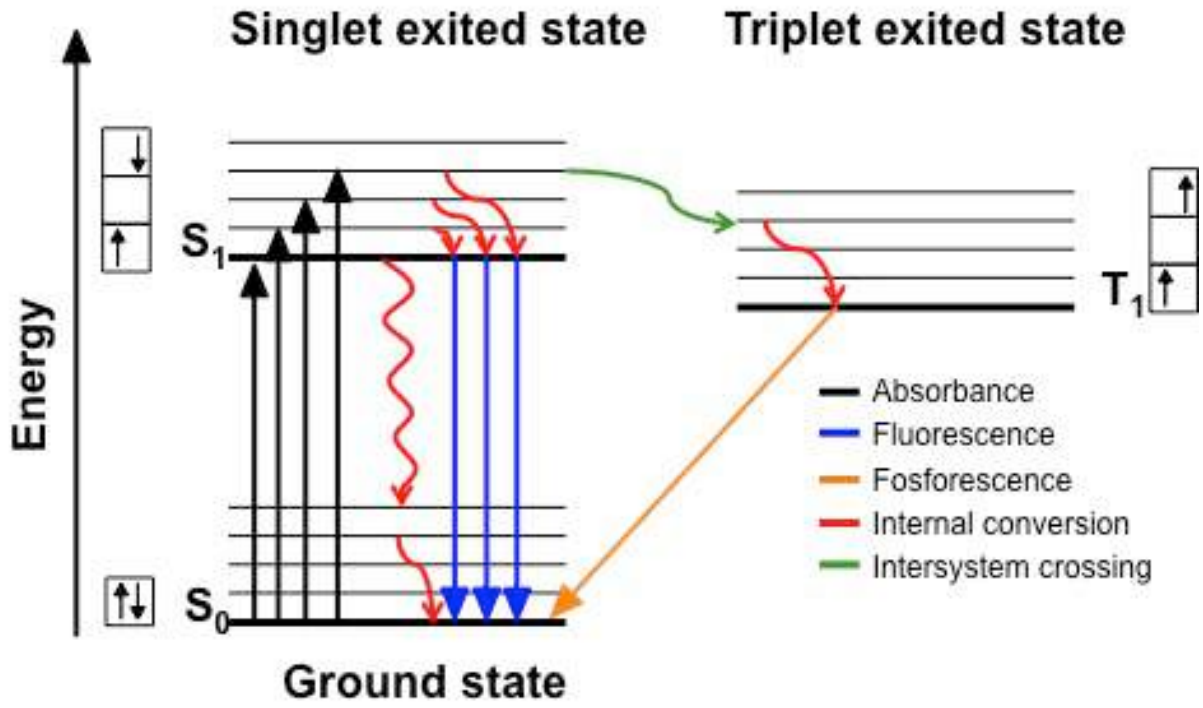

Figure 15: Jablonski energy diagram

After absorption electrons move, from a higher vibronic level, to the lower energy exited state, this mechanism is the internal conversion. Thereafter the fluorescence process occurs, with the emission of a radiation with a lower energy respect to the incident one, for the above the fluorescent bands are always at higher wavelength respect to the absorbance.

The electrons involved in fluorescence phenomena are π electrons, chromophores giving π–π* transitions are able to give fluorescence.

During the excitation we can consider nuclei having a fixed position respect to electrons, they are not involved in electronic transition. The probability of a transition to occur is higher if the wave functions of the two vibrational levels are overlapped; this is the Frank Condon

principle, it explain the reason for different intensities in vibronic transitions. However during the fluorescence process many transitions occur giving rise to a continuum spectrum.

Fluorescence is not the only one emission process. If after absorption a change in the spin multiplicity occurs, fosforescence can be observed. This second emission process is forbidden by the selection rules, but allowed because of the interaction spin-orbit. The time for a fluorescence process to occur is estimated in the range 10ps-10μs, the changing in spin multiplicity cause a delay in the emission, so fosforescence process take place in the range 10μM-hours.

Fluorescence is a high sensitive technique that can give information about the molecule structure; variation in the molecules environment or in their geometry can be estimated even at low sample concentration.

1.4.4 Resonance light scattering

When a supramolecular assembly interact with light two processes can occur. The electromagnetic radiation can be absorbed (see previous paragraph) and, when the aggregate size is smaller than the incident wavelength, the Rayleigh light scattering can be observed (together with absorbance).

If there is a strong communication between the chromophores in the aggregated specie, the Resonance light scattering (RLS) can occur. The RLS effect is observed as increased scattering intensity at or very near the absorption wavelength of an aggregate, because of the relation between the volume of the aggregate and its absorption (absorption depends on the polarizability and the polarizability depends on the volume of the aggregate).

Scattering is the diminution of the light intensity due to the radiation in all directions of the ray; it is a consequence of the oscillating dipole formation following the light-aggregate interaction. If the aggregate is small compared to the incident wavelength, the induced dipole can be considered ideal.

The ratio between the quantity of absorbed energy of the incident beam and the intensity of the initial beam is called "*absorption cross section*"; the ratio between the quantity of scattered energy (in all the directions) and the intensity of the incident beam is called "*scattering cross section*" the two "*cross sections*" depend on the polarizability (α) of the aggregates.

Polarizability is a complex quantity; its real and imaginary parts depend similarly on the wavelength; the two components assume a maximum in the absorption band of the chemical

specie. For the above, the RLS signal can be observed at the same wavelength as the absorbance and one can prevail on the other. In fact, the "*absorption cross section*" depends only on the imaginary part of the polarizability, while the "*scattering cross section*" depends on the square of both the real and the imaginary components.

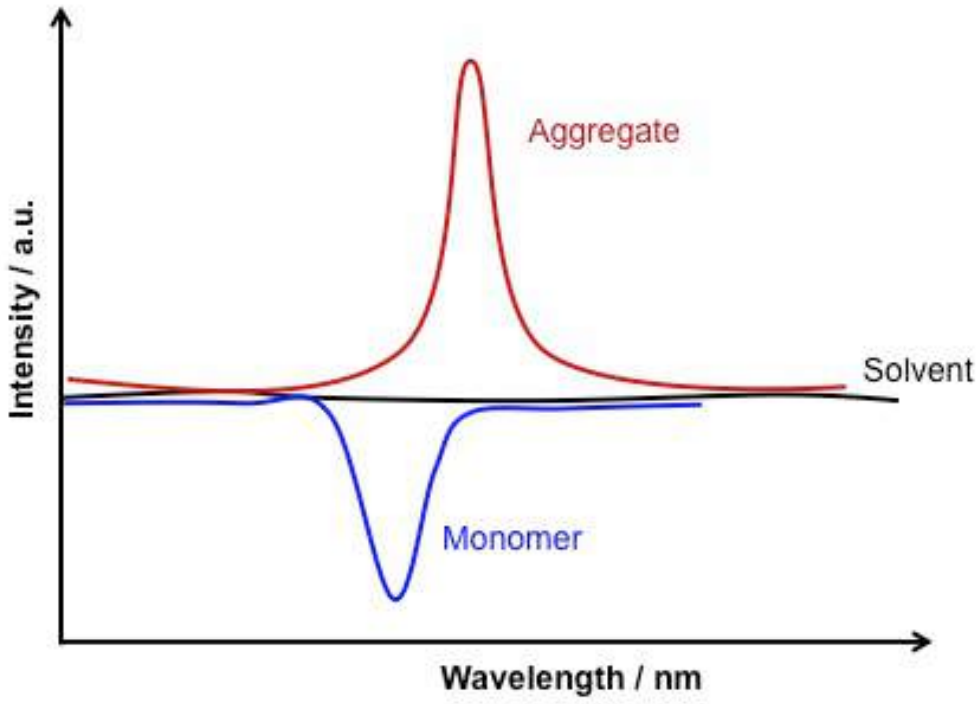

Figure 16: Examples of RLS spectra of monomer (blu curve) and aggregate (red curve).

If the RLS measurement is conducted on a monomeric specie solution, absorption prevail o scattering and a photon lack can be observed in correspondence of the absorption band. While the RLS spectrum of an aggregate displays an intense RLS signal at the same wavelength as the aggregate absorption band (figure 16). The last is due because of the dependence of the RLS on the square of the polarizability that prevails on the absorbance.

The bigger is the aggregate volume and, the communication among the chromophores in the aggregate, the higher is the RLS signal.

1.4.5 Raman spectroscopy

The Raman spectroscopy is an important analysis technique able to give detailed information about molecules structure (bonds, chemical environment etc.).

Photons that interact with sample molecules can be diffused, giving no energetic transitions, the diffusion follows an elastic interaction and in this case the Rayleigh diffusion take place (the scattered radiation has the same frequency as the incident one). When the diffusion occur following an inelastic interaction there is the energy transfer from the radiation to the particles; the scattered photon has lower or higher energy respect to the incident one, this is the Raman effect.

Molecules interacting with the light move toward a virtual non-quantised energetic state $h\nu_0$, after than they decay emitting photons that can be at higher or lower energy depending on the initial vibronic state. The lower energy photons are generated when the particles are in their fundamental state (most populated state at room temperature), following the interaction they decade to a vibrational exited state, this phenomena give signals called Stokes lines. On the other side, if particles start from an exited state and, after decay, they go to the fundamental state they give a higher energy photon generating anti-Stokes line (figure17).

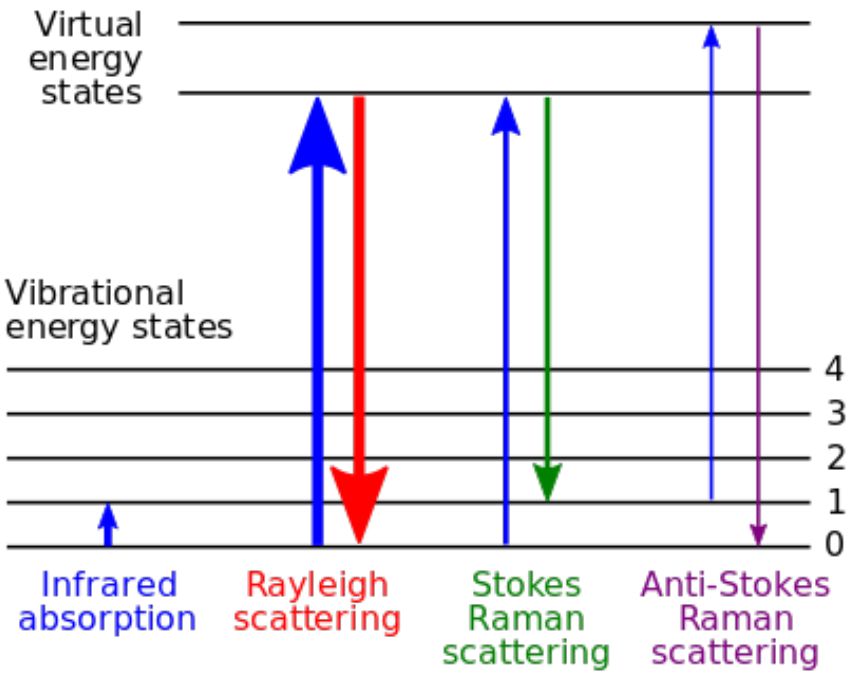

Figure 17: Energetic diagram in Raman

In the typical Raman spectra it is possible to observe signals from both elastic and inelastic interactions; the Rayleigh signal intensity is the higher in the spectrum but it doesn't give any information about the molecule. Anti-Stokes lines have low frequencies and cannot be easily

revealed; Stokes lines are the signals that give structural information on the molecules, their frequencies are related to the functional groups in the molecule. The information that can be given by a Raman spectrum are similar to those that can be find in a IR spectrum; of course the two techniques (Raman and IR) give similar but not the same information due to the different selection rules that control allowed and forbidden vibrational levels.

The data reported in a Raman spectrum are the emission intensity *vs* the Raman shift defined as the wave number difference between the observed and the incident radiations.

1.4.6 Zeta Potential

A colloidal system is a solution or better dispersion, where a solid is finely dispersed in a solvent.

A dispersion of nano particles in water is a typical example of colloid, depending on circumstances particles tend to adhere one to another to form aggregates; the stability of particles in solution is relates on its total potential energy function, whose value depends on several contribution. The attractive and repulsive contributions are the two most important; Derjaguin, Verwey, Landau and Overbeek developed the so-called DVLO theory. The theory proposes that, the stability of a colloidal system is determined by the contemporary contribution of attractive (van der Waals) and repulsive (electrical double layer) forces. If particles posses high repulsion contribution they show a higher stability in the dispersion.

The network of charged particles in solution consist of two layers (figure 18), the first layer or inner region, were ions are strongly bound, is called Stern layer; the outer layer is called diffuse, the presence of the Stern layer shield the charges in this region. In the diffuse layer we can find an ideal distance where ion and particles form a stable entity. Ions that are beyond the limit stay with the bulk, wile ion within the limit move with the particle; the limit potential is called zeta (ζ) potential, it can be positive or negative. The higher is the ζ potential value the higher is the colloidal system stability. Particles with a ζ potential value between +30 and -30 mV are considered unstable, while on the other side more positive or more negative ζ potential values are indicative of higher stability of the system.

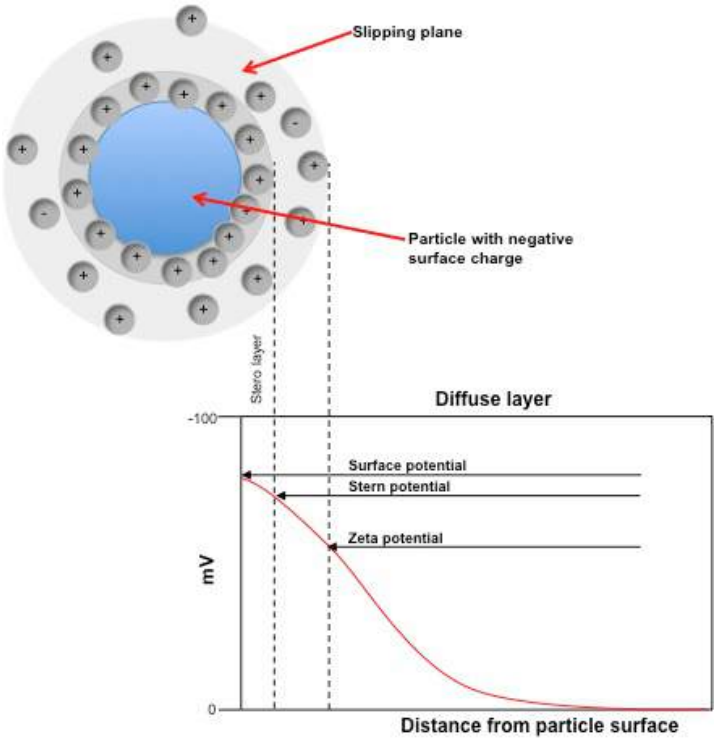

Figure 18: Schematic representation of zeta potential

Changing in the surface charge of particles can occur in non covalent way, for the interaction with oppositely charged molecules or, in a covalent manner with the functionalization with opportune molecules; ζ potential measurements in these cases is a useful technique that can give information about the reaction outcome. Of course in water solution pH such as ion strength can affect the surface charge of the particles, changing the stability of the solution.

1.4.7 Ciclic Volatmmetry

Cyclic voltammetry (CV) is an electrochemical technique employed to investigate the oxidation and reduction processes of molecular species.

During the CV measurement the current developed in an electrochemical cell is quantified against a reference electrode that maintains a constant potential; the voltage is swept between two values at a fixed rate, however when the voltage reaches the final voltage the scan is reversed and the voltage is swept back to the initial one.

The typical signal in a CV measurement is a voltammogram (see fig. 19) in the x axes there is the applied potential, while in the y axes there is the measured current (i). A crucial

parameter is the scan rate, it indicates that during the experiment the potential is varied linearly at a wanted mV per second. Changing the scan rate the amplitude of the voltammogram can change. Faster scan rates lead to a decrease in the size of the diffusion layer.

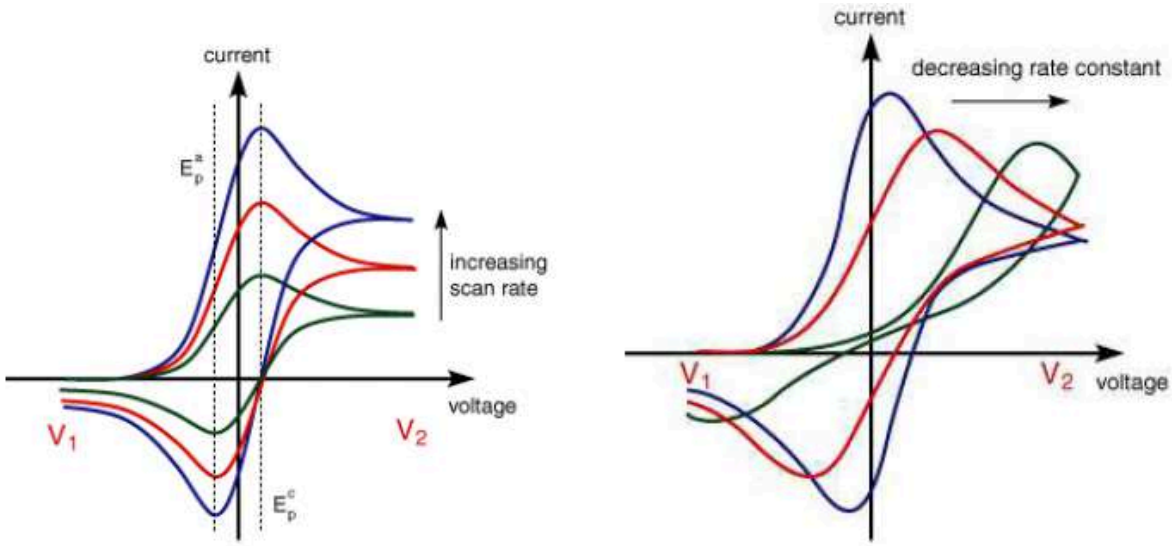

Figure 19: Scan rate and rate constant dependence of the I-V curves.

By analysing the variation of peak position as a function of scan rate it is possible to gain an estimation of the electron transfer rate constants.

The integral of the voltammogram is related to the charge stored by the sample an on its specific capacitance

$$Q = \frac{A}{2\,\frac{\delta E}{\delta t}} \qquad (1)$$

$$C = \frac{Q}{V} \qquad (2)$$

$$C_s = \frac{C}{m} \qquad (3)$$

All cyclic voltammetry measurements was recorded using a Reference 600/EIS300 Gamry potentiostat/galvanostat.

1.4.8 Experimental

Effect of preorganization in porphyrin aggregation and chirality transfer

ZnTPPS solutions were prepared in quartz cuvettes and porphyrin concentration was estimated by following the intensity of the Soret band at λmax = 421 nm (ε = $6.83x10^5$ $M^{-1}cm^{-1}$). The porphyrin solutions were kept in the dark to avoid undesired photochemical reactions. In all experiments the concentration of ZnTPPS is 2 μM.

Poly-D-glutamate sodium salt (PDG, Dp 20), and poly-L-lysine hydrobromide (PLL, Dp 68), purchased from Sigma-Aldrich, were dissolved in ultrapure water, and their concentration was detected by UV-vis measurements monitoring the signal at 205 nm (εPLL = 3300 $M^{-1}cm^{-1}$ and ε PDG = 3500 $M^{-1}cm^{-1}$). In all experiments the concentration of polyelectrolytes (PLL and PDG) is 50 mM.

The kinetic studies were performed by adding ZnTPPS to PLL (or PDG) solutions, and the aqueous demetalation of the ZnTPPS was measured by monitoring the absorbance variations for 7 h of the corresponding experiments at different pH (7.0–4.5–3.0–1.5). Acid pH was achieved by adding HCl 6 M in the PLL (or PDG) starting solutions.

Poly-L-Lysine hydrobromide (PLL) stock solutions dp from 36 to 2060 were obtained by dissolving a certain amount of freeze-dried polyelectrolites directly into ultrapure water. Their concentrations, expressed as moles of lysine residues per litre, were calculated spectrophotometrically monitoring the absorption of the lysine residues at 205 nm, UV/Vis (water): λmax(ε)=205 nm (3300 $M^{-1}cm^{-1}$). Despite the several chain lengths, all experiments were performed with a lysine residues concentration fixed at 50 μM.

Acid pH values were achieved in the PLL working solutions by adding small amounts of HCl 6 M.

To investigate the self-assembly of ZnTPPS with polylysine, we prepared the working solution by adding the ZnTPPS into neutral PLL solution (50 μM, neutral pH) and then decreasing the pH to 1.5 with HCl.

In all spectroscopic measurements a 1 cm quartz cuvette was used.

Chiral recognition of L and D amino acids by porphyrin aggregates

The H_2TPPS stock solutions were prepared in ultrapure water and their concentrations (ranging from 10^{-4} M to $2x10^{-4}$ M) were estimated by using the maximum intensity of the Soret band at 412 nm, using an extinction coefficient of $4.8x10^5$ $M^{-1}cm^{-1}$. The porphyrin solutions were kept in the dark to avoid undesired photochemical reactions. In all experiments the H_2TPPS concentration was fixed at 6 μM.

The amino acids stock solutions were prepared by dissolving the exact weight of solid in ultrapure water in order to obtain concentration 0.1 mM. The work solutions were prepared in ultra clean conditions: (i) the operators wore a lab coat, hair cap, gloves, and mask during the preparation of samples; and, (ii) the tips of the pipettes were washed three times with ultrapure water while the vials were treated with an ultrasonic system three times by dipping them in ultra-pure water, before being used. The samples were prepared as follows: (i) in the case of the "acid first" procedure, the needed volume of the amino acid stock solution was diluted in water to reach the desired concentrations (0.5 mM; 1 mM; 2 mM; and, 4 mM); the NaCl (0.3 M) and

HCl (pH 2.5) were then added and the porphyrin (H_2TPPS) was inserted at the opportune volume in order to obtain 6 μM concentration. Finally, the solutions were left to equilibrate for one night prior to record the spectra; and, (ii) in the "acid last" procedure, the porphyrin compound was mixed with the amino acid and NaCl at a pH of 6.5 then left for one night. HCl was then added as the last reagent in order to reach pH 2.5. The solutions, with all reagents, were left to equilibrate for one night prior to perform any measurements.

All spectoscopic measurements were performed at room temperature using a 1 cm quartz cuvette.

Morphological study of chiral J-Aggregates

Samples for morphological study was prepared using the above described acid first procedure.

Porphyrins in heavy metal sensing

H_2T4 stock solution ($1x10^{-4}$ M) was prepared by dissolving the solid in ultrapure water at pH 5.5, the concentration was extimated using ε at 422 nm $2.08x10^5$ $M^{-1}cm^{-1}$. H_2T4 work solutions were achieved directly in cuvettes, by adding a microliter of the stock solution in 2.5 mL of water (pH = 7). $Pb(NO_3)_2$ and $Zn(NO_3)_2$ stock solutions ($1x10^{-3}$ M) were prepared in ultrapure water at pH = 7 weighing the necessary amount of solid.

Microscope glass slides were polished by sonication in water, isopropyl alcohol, and ultrapure water before use.

H_2T4 deposition is achieved by dipping (dipping time =1.5 hours) glass slides into [H2T4] = 10 mM solution at pH 5.5; afterwards, glass slides were rinsed with water to remove the excess of porphyrins.

The UV-Vis spectra of H_2T4 deposited on glass were recorded from λ = 700 nm to λ = 350 nm (data pitch 0.5 nm; band width 2.0 nm; and scanning speed 100 nm min^{-1}) before and after dipping in water containing Pb^{2+} (concentration range between 1 mM and 10 mM at pH 7), Zn^{2+} (concentration range between 1 mM and 10 mM at pH 7) or both ions in different Pb^{2+}/Zn^{2+} ratios (1 mM/5 mM; 5 mM/5 mM; 10 mM/5 mM pH 7; 3 mL).

Absorption spectra were recorded immediately after dipping (t = 0) and at intervals of 5 minutes, up to 30 minutes.

Porphyrins deposited on glass are desorbed after dipping (2 hours) in a SDS 10% solution.

Porphyrins in energy storage

The H_2TPPS and H_2T4 stock solutions were prepared in ultrapure water (or in NMP) and their concentrations ***4.*** (ranging from $1x10^{-4}$ M to $2x10^{-4}$ M) were estimated by using the maximum intensity of the Soret band respectively at 412 and 422 nm, using the extinction coefficients $4.8x10^5$ $M^{-1}cm^{-1}$ for H_2TPPS and $2.08x10^5$ $M^{-1}cm^{-1}$ for H_2T4. Solutions were stored in the dark to avoid undesired photochemical reactions.

MnO_2 nanosheets NMP dispersions was obtained by LPE following the procedure in ref. 114.

The MnO_2 was centrifuged and washed using ultrapure water, than weighed and dispersed in water to obtain the working solutions 0.025mg mL^{-1}.

The opportune volume of porphyrins stock solution was added to the MnO_2 solutions to reach the concentration 1.5μM.

All spectroscopic and zeta potential measurements were performed using 1cm path length disposable plastic cuvette.

ITO coated glass slides where washed using isopropanol, acetone and water. A functionalized MnO_2 layer, having thickness ranging from 100 to 250nm was then sprayed onto the glass substrate.

These MnO_2 electrodes, and H_2T4 functionalized MnO_2 electrodes were tested in a half-cell configuration using an Ag/AgCl reference electrode and a platinum coil as counter electrode. The electrolyte used for all testing was 0.5 M K_2SO_4. Cyclic voltammetry experiments were performed in a potential range of 0 to 1 V versus Ag/AgCl using scan speeds from 5 to 10000 mV/s.

2 CONTROL OF PORPHYRINS AGGREGATION AND CHIRAL INDUCTION

2.1 State of the Art

We can find several studies on the porphyrin self-assembly process, in particular there are many reports on the hierarchical effect governing aggregates formation.

One of the more exemplifying study was conducted on the porphyrin *meso*-tetrakis(4-phosphonatophenyl)-porphyrin (H_2TPPP) (figure 20). [57]

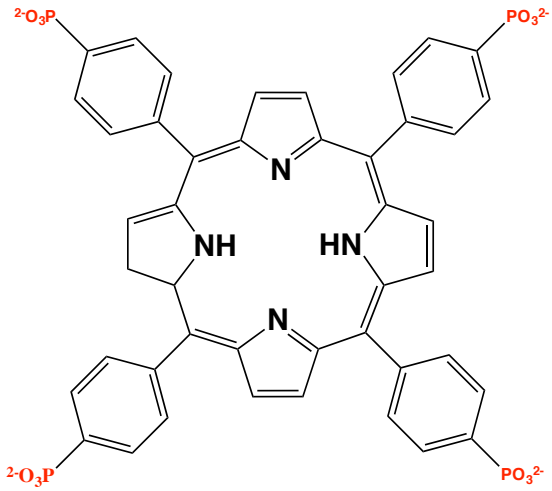

Figure 20: Schematic representation of the porphyrin H_2TPPP

The hierarchical self-assembly of the titled porphyrin was described clarifying the effect of time and reagent addition order on the final assembly. The strict control on the three protonation steps of the H_2TPPP, allow to drive the system toward the *i)* thermodynamic pathway, where the final product is the protonated specie; *ii)* the kinetic pathway having as final product the aggregate. Protonation is a more rapid process respect to the aggregation, the last can be achieved even after hours; the different speed is the parameter that allow to control the final product in the solution.

As stated before, H_2TPPP shows three protonation steps (see scheme 3 a): 1) below pH 7.8 we can observe the first protonation of the phosphonate groups; 2) the protonation of the

porphyrin core occurs at pH value lower than 5.4; 3) the phosphonate groups can bind the second proton at pH lower than 2.4. After the second protonation step the porphyrin is in its zwitterionic form, this allow H_4TPPP to aggregate thanks to the capability to give both hydrogen bond and π–π interaction. The as obtained aggregates are in a kinetic trap; simply decreasing the solution pH is not sufficient to overcome the energetic barrier to give the thermodynamic product.

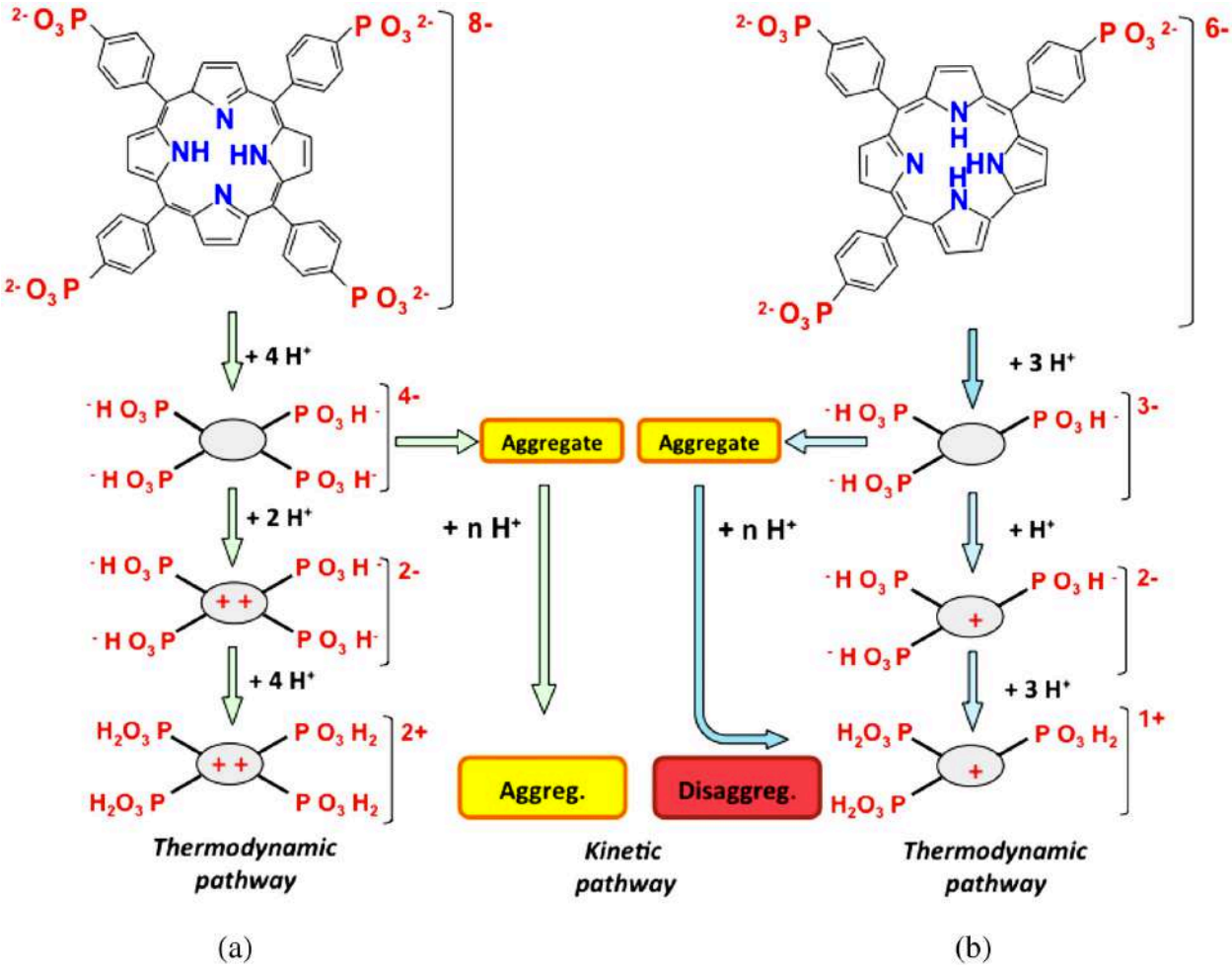

Scheme 3: (a) HTPPP protonation and aggregation pathways; (b) TPPC protonation and aggregation pathway

To demonstrate the kinetic inertia of the described system two UV-Vis pH-metric titrations was performed on porphyrin solutions, changing the acid addition time.

A first quick titration was performed from pH 10 to 2.5; it leads to the formation of the monomeric protonated specie, the UV-Vis spectra show the shift of the Soret band from 414 to 438 nm (figure 21). Following the quick titration a slower one was performed as showed in figure 22, slowly lowering the pH cause a broadening in the Soret band and a high hypochromic effect.

The final aggregate growth is consequential to the formation of small aggregates that act as "seeds"; if the acid addition is rapid protons reach quickly the binding avoiding seeds formation. During the slow titration the lag time between acid additions is sufficient to small aggregate formation, they are able to catalyse the growth of a big homoaggregate.

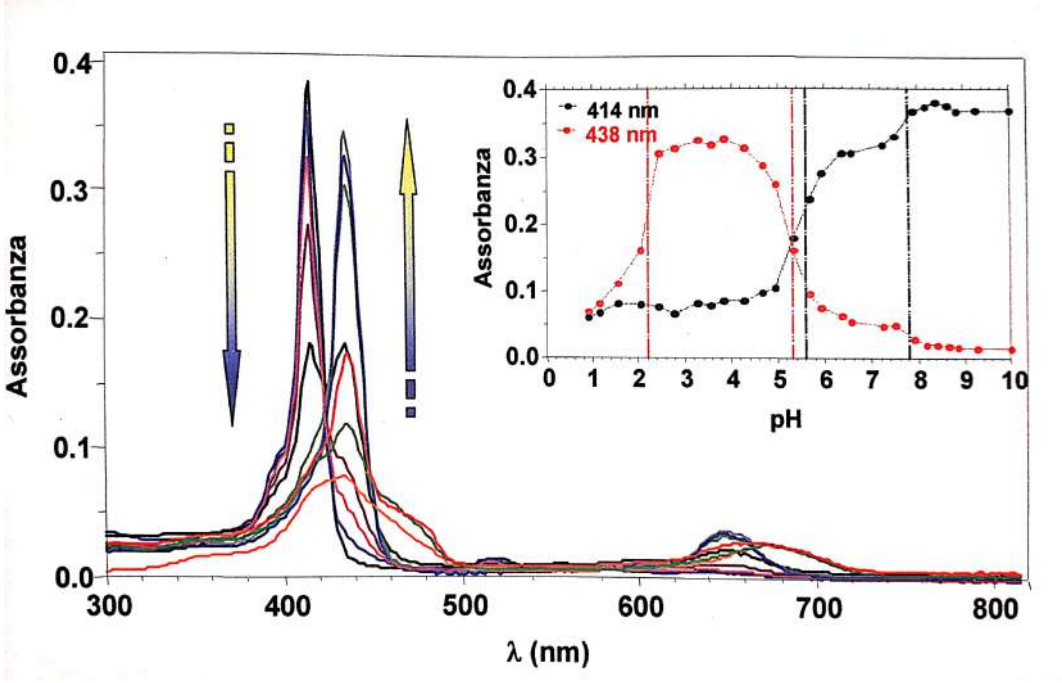

Figure 21: Absorption spectra of the quick titration performed on a H_2TPPP solution.

Figure 22: Absorption spectra of the slow titration performed on a H_2TPPP solution.

Interestingly, we observed that changing the macrocycle size and, consequently restricting its capability to form H-bods, has consequences on the aggregate formation (Scheme 3).

We studied the aggregation pathway of the *meso*-tris(4-phosphonatophenil) corrole (TPPC) (figure 23);[66] corroles are macrocyclic molecules having a smaller cavity to that one of porphyrins because of the lack of a methinic bridge, they still have 18 π electron system making the core more electron-rich respect to porphyrins.

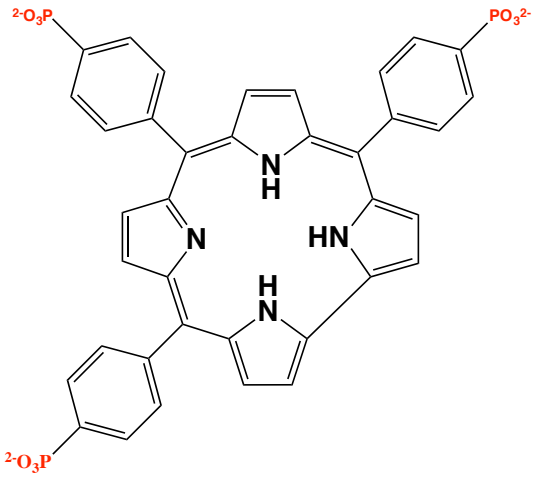

Figure 23: Schematic representation of the porphyrin TPPC

To evaluate the differences in H_2TPPP and TPPC aggregations we recorded spectra of TPPC solutions at various pHs (independent solutions experiments) after that, we performed a slow titration of the corrole solution. The independent solutions method is a useful approach that allows evaluating the pK_a in water solution, avoiding aggregation of the molecule (see figure 24).

The shift of the absorption band from 413 to 432 nm showed in figure 24, displays the typical protonation process; in the inset the three protonation steps are highlighted by pKa values: 1) pKa 7.7 for the first protonation of the phosphonate groups; 2) pKa 5.2 for the protonation of the core nitrogen atoms; 3) second protonation of the phosphonate groups.

Despite similarities among the quick titration experiments conducted in H_2TPPP solution and independent TPPC solutions, the slow titration experiments doesn't show the same results.

In Figure 25 the UV-Vis spectra of the TPPC slow titration (from pH 11.5 to 1.6) show that up to pH 4 the protonation together with the aggregate formation occurs, the hypochromic effect and the broadening of the band at 413 nm evidence this last, immediately after the first protonation step (see Scheme 3). Further acid addition cause an increase in the band at 432 nm indicates that both the corrole protonation and the disaggregation are ongoing. Increasing the positive charge in the TPPC favour the disaggregation.

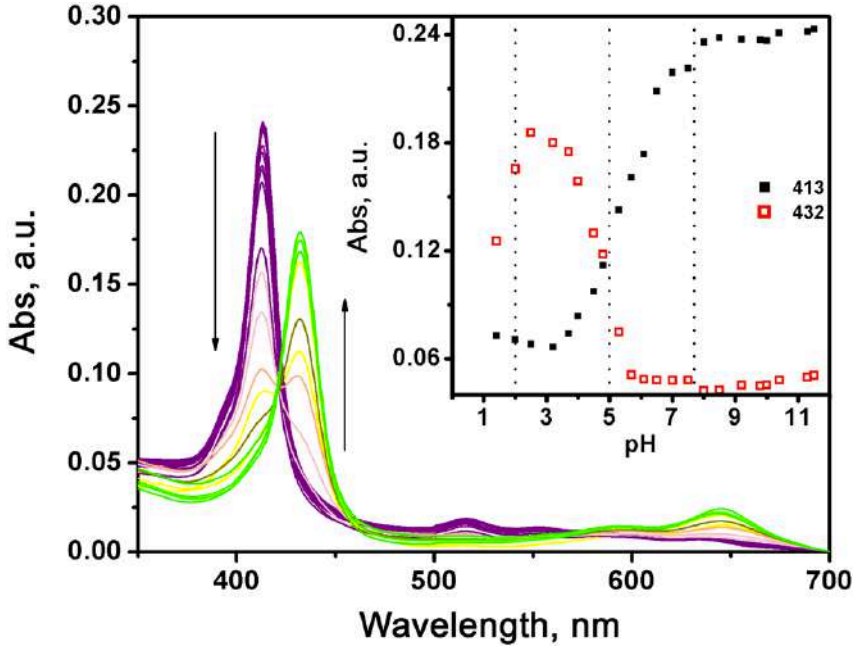

Figure 24: Absorption spectra of independent solutions of TPPC 10 mM at different pH. Inset: absorbance *vs.* pH for independent solutions of TPPC.

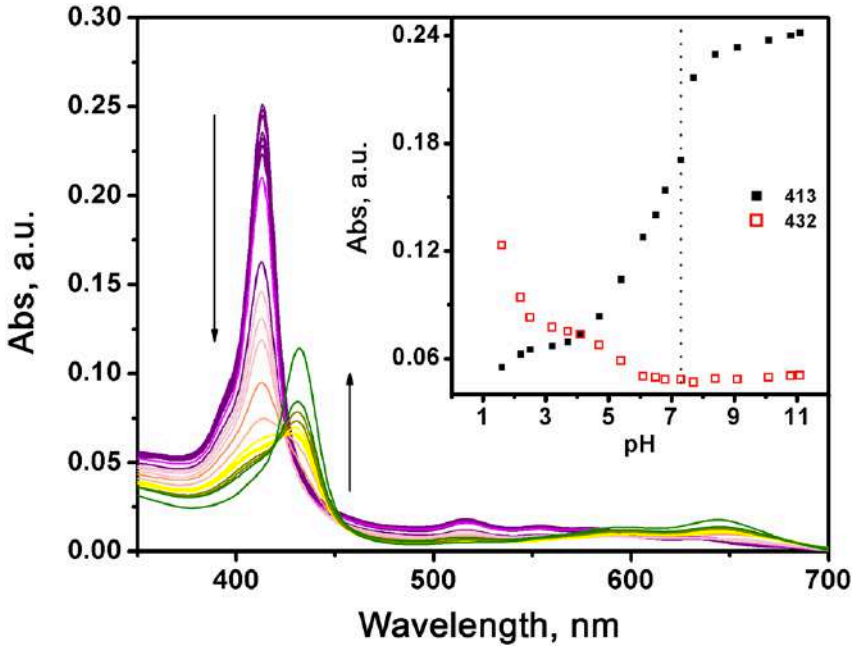

Figure 25: pH titration of a solution 10 mM of TPPC. Inset: absorbance *vs.* pH for the titration of a solution of TPPC

In TPPC solutions the aggregate formed after the first protonation step easily undergo from the aggregate (kinetic controlled product) to the protonated form (thermodynamic controlled

product) decreasing the pH; on the opposite the H_2TPPP aggregate formation prevent further protonation of the porphyrin, to obtain the monomeric protonated porphyrin the first protonation step must be skipped.

One of the most studied porphyrin aggregate system are the H and J aggregates of the protonated *meso-tetrakis-(4-sulfonanophenyl)porphyrin* $H_2TPPS_4^{4-}$ (figure 26).

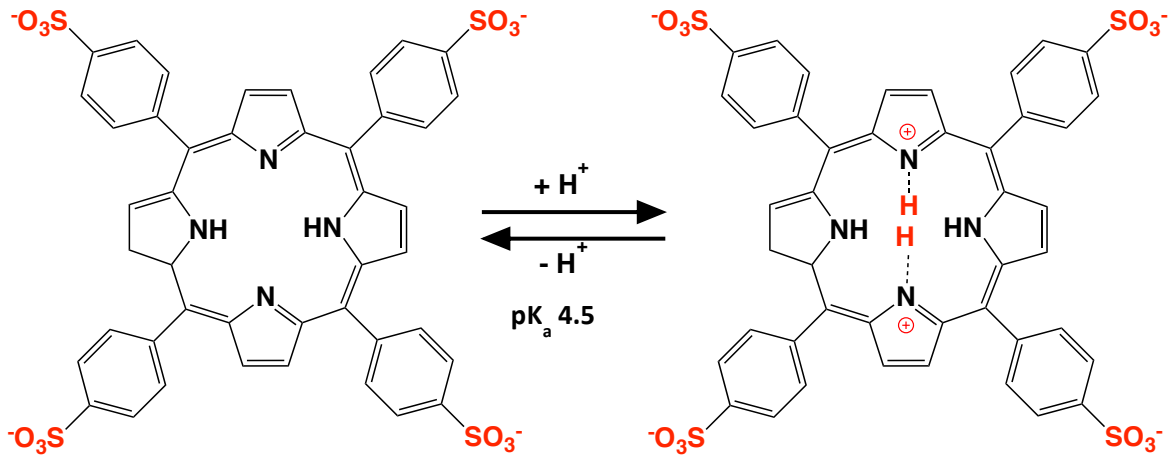

Figure 26: Schematic representation of the porphyrin $H_2TPPS_4^{4-}$ and the protonated $H_2TPPS_4^{2-}$

The kinetic formation of H_4TPPS4^{2-} J-aggregates is an intriguing aspect, studied since long time;[67-72] it is a self assembly process hierarchically controlled;[73, 74] this means that the adding order of the reagents (porphyrin, salt, acid) in the working solution lead to a different final product. Because of the dependence of the final aggregate architecture on the addition order, the structure of J-aggregates is not known. The different species that can be obtained can show similar UV-Vis absorption spectra and similarities in morphologies at nanoscale level, but deep differences in their structure.[67]

The pK_a value for the nitrogen of the porphyrin core is 4.5; at lower pH, the core is protonated giving the $H_4TPPS_4^{2-}$, this cause a shift of the Soret band from 413 nm to 435 nm (see figure 27 black and red curves respectively), increasing the ionic strength in an $H_4TPPS_4^{2-}$ solution leads to the formation of aggregate (figure 27 green curve) with an initial induction time, the kinetic of the aggregate formation depend on pH, ionic strength but also porphyrin concentration and nature of the salt.

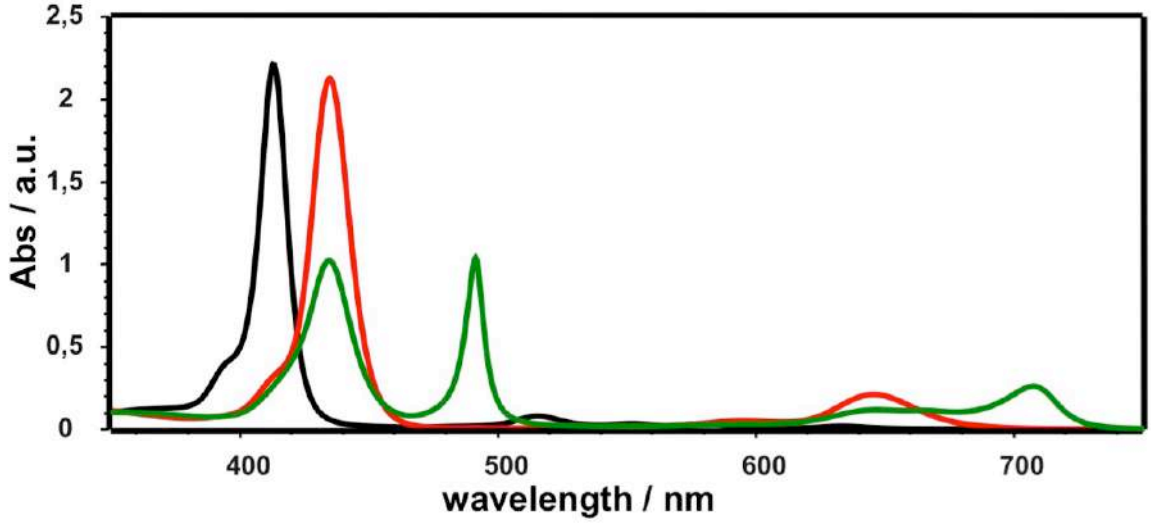

Figure 27: Absorption spectra of the porphyrin H_2TPPS at pH=7(black curve), at pH=2.5 (red curve) and at pH =2.5 with NaCl 0.3M (green curve).

H_2TPPS J and H type aggregates absorption bands are respectively at 490 and 422nm; their formation can be elucidated by an energetic and a steric contribution. The minimization of the repulsion between negatively peripheral charges is possible because of the presence of two positive charges inside the macrocyclic ring, in the protonated porphyrin (energetic contribution). The capability of bonds to stretch allows the benzensulphonic groups to rotate in a quasi-planar conformation respect to the macrocycle; consenting porphyrins to place one near the other to interact (steric contribution).

As before stated there are many parameters involved in H_2TPPS aggregate formation, one of that is the porphyrin concentration, amount of porphyrin lower than 2 μM , even at pH 2, prevent aggregation. The aggregation follows a sergeant soldiers process, the growth of big aggregates is a consequence of small aggregate "seeds" formation in the solution, of course increasing the H_2TPPS concentration allows porphyrins aggregation because of the higher possibility of molecules to interact each other.

It is important to underline that the protonation is a necessary condition but it is not sufficient to allow H_2TPPS to aggregate.

To overcome the limit given by concentration, one of the parameters that can be considered is the ionic strength, a high ion concentration in the solution allow to shield the charges and to stabilize the aggregate. Adding NaCl to an acid porphyrin solution is a useful tool to increase the aggregate formation rate, moreover the presence of salt is useful to observe

aggregates at higher pH (around pH=3). Moreover a huge contribution in the aggregate kinetic is played by anion nature, the growth rate is slow down in the order H_2SO_4 > HCl > HBr > HNO_3 > $HClO_4$.[75]

The reagents addition order in a H_2TPPS solution plays a pivotal role in the kinetic of the aggregate, adding the porphyrin before or after respect to the salt can accelerate or slow the growth of the final product. In particular adding the porphyrin before respect to the slat can avoid the aggregate formation if the porphyrin concentration is below 2 μM, at higher porphyrin concentration, the kinetic is very slow, it can take even weeks.

Aggregate seeds can undergo towards two different routs *i)* once formed without any stabilization from the environment (no salt in the solution) they disaggregate because of the repulsion among the positive charges in the porphyrin core, *ii)* in the presence of shielding charges in the solution small aggregates are stable an they can catalyse aggregate growth.

Porphyrin aggregate seeds can be formed at neutral pH if the stock solution of porphyrin has a high concentration, in order to avoid small aggregates in the stock solutions the amount of porphyrin must be between 0.15 and 0.2 mM.

Despite the achiral origin of the porphyrin H_2TPPS its J aggregates are chiral. Studies on this phenomenon are of considerable importance to shield light on symmetry-breaking mechanism; the spectral properties and the tendency of H_2TPPS to self assemble into chiral supramolecular structure both in the presence and not of a chiral templating agent are useful tools able to understand the mechanism of self assembly in a chiral fashion.

J aggregates CD spectra show positive or negative coupling related to P or M helices randomically (see figure 28).

There are different explanations regarding the spontaneous chirality of the J aggregates: [76,77] *i)* they aren't chiral but can became chiral due to the presence of picomolar traces of chiral pollutants, that can act as template and can induce a phenomena of chiral amplification; *ii)* they are intrinsically chiral and their distribution 1:1 obey to the statistical breaking of the parity rule; *iii)* they are intrinsically chiral and trace of contaminants move the equilibrium of the racemate to one of the two enantiomers.

The last two hypotheses seems to be the more plausible, because when ultrapure water is used to prepare aggregates solutions just a little signal is observed in the porphyrin absorption range.

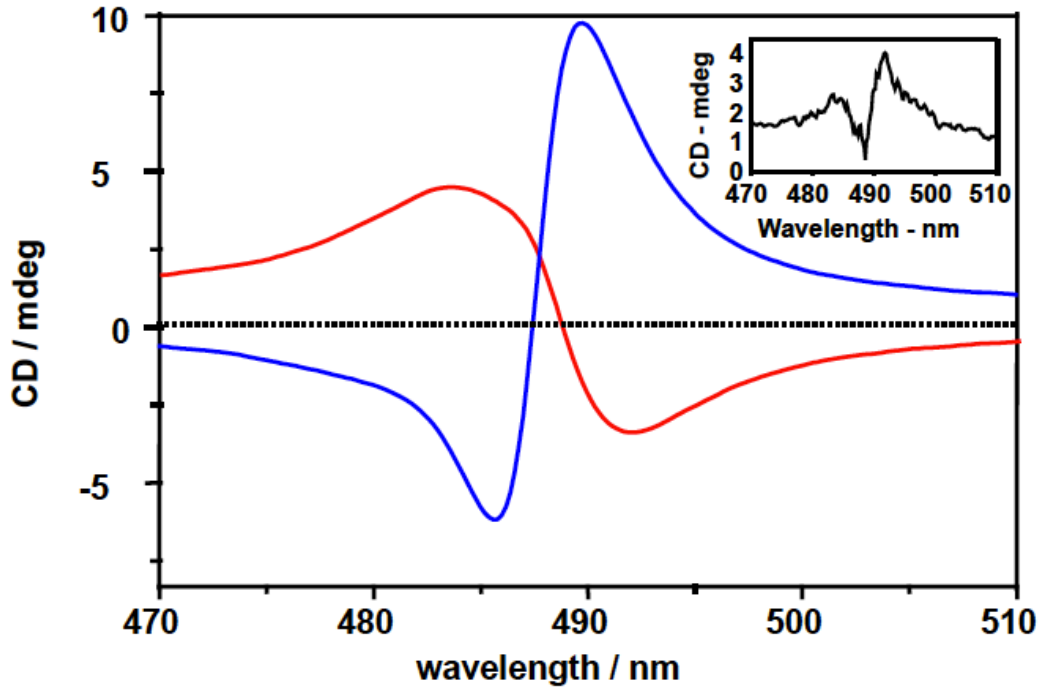

Figure 28: CD spectra of $H_4TPPS_4^{2-}$ aggregates, M helix (black curve) and P helix (red curve).

Understanding the driving force behind the aggregate formation is an open issue, as well as the orientation and packing between the single molecules, a deep knowledge is useful for controlling and fine-tuning the photophysical properties of the aggregates, also it has a lot of consequence in the design of new nanomaterials and in the knowledge of biological systems self-assembly.[78]

2.2 Effect of preorganization in porphyrin aggregation and chirality transfer

The aggregation pathway of the porphyrin H_2TPPS can be affected by the presence of even low amount of the metal Zn. It was demonstrate that neutral porphyrin stock solutions are able to extract Zn from vials; the metal ions are present because of the use of zinc oxide in glass fabrication. The presence of traces of the metalated porphyrin can slow the kinetic formation of the J-aggregates.[79]

The demetalation of the zinc tetra-anionic meso -5,10,15,20-tetrakis-(4-sulfonatophenyl) (ZnTPPS) (Figure 32) and the role of poly electrolytes in the pathway was studied in order to shield light in the self assembly process of the porphyrins.[80]

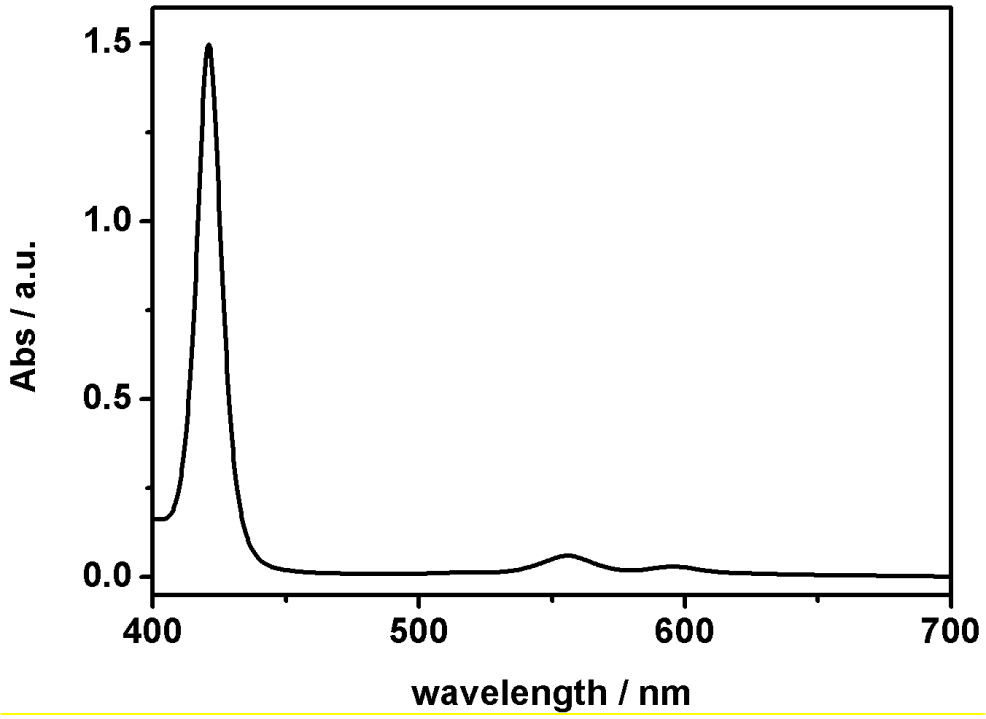

Figure 29: Absorption spectrum of a ZnTPPS solution at neutral pH

Metalloporphyrins are able to loose the central metal in different experimental conditions, depending on the metal oxidation state and size as well as the coordination and degree of covalent bonding.[81]

A 2 μM ZnTPPS solution was prepared in water at different pHs (respectively 7, 4.5, 3 and 1.5) in order to evaluate the demetalation kinetic, ZnTPPS shows a Soret band with a maximum at 421 nm (Figure 30), the reduction at the maximum absorption wavelength of the metalated

porphyrin was monitored for 7 hours, together with the increasing in absorbance of the protonated at 434 nm, (Figure 31).

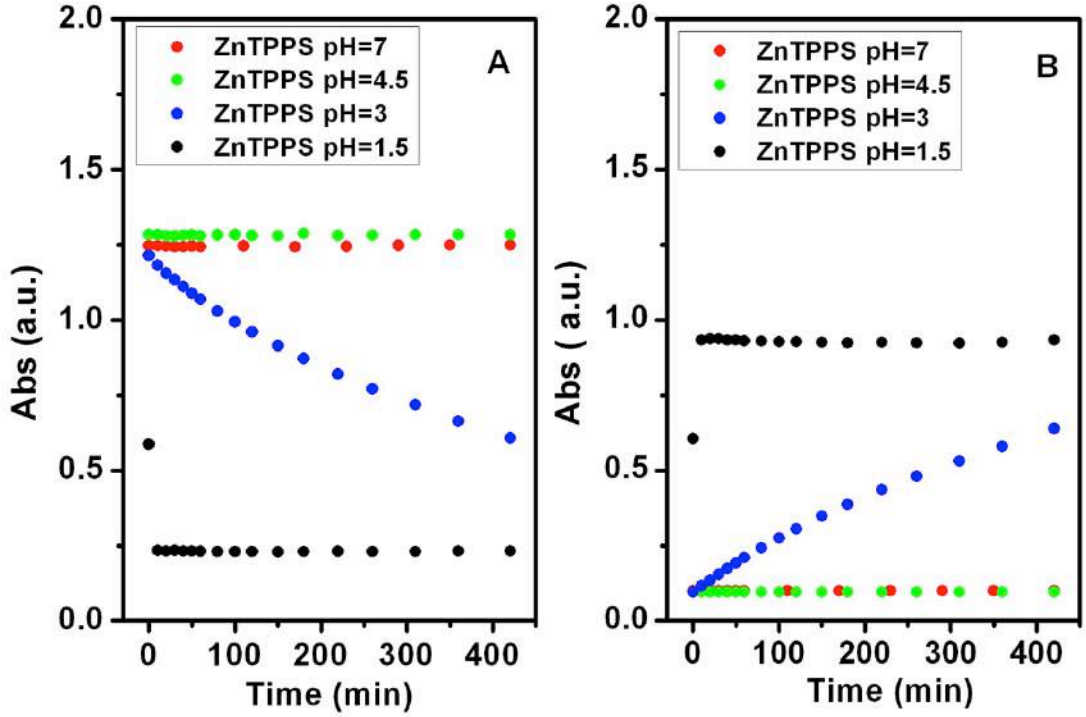

Figure 31: Absorption variation at 421 nm vs. time of ZnTPPS solution at pH 7 (red circles), pH 4.5 (green circles), pH 3 (blue circles) and pH 1.5 (black circles). (b) Absorption variation at 434 nm vs. Time of ZnTPPS solution at pH 7 (red circles), pH 4.5 (green circles), pH 3 (blue circles) and pH 1.5 (black circles).

The protonation of the porphyrin core starts at pH lower than 4.5, this is the pK_a value relative to the two nitrogen of the free base porphyrin, the demetalation process became quick at lower pH values; as showed in figure 31a at pH = 1.5 the absorbance value is almost half respect to the expected value at time zero, demonstrating that the protonation occur immediately.

The porphyrin concentration is under the minimum value that allows aggregate formation; just increasing the ionic strength in solution should help to observe the aggregate growth.[69, 82]

Electrostatic allow porphyrins to interact with polymeric chain having opposite charge. [83,84] It was reported that the anionic porphyrin H_2TPPS is able to interact with poly-L-lysine (PLL) (figure 32), the presence of the polypeptide in solution promote porphyrin binding ad self-aggregation.[83] Poly-D-glutamate (PDG) (figure 32) on the other hand is negatively charged, even this polyelectrolyte was used to control the aggregation of porphyrins in solution.[84]

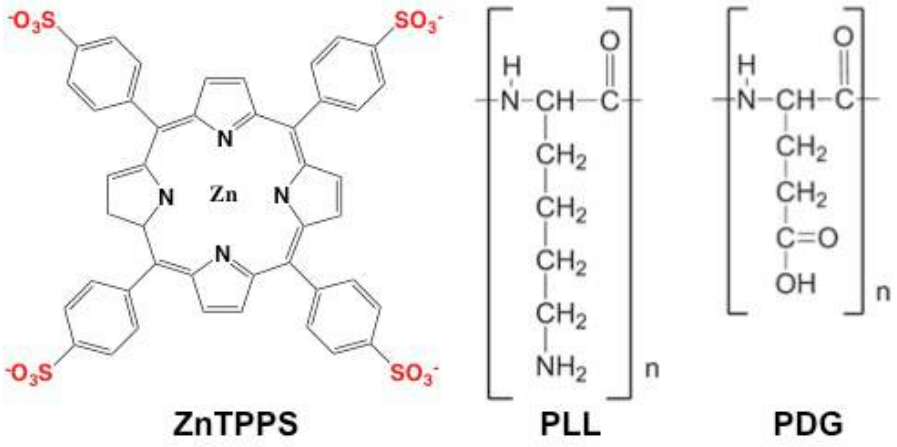

Figure 32: Molecular structures of ZnTPPS, Poly-L-Lysine and Poly-D-Glutamate.

The demetalation process of the ZnTPPS was monitored in the presence of the titled polyelectrolyte (50 μM) to evaluate if they have any effect on the final specie.

PDG is an anionic polyelectrolyte; its pKa value is 4.9 meaning that at pH higher than the pKa it is negatively charged. Of course this inhibits any interaction between the porphyrin and the PDG at pH higher than the pKa. Lowering the pH under 4.9 most of the negative charges are lost from the polymeric chain leading to a possible interaction with the Zn porphyrin.

However, spectroscopic behaviour of ZnTPPS in the presence of PDG is almost the same of that of bare ZnTPPS, ranging from neutral to strong acidic conditions. Figure 33 points to the negligible role of PDG in influencing ZnTPPS demetalation; a more careful analysis of the UV-Vis spectra of the ZnTPPS in the presence and not of PDG reveals an initial inhibition of the metalated porphyrin protonation at pH=1.5 at time zero (see below).

A more pronounced effect on the delay, on protonation of porphyrin, can be observed after the porphyrin interaction with PLL, the polypeptide chain is protonated even at pH 7, meaning that it is able to interact with the porphyrin even at higher pHs (Figure 34).

It was previously observed that ZnTPPS Soret band broadening and blue shift at 414 nm (attributed to formation of dimers in a face to face arrangement) associated to a significant hypochromic effect were due to interaction with PLL.[83]

The comparison at time zero of the solutions prepared at pH 1.5, figure 35, shows that the ratio between the two maxima at 434 an 421 nm is different in the ZnTPPS and ZnTPPS-PDG systems, while only one absorption band can be observed in the ZnTPPS-PLL solution. This band is slightly shifted at 424 nm and confirms the deposition of the anionic porphyrin on the PLL.

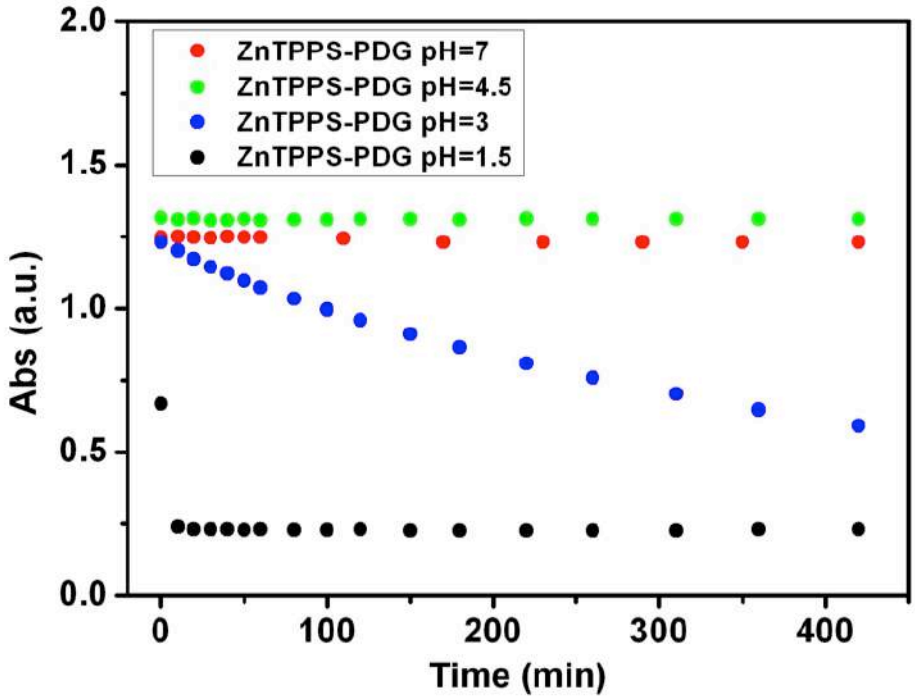

FIGURE 33: Absorption variation at 421 nm vs. time of ZnTPPS-PDG solution at pH 7 (red circles), pH 4.5 (green circles), pH 3 (blue circles) and pH 1.5 (black circles).

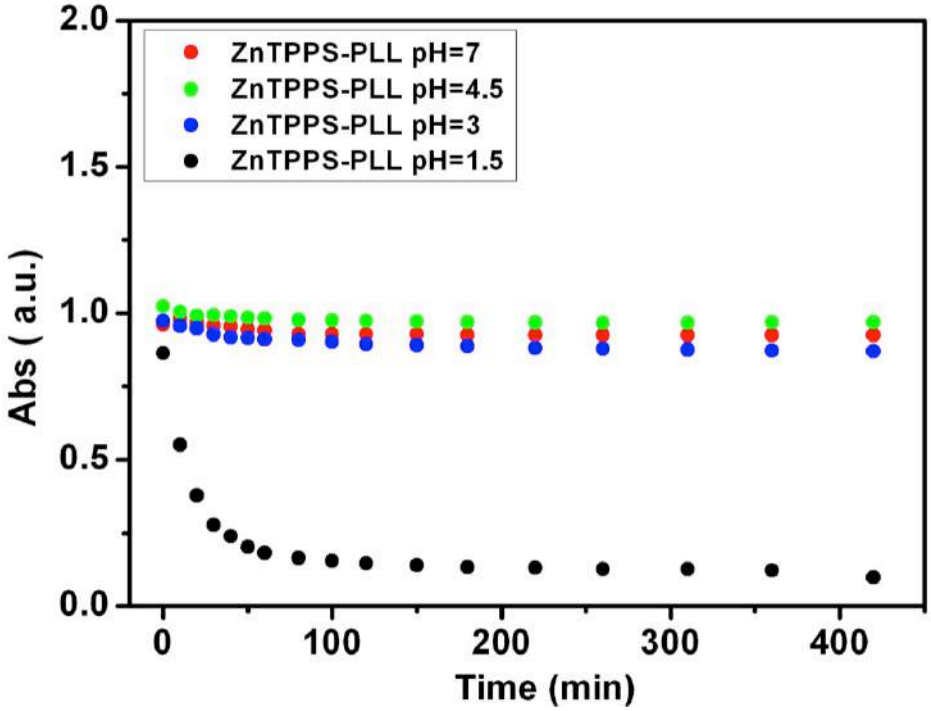

Figure 34: Absorption variation at 424 nm vs. time of ZnTPPS-PLL solution at pH 7 (red circles), pH 4.5 (green circles), pH 3 (blue circles) and pH 1.5 (black circles).

The capability of PLL to bind the porphyrin and delay its protonation affect the pathway followed by the macrocycle. PLL trap the protons, ZnTPPS can bind the positive chain in its free binding sites, and the lower proton availability in solution maintains the metal inside the porphyrin core. At pH= 1.5, porphyrins are able to protonate the core and the presence of the polyelectrolyte act as a catalyser for the J aggregate formation (see figure 36).

On the other hand, at pH 1.5 the bare porphyrin ZnTPPS and that in the presence PDG doesn't lead to J aggregate.

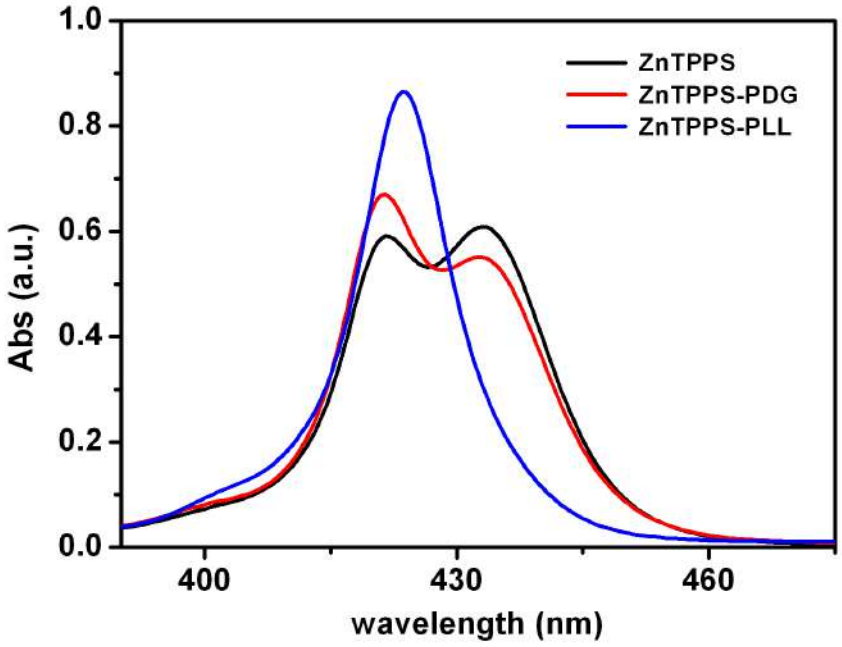

Figure 35: Absorption spectra of ZnTPPS (black curve), ZnTPPS-PDG solution (red curve) and ZnTPPS-PLL solution (blue curve) at pH 1.5 as prepared.

To have a strict control of the demetalation and aggregation kinetic of the ZnTPPS a study on the role of the length of the polylisine chain was performed.[85]

Several experiments using PLLs with different polymerization degrees, ranging from dp 36 to 2060 was performed. PLL (50 μM) and ZnTPPS (2μM) were incubated for 15 minutes at neutral pH to favour a spatial pre-organization.

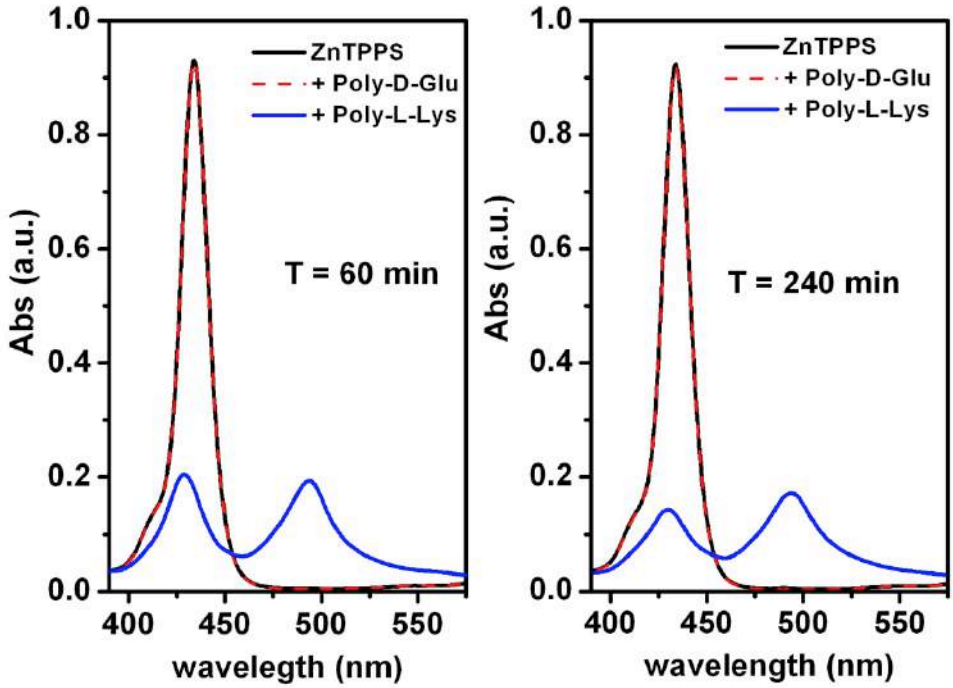

Figure 36: Absorption spectra of ZnTPPS (black curve), ZnTPPS-PDG solution (dashed red curve) and ZnTPPS-PLL solution (blue curve) at pH 1.5 after 1h (left) and 4h (right).

The UV-Vis characterization of the system composed by the ZnTPPS-PLL clearly indicates the presence of different species when the 2 μM porphyrin was added to the 50 μM polyelectrolyte solutions at neutral pH (figure 37), one specie are the porphyrin dimers with absorbance at 414 nm, the other are porphyrin hybrids on the PLL chain.

In the presence of short PLL chain the formation of ZnTPPS dimers is predominant, the presence of the component at 414 nm is evidenced by the derivative reported in figure 37 inset. The reason of the dimers formations lies in the number of binding sites, in short PLL chain it is limited, and thus each dimer taking up a significant space hinders the formation of other dimer.

On the contrary, adding ZnTPPS in the presence of long PLL, the combination of electrostatic and solvophobic interactions (as observed in figure 7) suggests that once a single porphyrin binds to PLL the affinity of other sites becomes higher as in a positive cooperative binding. [86]

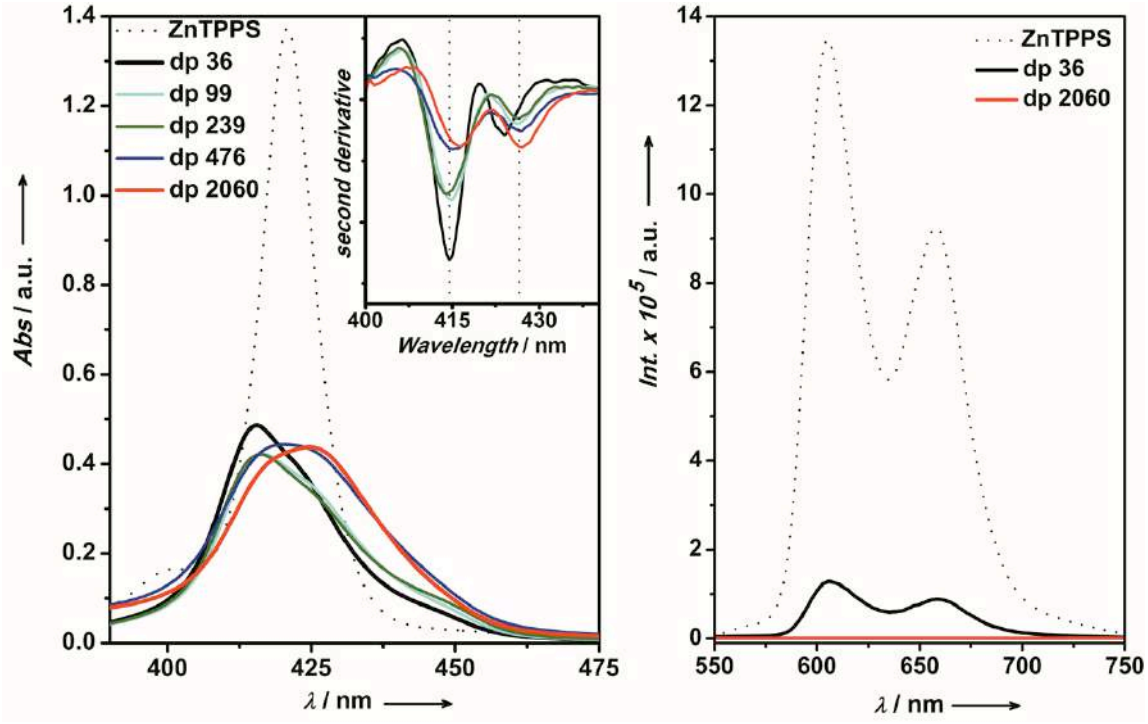

Figure 37: UV-Vis (inset: second derivative) and fluorescence (λex = 421 nm) spectra at neutral pH of ZnTPPS (2μM) alone (dotted curves) and of various PLL/ZnTPPS (50μM/2μM) complexes (PLL dp 36 black curves, dp 99 cyan curve, dp 239 green curve, dp 476 blue curve and dp 2060 red curves).

The stronger affinity of porphyrin respect to the longer PLL is confirmed in the fluorescence spectrum (figure 37 right panel), where a complete quenching of the fluorescence can be observed.

After a15 minutes incubation time the pH has been lowered from 7 to 1.5 using HCl (figure 38); the comparison of absorption band at 434 nm, immediately after the acid addition, indicate the protonation of the porphyrin core. The UV-Vis spectra registered after 10 minutes show a band around 490 nm, evidencing that even if the porphyrin concentration is low and there is no ionic strength, the role of the polyelectrolyte is to induce the porphyrin aggregation as already observed. The band intensity at 490 nm increases during time as the length of the polypeptide chain increase (figure 39).

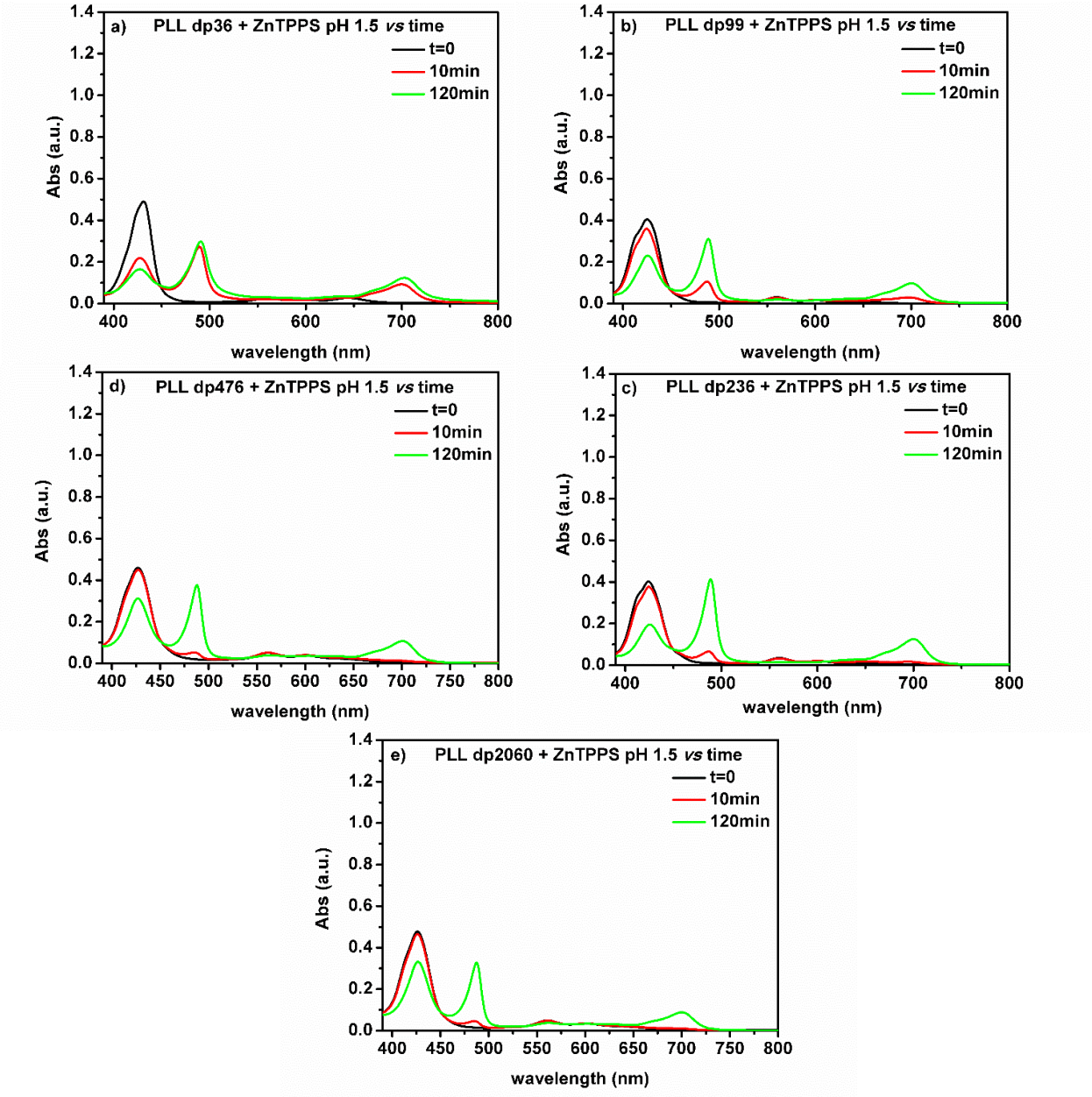

Figure 38: Absorbance variations of 2µM ZnTPPS solutions at pH 1.5 (t = 0 - 10 min – 120 min) in presence of PLL a) dp 36 b) dp 99 c) dp 239 d) 476 e) dp 2060.

The chain length has effects on the kinetics of the aggregation process, as evidenced in the calculation of the rate constant obtained plotting the band intensity trend at 490 nm upon increasing time (figure 40).

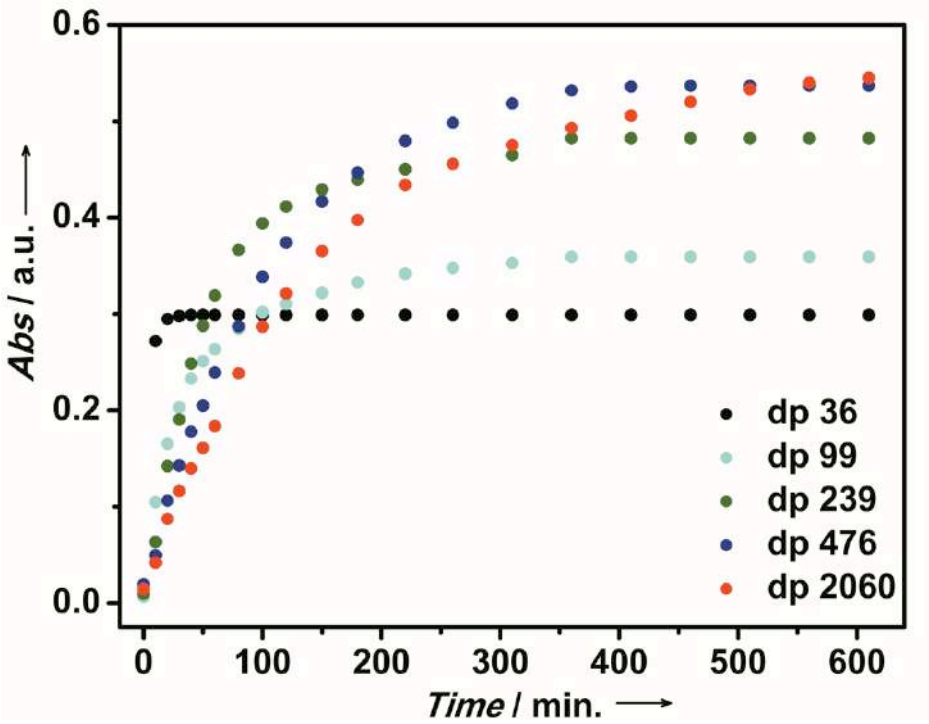

FIGURE 39: Absorption values of band at λ=490 nm of ZnTPPS/PLL solutions at pH=1.5 (PLL dp 36 black dots, dp 99 cyan dots, dp 239 green dots, dp 476 blue dots and dp 2060 red dots).

In the presence of the dp = 36 PLL (black dots), the two processes demetalation of ZnTPPS and protonation of H_2TPPS occur very quickly; the instantaneous formation of J-aggregates (K_{dp36}= 5.55 x 10-3 s^{-1}) is spectroscopically revealed by the comparison of band at λ=490 nm. Noteworthy, the intensity of the H_4TPPS^{2-} aggregate band remains constant as soon as aggregate species are formed, demonstrating the absence of any structural evolution. On the contrary, the presence of longer PLLs chains from dp = 99 (cyan dots) to dp = 2060 (red dots), leads to a slower formation of J aggregates (K_{dp99} = 3.55 x 10-3 s^{-1}; K_{dp239} = 2.59 x 10-3 s^{-1}; K^{dp476}= 1.44 x 10-3 s^{-1}; K_{dp2060} = 1.20 x 10-3 $^{s-1}$), resulting in a more intense band at λ ≈ 490 nm whose intensity reaches a maximum value over a longer time frame. These data provide an interesting insight on the mechanism of ZnTPPS/H_4TPPS^{2-} aggregation onto PLL confirming the pivotal role of PLL in the demetalation aggregation process of the porphyrin.

It has been extensively demonstrate that the PLL is able to transfer chirality on the J-aggregate of the protonated form of the H_2TPPS, we performed CD measurements on the above reported systems, the spectra confirm that we are under the presence of a different organization pathway of the porphyrin aggregates depending on the PLL length.

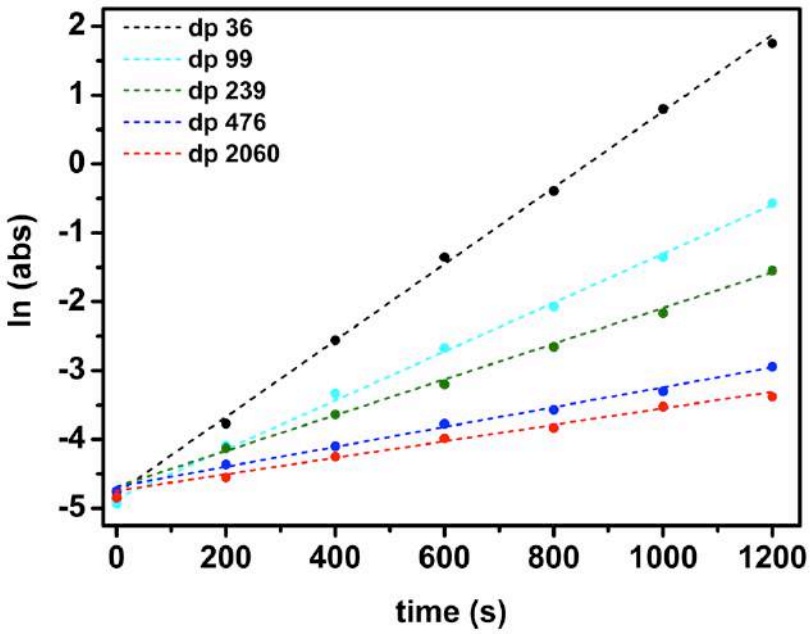

Figure 40:. ln abs (λ = 490nm) vs. time of ZnTPPS/PLL solutions at pH = 1.5 in a kinetics experiment (PLL dp 36 black dots, dp 99 cyan dots, dp 239 green dots, dp 476 blue dots, dp 2060 red dots); [ZnTPPS] = 2μM, [PLL] = 50μM, 25°C. Here, the slope of the best linear fit of each curve (dashed lines) defines the first-order rate constant: K_{dp36}= 5.55 x 10^{-3} s^{-1}, K_{dp99}= 3.55 x 10^{-3} s^{-1}, K_{dp239}= 2.59 x 10^{-3} s^{-1}, K_{dp476}= 1.44 x 10^{-3} s^{-1}, K_{dp36}= 1.20 x 10^{-3} s^{-1}.

The addition of the ZnTPPS to a neutral solution of PLL lead to the appearance of a CD signal in the absorption region of the porphyrin (figure 41), both in the case of the PLL dp36 and PLL dp2060 confirming the strong communication between the ZnTPPS and the PLL. The observed CD signals at pH 7 drastically change after the HCl addition to reach pH 1.5 (figure 42); the modification of the signal does not depend on the chain length.

J aggregate formation is confirmed by CD measurements. The CD signal observed in the case of the system PLL dp 36 plus ZnTPPS doesn't change during time; while in the case of the aggregate formed in the solution with the PLL dp 2060 there is an increasing intensity of the CD signal during time, confirming that the aggregate undergoes a structural evolution when the porphyrin interact with the longer chain.

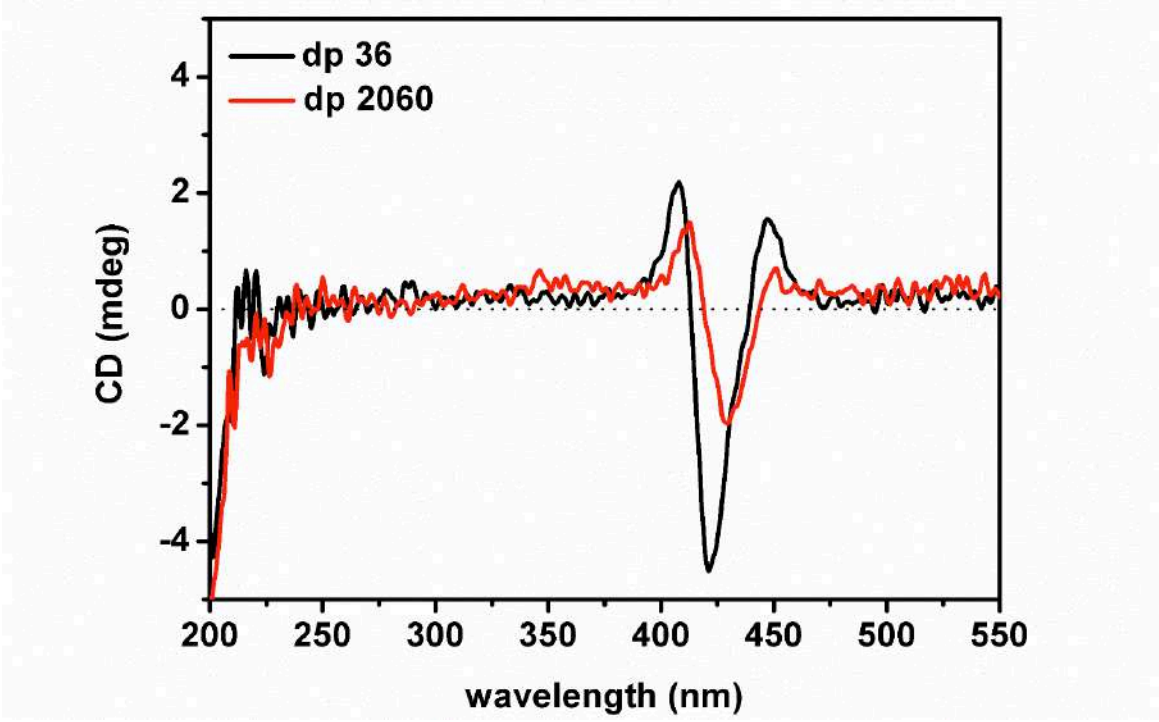

Figure 41: CD spectra of ZnTPPS/PLL solutions (dp = 36 black curves and dp = 2060 red curves) at pH 7; [ZnTPPS] = 2μ M, [PLL] = 50μ M, 25 °C.

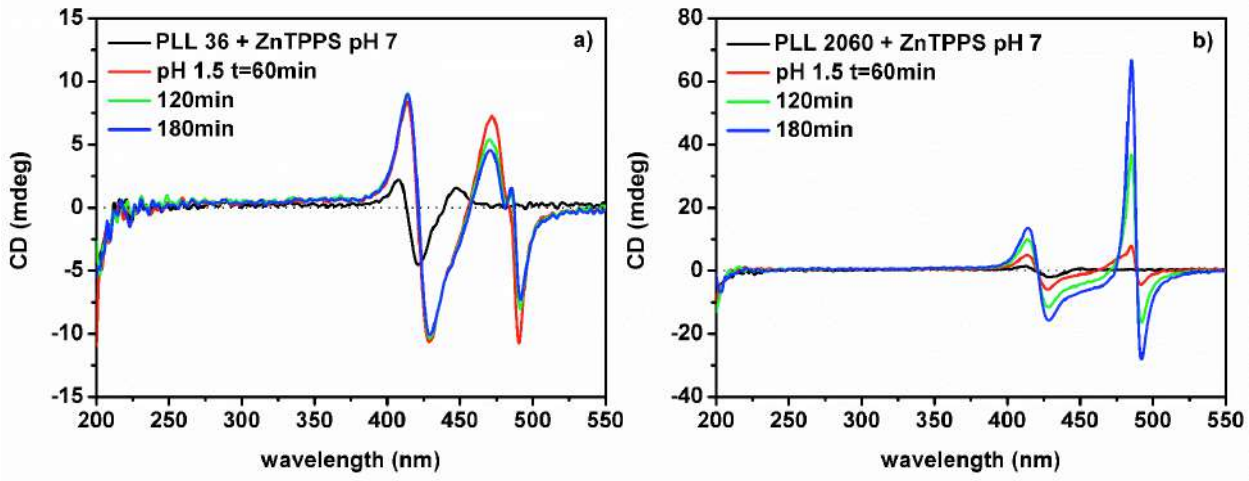

Figure 42: CD spectra of ZnTPPS in presence of PLL a) dp 36 b) dp 2060 vs. time at pH 1.5; [ZnTPPS] = 2μ M, [PLL] = 50μ M, 25°C.

In the figure 43 the comparison between the UV-Vis and CD spectra of the aggregates formed on PLL dp 36 and dp 2060 evidence the deep spectroscopic differences among the aggregates, confirming the better ability of long PLL (dp 2060) to act as chiral template and to induce chirality into porphyrins with which a strong electronic communication is established. Further confirmation can be given by the resonance light scattering spectra showed in figure 44.

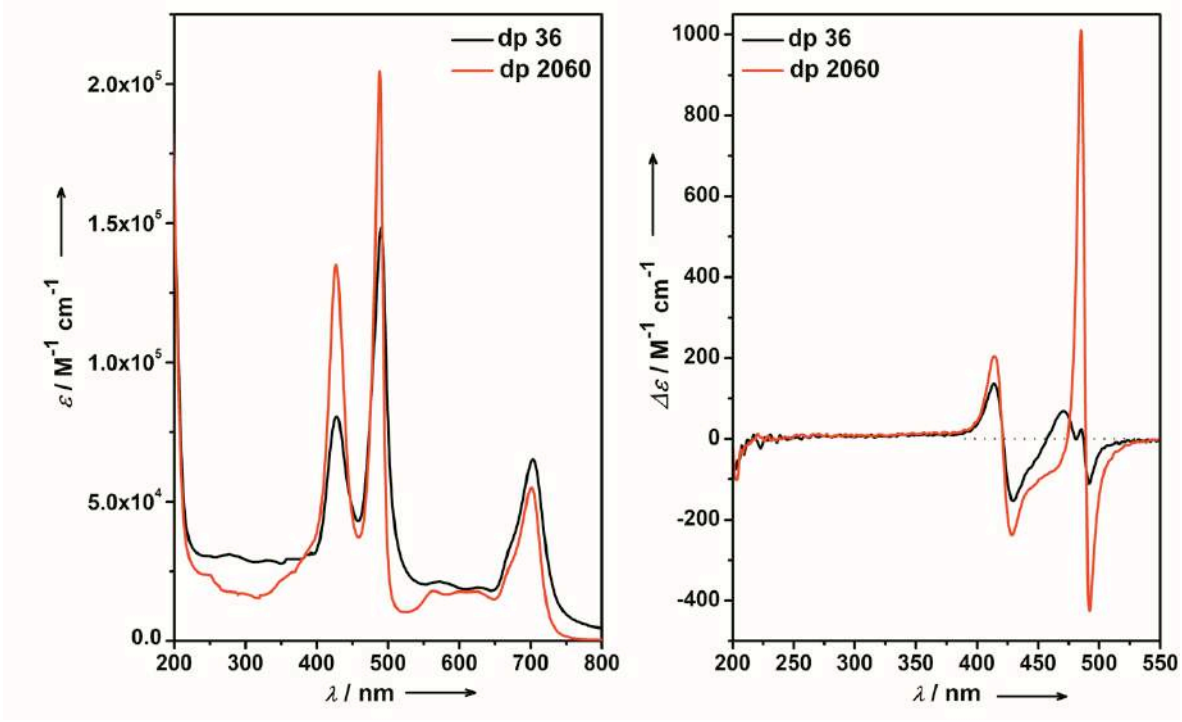

Figure 43: UV-Vis and CD spectra of ZnTPPS/PLL solutions (dp = 36 black curves and dp = 2060 red curves) at pH 1.5 after 3 h.

The resonance light scattering RLS, is a phenomena that occurs when there is a strong electronic coupling between adjacent cromophores in aggregates having a precise size and geometry whose monomers posses high molar extinction coefficient.

The RLS spectrum of a non aggregate porphyirin solution shows no signal (figure 44 blue curve), the signal became more sharp and intense when higher is the communication of the cromphores in the aggregate, the comparison between the aggregates obtained with PLL dp36 and PLL dp 2060 shows different RLS signal, underlining that the number and arrangements of porphyrins in the two aggregate is deeply different starting from different polyelectrolyte chains length.

To explain the experimental evidences, the group of professor Raudino from University of Catania performed Spinodal Decomposition (SD) Model. SD is the passage from a homogeneous solution to a patterned one, in thermodynamically unstable solutions. The titled system is well described by this theoretical model.

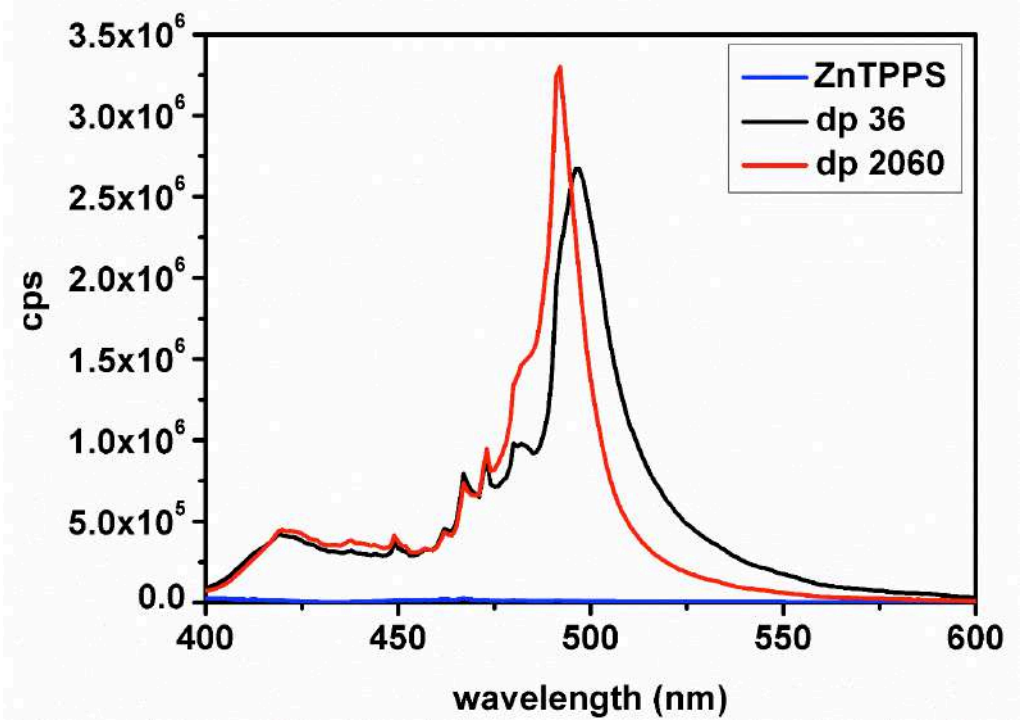

Figure 44: RLS spectra of bare ZnTPPS (blue curve) and in presence of PLL dp 36 (black curve) or PLL dp 2060 (red curve) at pH 1.5 after 3h; [ZnTPPS] = 2 µ M, [PLL] = 50 µ M, 25°C.

2.3 Chiral recognition of L and D amino acids by porphyrin aggregates

The formation of the J-aggregates is a non-covalent polymerization process, it follows a critical nucleation step that drives the aggregation.[87] If the polymerization occur in a chiral network or in the presence of a chiral templating, homochiral complexes can be achieved.

Using polymeric chain as templating agent is a functional approach to induce chirality at supramolecular level; the induction of chirality in this case has a conformational origin.

Moving from long chain to smaller molecule to induce chirality is not easy, monomeric molecules cannot transfer chirality onto the achiral porphyrin aggregates, but if the chiral moieties are able to aggregate in a chiral fashion, can transfer its handedness at supramolecular level.

Single amino acids have been employed by researchers to transfer chirality to porphyrin's homo and hetero-aggregates using either covalent [88-95] or non-covalent approaches.[77,96,97] However, minimal research reports on the chiral properties of the J-aggregates of H4 TPPS in the presence of amino acids.[98-100]

It was demonstrated from Purrello et al. that phenylalanine is able to aggregate in water solution at concentration higher than1 mM, the amino acid aggregate can induce chirality in hetero aggregate of a positively charged CuT4 and the negatively charged H_2TPPS, the obtained porphyrin aggregate are also able to store the information, even if the amino acid is removed from the solution using ultrafiltration.[77]

We studied the capability of the two enantiomers of four amino acids to transfer chirality at supramolecular level in homochiral H_4TPPS aggregates. The four chosen amino acids are Arginine (Arg), Lysine (Lys), Hystidine (His) and Phenylalanine (Phe) (Scheme 4).

Depending on the characteristic of their side chain, amino acids can be classified as non-polar, polar, acid and basic. We chose to use the three basic amino acids Arg, Lys and His and the non-polar Phe to induce chirality in the aggregate of the protonated form of the anionic porphyrin H_2TPPS.

The aggregation of the H_2TPPS is a hierarchically controlled process; the kinetic strictly depends on the addition order of the reagents in solution. We decided to use two protocols to study the chiral induction from amino acids to porphyrin homoaggregates.

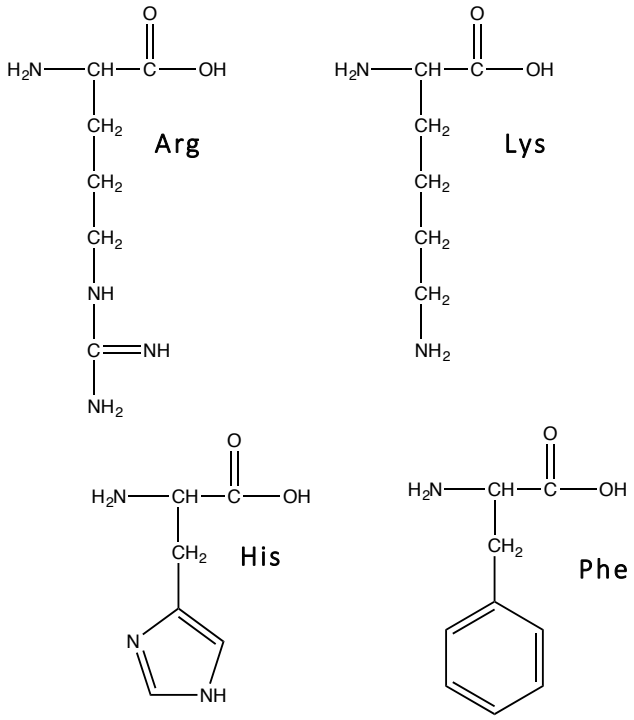

Scheme 4: molecular structure of the amino acids

The so-called *acid first* protocol consists in adding porphyrin (6 μM) as last reagent in solution (0.3 M NaCl pH=2.5), if there are no chiral inducer the aggregate CD signal is the one showed in figure 45.

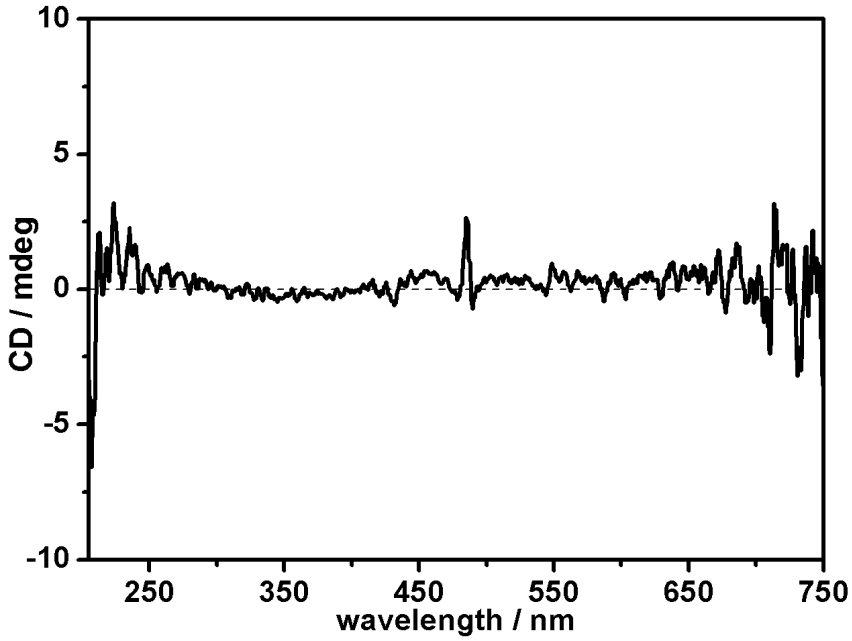

Figure 45: CD spectrum of a solution of J-aggregate obtained by adding 6 μM porphyrin to NaCl 0.3M at pH=2.5

The *acid first* protocol was performed adding 6 μM H_2TPPS to an acidic solution of NaCl containing 1mM amino acid. After one night the CD spectra of the four amino acids solutions were recorded. An induced CD signal (iCD) in the absorption region of the porphyrin aggregate was observed in Arg and Lys solutions, in the same conditions His and Phe were not able to transfer the chiral information to the supramolecular complex (figure 46).

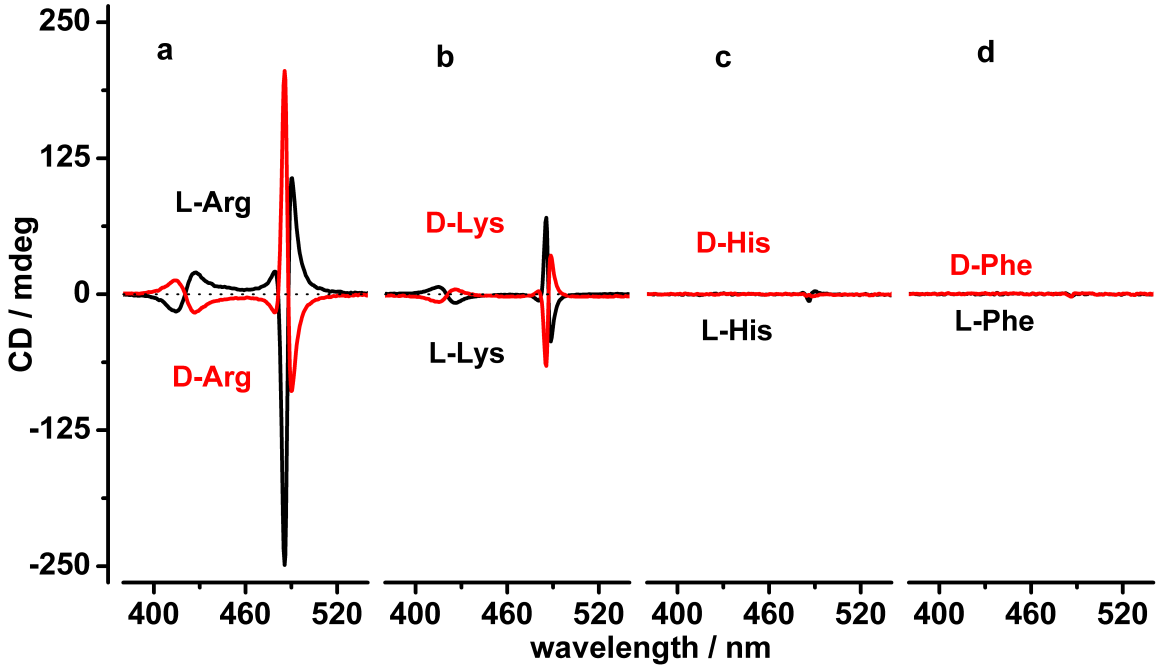

Figure 46: The CD spectra of the J-aggregates obtained with the protocol "acid first" template on: (a) 1 mM Arg; (b) 1 mM Lys; (c) 1 mM His; and, (d) 1 mM Phe (black curves represent the L- amino acids and red curves represent the D- amino acids).

L and D-Arg are able to transfer chirality in H_4TPPS aggregates, the observed iCD are mirror images the one of the other; the same results was obtained for aggregates growth in the presence of the two enantiomers of Lys. The iCD intensities of the aggregates obtained with Arg and Lys are different; moreover the two L enantiomers (as well as the two D enantiomers) give opposite Cotton effects.

Intensity and shape of the J-aggregates iCD signal strongly depend on the type and configuration of the amino acids used as inducer, therefore, indicate that the side groups (in terms of size and charge) affect the formation of the supramolecular chiral assembly process.

The lack of CD signal in the absorption range of the porphyrin aggregate growth in the solutions containing His and Phe suggest us to investigate the possible reasons for this ICD absence.

The chirality induction from a non–covalent polymer to a supramolecular porphyrin aggregate is a complicated process; a fine control of the inducer dimension must be accomplished in order to allow the development of the wanted supramolecular structure. Amino acids clusters are ours non-covalent polymers; the monomer concentration in the final solution is an essential parameter for the control of their aggregation, the evaluation of this aspect is fundamental to shield light on the results showed above.

Following the procedure *acid first* we prepared amino acid solutions at concentration 0.5, 1, 2 and 4 mM, after the addition of the porphyrin we wait one night before the measure of the CD spectra (figure 47).

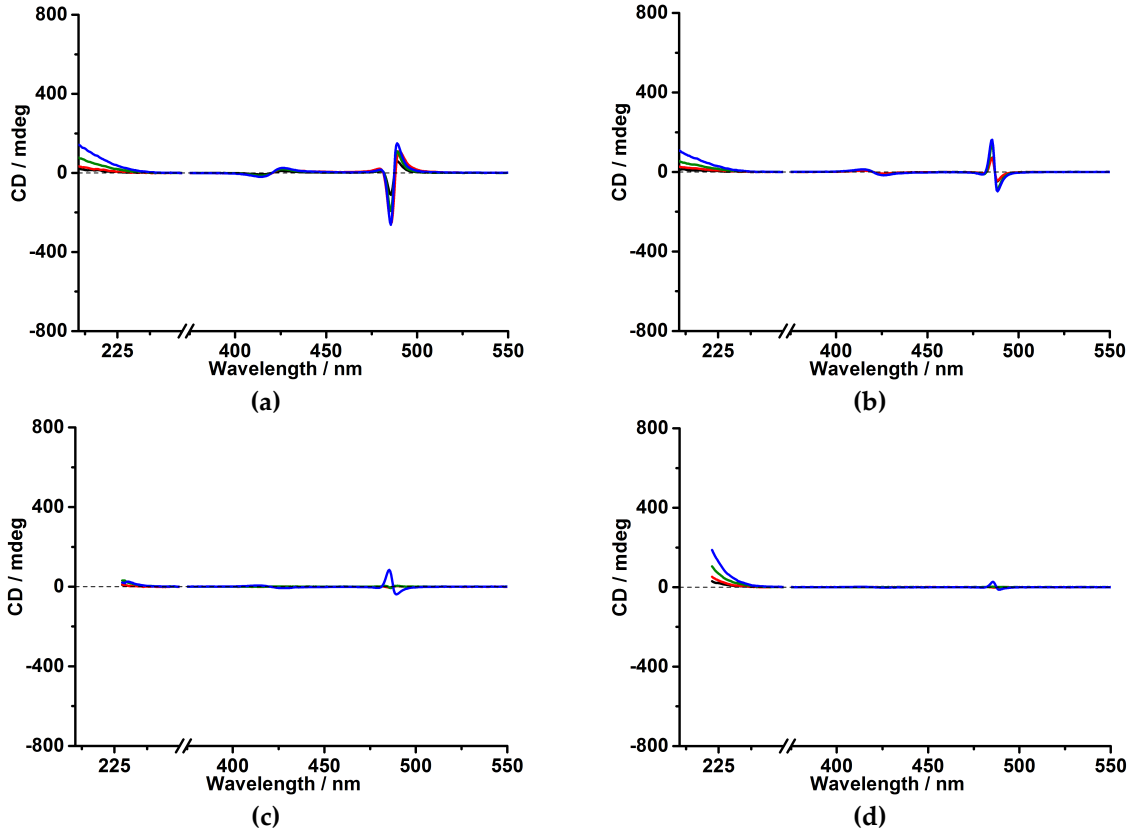

Figure 47: CD spectra of H_4TPPS J aggregates obtained using the protocol *acid first* at different amino acids concentrations (black curves 0.5mM, red curves 1mM, green curves 2mM and blue curves 4mM). a) L-Arg, b) L-Lys, c)L-His and d) L-Phe.

In figure 48 we plot the CD intensity at 489 nm vs the amino acid concentration to determine the minimum amount of amino acid required to induce chirality in H_4TPPS J-aggregates. The graph shows clearly that, using the *acid first* protocol, both Arg and Lys are able to induce chirality in J aggregates even at the lower concentration, also the iCD increase linearly with the concentration of the inducer, while the minimum concentration required for His and Phe is 4 mM, under this value no iCD was detected.

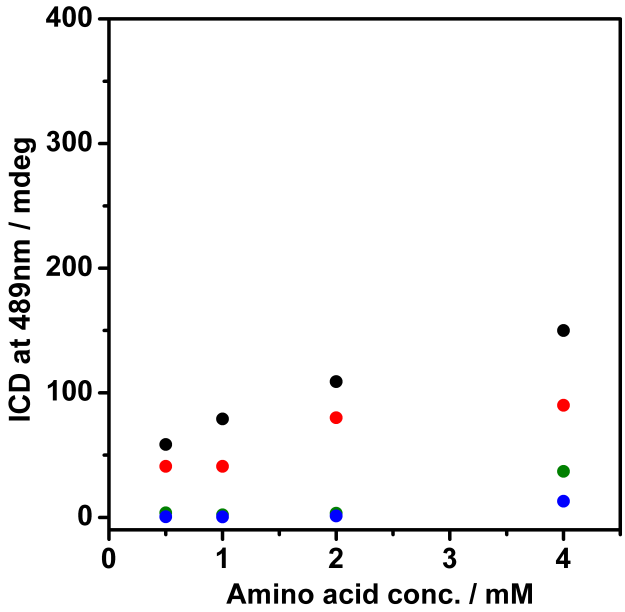

Figure 48: Intensity of the iCD at 489 nm (absolute values) versus the amino acid concentrations. Black dots represent Arg; red dots represent Lys; green dots represent His; and, blue dots represent Phe

Changing the kinetic pathway of the supramolecular complex formation, size and shape can vary; in the second procedure, called *acid last*, we give to porphyrin and amino acid time to interact at neutral pH (in the presence of 0.3 M NaCl), only after one night incubation we decrease the pH using HCl to reach pH 2.5.

The starting pH was 6.5, at this pH value more than the 50% of the side chains of basic amino acids are protonated and the porphyrin has four negative charges on its substituents. Despite of that no evidence of chiral induction in the Soret region can be observed even after one night.

Decreasing the pH from 6.5 to 2.5 leads to the formation of chiral H_4TPPS aggregate (figure 49) in all the four amino acids solutions; even if there was no evidence of interactions at

pH 6.5 the amino acids can transfer the chiral information to the protonated porphyrin aggregates.

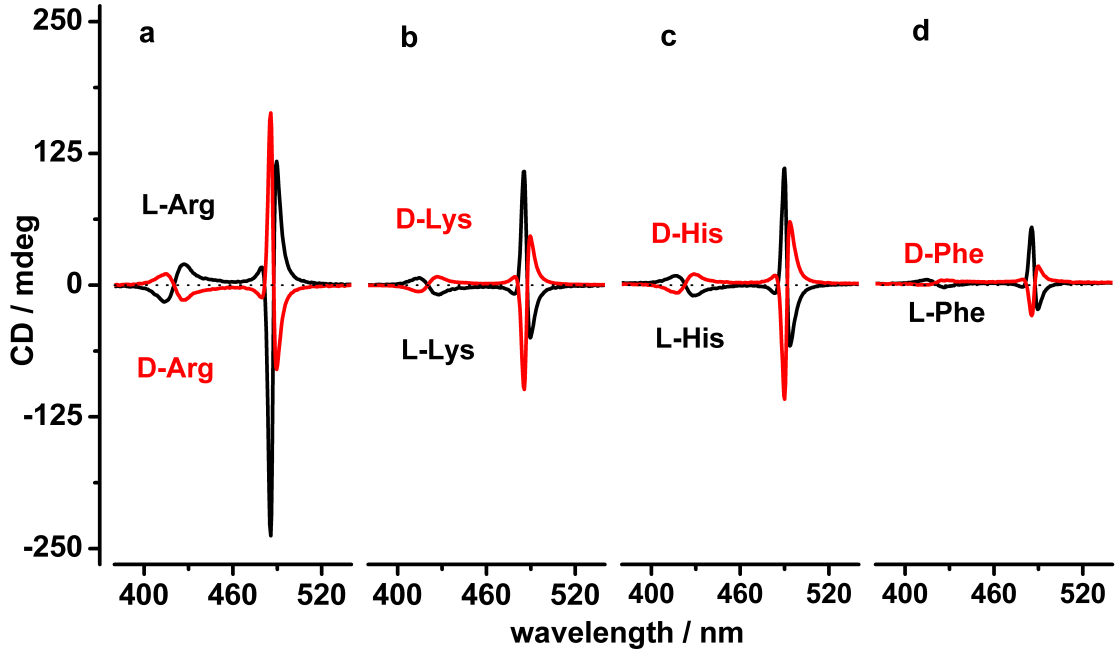

Figure 49: The CD spectra of J-aggregates obtained with the procedure "acid last" template on: (a) 1 mM Arg; (b) 1 mM Lys; (c) 1 mM His; and, (d) 1 mM Phe. Black curves represent L- amino acids and red curves represent D- amino acids.

Using the protocol *acid last* we are able to observe a iCD in Arg and Lys 1mM, but also in His and Phe solutions. This second approach seems to be more efficient. As observed previously the iCD intensities are different depending on the amino acid used as templating agent; L and D enantiomers give mirror image iCD and aggregates growth in L-Arg (D-Arg) solutions show opposite Cotton effect respect to supramolecular complexes growth in other L (D) enantiomers solutions.

We performed experiments using different amino acids concentrations from 0.5 to 4 mM in order to confirm that the minimum amino acid concentration to transfer chirality is lower using the *acid last* protocol (figure 50).

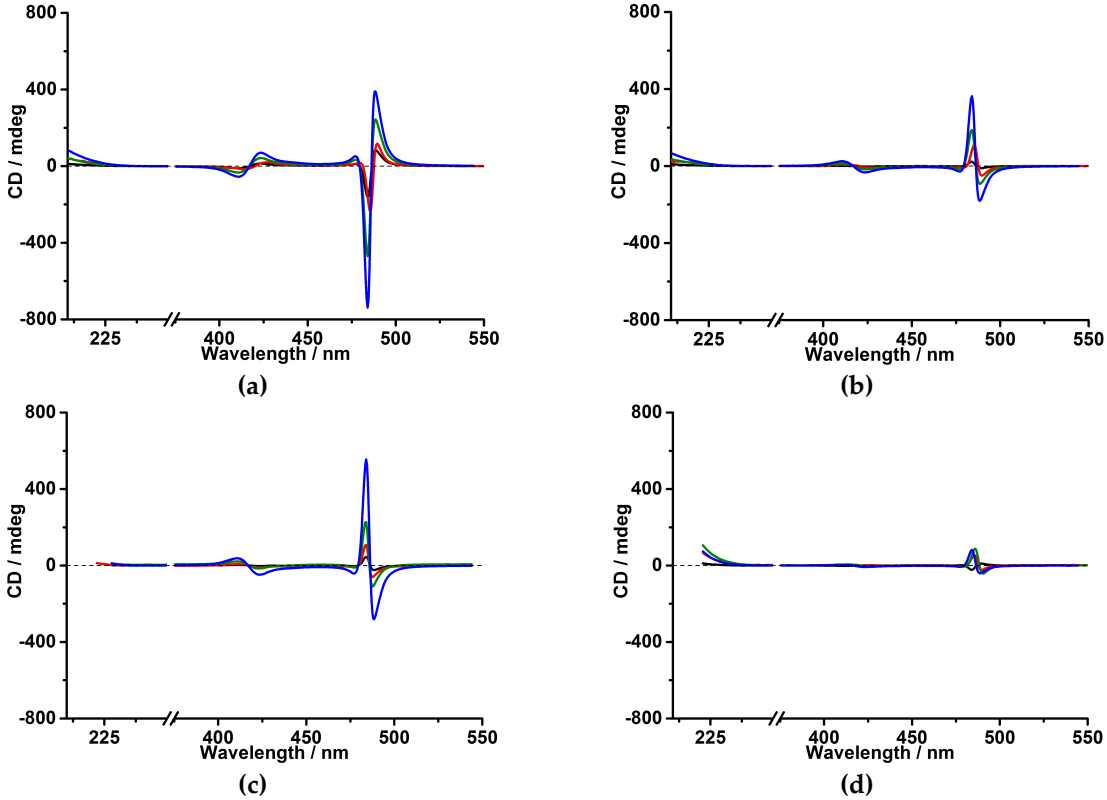

Figure 50: CD spectra of H_4TPPS J aggregates obtained using the protocol *acid last* at different amino acids concentrations. a) L-Arg, b) L-Lys, c) L-His and d) L-Phe. Black curves amino acids concentration 0.5mM, red curves amino acids concentration 1mM, green curves amino acids concentration 2mM and blue curves amino acids concentration 4mM.

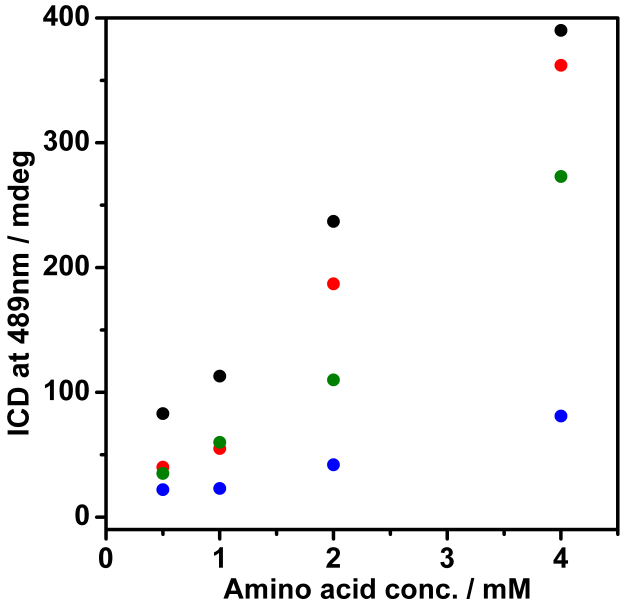

Figure 51: Intensity of the iCD at 489 nm (absolute value) versus the amino acid concentration. Black dots represent Arg; red dots represent Lys; green dots represent His; and, blue dots represent Phe.

The data reported in figure 51, confirm that the minimum concentration required for chiral induction in H_4TPPS aggregate using the *acid last* procedure is 0.5 mM for Arg and Lys and His. Phe is the only one amino acid not able to induce chirality at concentration lower than 1mM, however the minimum concentration limit results lower respect to the one observed using the protocol *acid first*.

Looking at the intensities of the iCD obtained using the two different procedures, what is extremely evident is that in the acid last protocol the resulting aggregates show a more intense iCD signal. We can speculate that the different intensity can be attributed to the different kinetic of the J-aggregate formation.

As reported from Ribò et al. [73] adding porphyrin as the last reagent, in the *acid first* procedure, influence the J-aggregate kinetic increasing the formation rate. The CD signal in the J aggregate absorption range reveals the strong interaction between the inducer and the achiral moieties; at pH 2.5 amino acids possess positive charges and the protonated form of the porphyrin still have two negative charges. The electrostatic interactions that occur between the amino acids and the porphyrin have a fundamental role in the supramolecular chiral induction process.

In the *acid last* procedure the J-aggregate kinetic is slower respect to that of the *acid first*, porphyrins have more time to arrange in a more ordered fashion around the amino acids, this organization is reflected in the more intense CD signal.

The comparison between UV-Vis, CD and RLS spectra of the aggregates obtained with the two different procedures give more details about the dissimilarities of the aggregates.

In figure 52 a) the CD spectra shows a more intense and narrow signal for the J-aggregate template on L-Lys 4mM using the protocol *acid last*, in the UV-Vis spectra the differences between the aggregates obtained with the two different procedures are not so big, while in the RLS spectra (fig 52 c)) a higher intensity is observed for the acid last J-aggregate, confirming the formation of ordered J-aggregates where the chromophores have a stronger electronic communication.

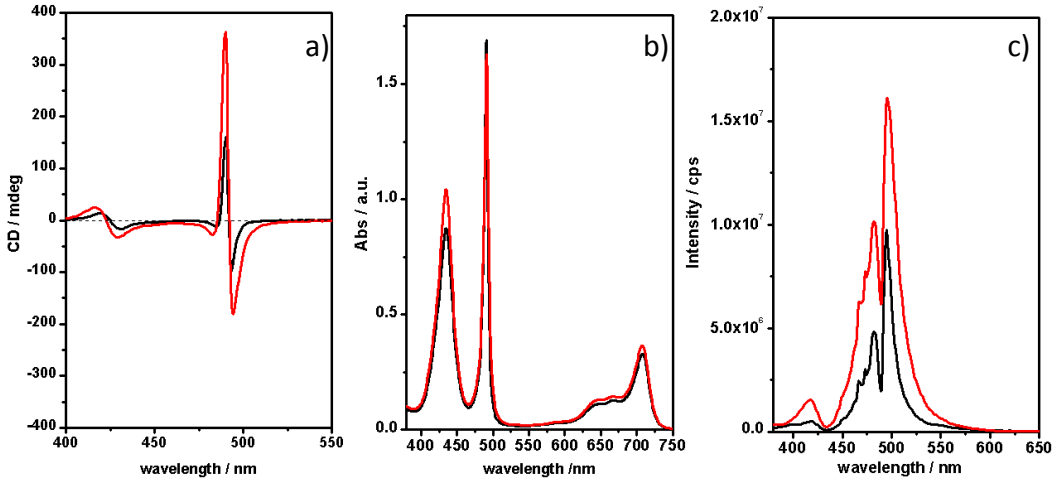

Figure 52: (a) CD spectra; (b) UV-Vis spectra; and, (c) RLS spectra of the solutions of the J-aggregates template on L-Lys 2 mM (black curves represent the "acid first" procedure, and red curves represent the "acid last" procedure).

We can explain the different interactions between the porphyrins complexes and amino acids looking at the iCD observed using the two procedures, and relating it to the isoelectric point of the chiral molecules reported in Table 1.

Amino acid		pK$_a$ α-CO_2H	pK$_a$ α–NH_3	pK$_a$ side chain	IEP
Arginine	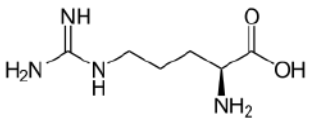	2.01	9.04	12.48	10.76
Lysine	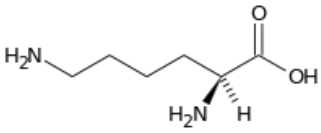	2.18	8.95	10.53	9.47
Histidine	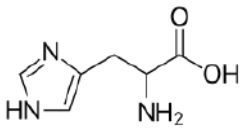	1.77	9.18	6.10	7.60
Phenilalanine	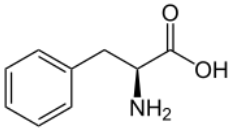	2.58	9.24	-	5.48

Table 1. pKa and IEP values of the amino acids.

As exhibited in table 1 and figure 53, Arg is the amino acid with the higher value of IEP and looking at the iCD intensities, it is also the chiral molecule that in the two used procedures, has transmitted the chiral information stronger than the others molecules. In figure 23 we reported all the intensities obtained for chiral induction at four different amino acid concentrations and using both the procedures, as is possible to observe, the lower ICD values are that of the aggregates template on Phe that is the amino acid with the lower IEP.

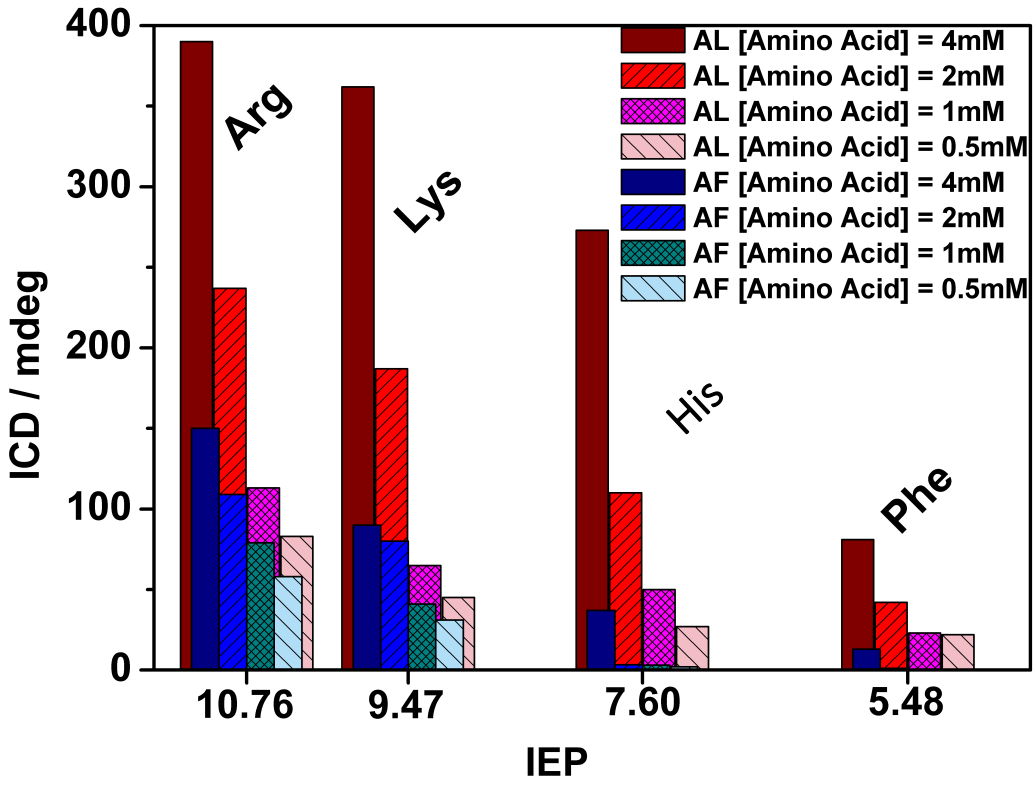

Figure 53: Induced CD signal at 489 nm of J Agg–amino acid complexes *vs* Isoelectric points (IEP). Each bar at the same IEP indicates different concentration of amino acid (wine and dark blue bars 4mM; red and blue bars 2mM; magenta and dark cyan bars 1 mM; pink and cyan bars 0.5mM). The two set of colours indicate the two procedures used: *acid last* (wine, red, magenta and pink bars) and *acid first* (dark blue, blue, dark cyan and cyan bars)

The final pH in both the protocols is equal to 2.5, meaning that the amount of positively charged side chain on the amino acid is higher for those amino acids with higher IEP, also the electrostatic interactions are the driving forces involved in the efficient chiral induction of J aggregate of H4TPPS.

In addition to electrostatic interaction the aggregate of the porphyrin H_4TPPS can be stabilized from other weak forces, hydrogen bonding interactions between NH and SO_3 groups

and, hydrophobic interactions between non-polar regions, i.e. those of the porphyrin ring and of the meso-aryl rings.

To prove if the chiral J-aggregate is stabilized by a contribution of all the titled interactions, we perform new experiments; adding an excess of the amino acid that was not used as chiral templating agent we tried to evaluate the time stability of the iCD.

The chirality transfer from amino acids to porphyrin homoaggregate is not a static process, meaning that the perturbation of the system (in the present case the addition of the second amino acid enantiomer) cause the lack of the transferred feature. It was reported in the case of induction of chirality in porphyrin H_4TPPS homoaggregate, that the addition of an excess of the amino acid not used as inducer cause the inversion of the CD signal after 72 hours.[82]

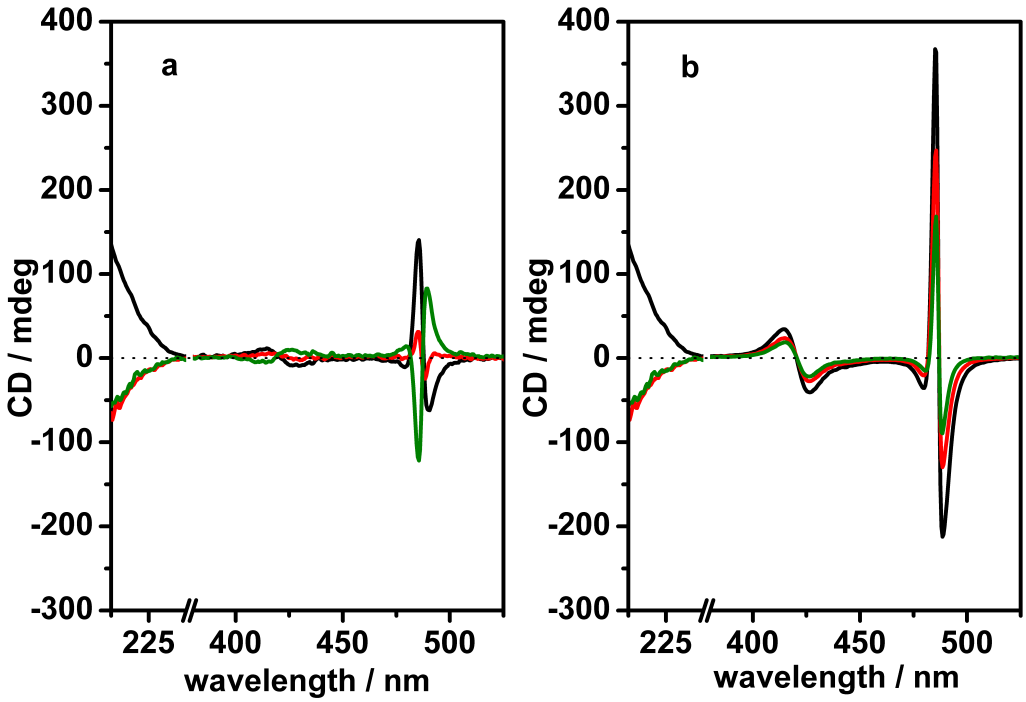

Figure 54: (a) CD spectra of the solution of the J-aggregate template on L-Lys 5 mM using the "acid first" procedure before (represented by the black curve), after 24 h (represented by the red curve), and 1 week (represented by the green curve) from the addition of D-Lys 7.5 mM. (b) CD spectra of the solution of the J-aggregate template on L-Lys 5 mM using the "acid last" procedure (represented by the black curve), after 24 h in the presence of D-Lys 7.5 mM (represented by the red curve), and after 1 week (represented by the green curve)

The stability of the aggregates was monitored during time; the CD intensity of the aggregate obtained with the *acid first* procedure decrease after only 24 hours and after 1week the

signal shows an opposite Cotton effect respect to the starting sign. Indicating the loss of the information transferred from the first added amino acid (figure 54).

On the contrary, the CD signal of the aggregate obtained with the *acid last* protocol remains the same but less intense. Respect to the *acid first* procedure a higher ordered structure was reached with the other protocol.

The aggregate obtained using the *acid last* protocol shows a higher stability to perturbation, this evidence that in the second used procedure, the slower growth of poprhyrins chiral complex allows a better equilibrium between the different interactions that contribute to the supramolecular chiral aggregate steadiness.

2.4 Morphological study of chiral J-Aggregates

The described J aggregates are widely studied systems, high interest is addressed in the correlation between the structure and the optical properties of the porphyrin J-aggregates.[78,87]

The CD signal showed in the spectra of the aggregates is not a consequence of artefact linear polarization (LD); in fact the same optical activity can be observed both in long shaped aggregates and round particles (different shape occur following different preparation protocols); to determine the different mesomorphs a combination of spectroscopic and physic techniques must be used.[71]

In the literature we can find models aiming to explain the J-aggregate structure, based on X-ray diffraction or scattering and also on AFM, SPM and TEM,[101-104] nevertheless at present the challenge is to correlate the origin of aggregate chirality to their structural pattern.

Electron microscopy techniques work with the samples in a vacuum and therefore normally must be dried, producing deformation and producing a lack of high resolution information on molecular features of the particles in solution. Tubular structures for example collapse to a tape, because of the absence of solvent inside the tube. Using Cryo-Electron Microscopy (Cryo-EM) assemblies are snap-frozen so quickly that they are maintained in their aqueous environment in vitreous ice maintained at Liquid Nitrogen temperature. Allowing a high physical stability against evaporation inside the microscope, together with more precise characterization of the structure.[105]

Cryo-EM measurement was performed, in the Institut de Microbiologie de la Méditerranée

In Marseille from Dr. Kosta, on the J-aggregates templated with amino acids in order to shield light on the item of correlation between structure and chirality.

In its study on the origin of chirality in J-aggregate Balaban et al. [78] reported that the J-aggregates are tubes and that the origin of chirality can be ascribed to a helical arrangement of the monomers perpendicularly oriented respect to the axes of the tube (see figure 55).

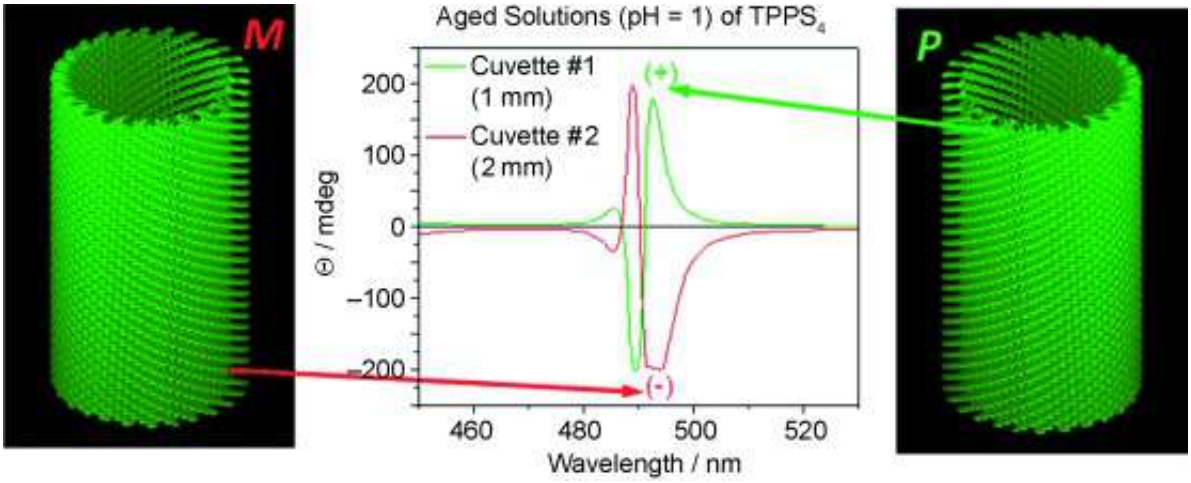

Figure 55: Three-dimensional reconstruction computed by helical tubes of M and P J-aggregates (reprinted with permition from ChemPhysChem 2013, 14, 3209 – 3214)

Using the templated J aggregate is advantageous because the handedness of the complex can be determined spectroscopically performing CD measurements.

Preliminary data achieved on samples obtained using L-Arg as templating agent and following the protocol acid first, confirm the tubular structure of J-aggregates, but even more interestingly they seem shown an helical shape of the tubes (see figure 56 b) that should confirm the Balaban theory about the supramolecular origin of chirality in H_4TPPS aggregates.

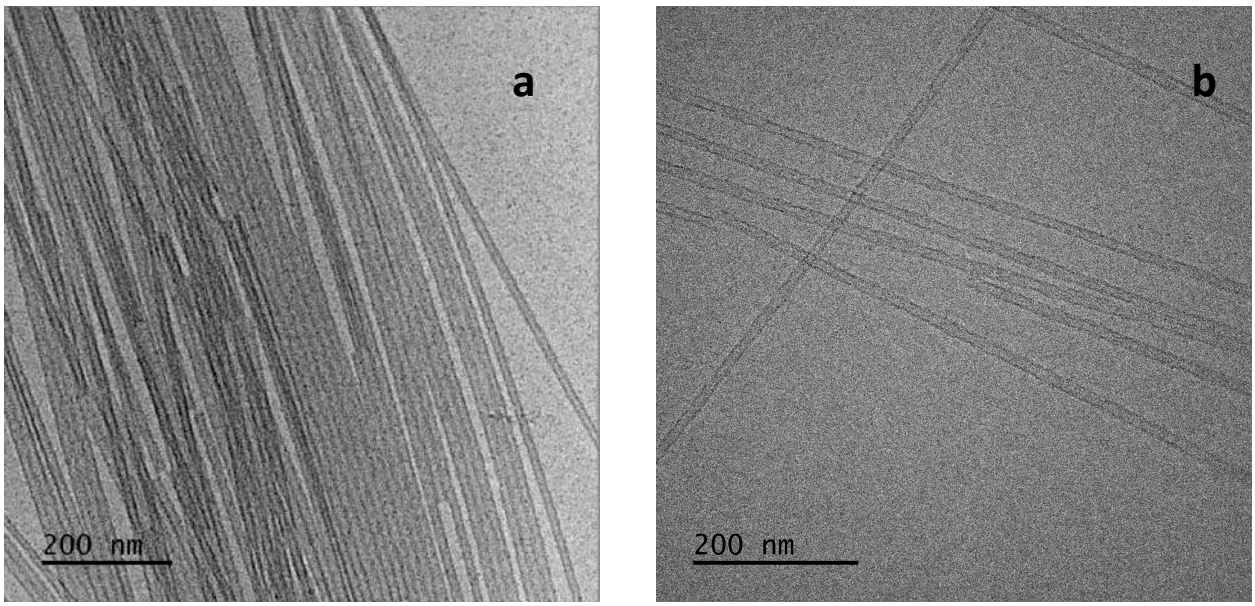

Figure 56: Cryo-TEM images of the J-aggregates template on L-Arg following the *acid first* procedure

The fine control of the J-aggregate handedness, its spectroscopic characterization followed by the microscopic analysis is a good approach useful to open the way to high precision design and fabrication of Nano-assemblies with increasing feature and potentialities.

3 PORPHYRINS IN HEAVY METAL SENSING

The increasing industrialization and the growth of population has a dramatic consequence in the water pollution; inadequate access to clean water and sanitization has contributed to the increasing interest in studying water purification.

In the last decade a tremendous amount of research to be conducted to identify robust new methods of purifying water at lower cost and with less energy, while at the same time minimizing the use of chemicals and impact on the environment.

One of the most used approaches in water purification is the application of membrane for ultrafiltration; the possibility to make advanced materials characterized by combined sieving and photocatalytic properties seems to be a promising procedure to improve the technology.

Water resistant ZnO decorated electrospun mats was proposed as a cost-effective, simple and easily scalable process both in term of materials choice, process time and cost system versatility and, even more relevant as photocatalysts in methylene blue degradation under UV irradiation; despite the effectiveness of the studied system it was observed a light release of the ZnO deposited on the surface of fibers.[106-109] Quantification and capture of the released metal is mandatory for the efficiency of the system.

Not only Zn, but also the content of other metal ions has risen enormously and the need for monitoring and capture these elements in solution has a huge impact.[107]

Recently, porphyrin-based probes have shown great promise for detecting heavy metal ions in solution.

Insertion of metal ions in porphyrins core can occur quite easily and the spectroscopic modifications of the macrocycle (shift of the Soret band and diminution of the Q bands) following the formation of metal derivative allow a fast and inexpensive detection.

Hydrosoluble porphyrins are fundamental for the development of sensing strategies in aqueous environment; unfortunately their capability to dissolve in water has the drawback of release and dispersion of porphyrins in the medium.

Meso-tetra(N-methyl-4-pyridyl)-porphyrin (H_2T4) was used as an efficient optical chemical sensor in solution; the immobilization of porphyrins on a transparent substrate instead of its use in solution is a useful approach able to by-pass the release of porphyrin in water.[108]

The use of a transparent substrate allows the easy measurement before and after the exposure to metal ions in water, also enabling to monitor the eventual release of porphyrin in water.

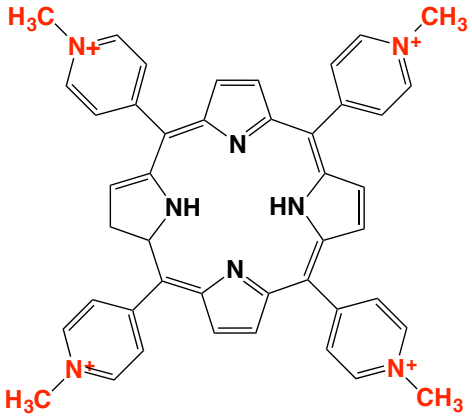

Figure 57: Schematic representation of H_2T4

H_2T4 (figure 57) can anchor to glass substrates by dip coating thanks to electrostatic forces, a clean glass slide was dipped for 1.5 hours in 10 μM H_2T4 solution whose pH was 5.5, after that the glass was rinsed to remove the porphyrin excess; the deposition of the tetracationic porphyrin was confirmed by UV-Vis spectra recorded on glass; the Soret band of the deposited porphyrin is broader and red shifted around 10 nm respect to the solution (figure 58).

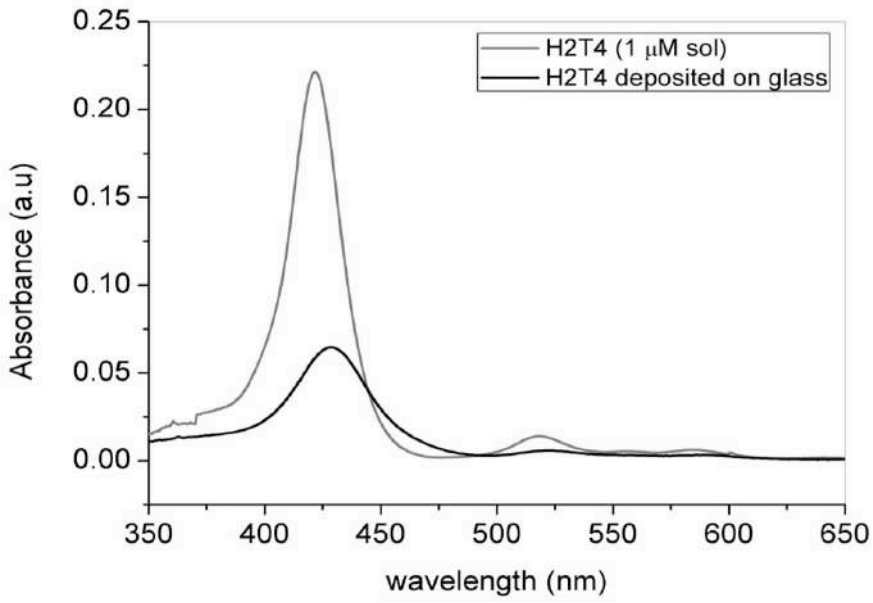

Figure 58: UV-Vis spectra of [H_2T4] 1μM (black line) in ultrapure water pH= 7 (grey line) and of H_2T4 deposited on glass (black line).

Dipping the functionalized glass in $Zn(NO_3)_2$ solutions at different concentration from 1 to 10 μM cause a hypochromic effect at 433 nm after only 15 minutes, and at concentration higher than 5 μM also a shift of the Soret band at higher wavelength can be observed (figure 59) in the same range of time.

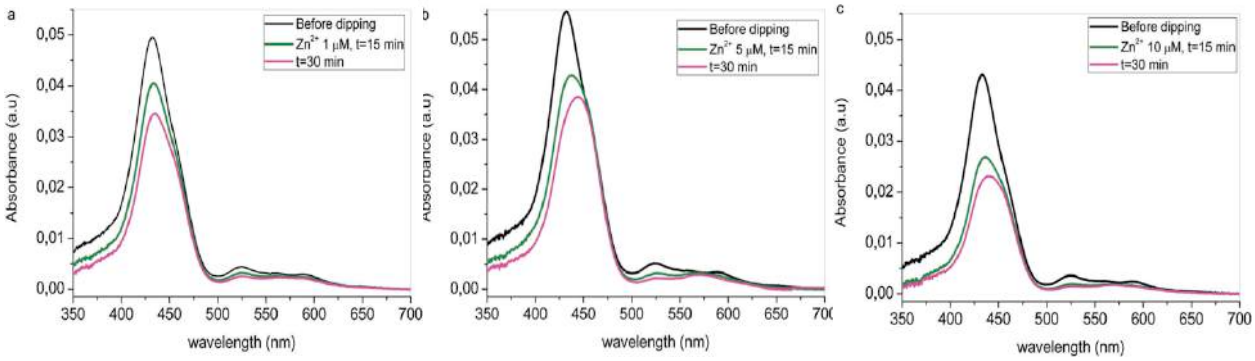

Figure 59: UV-Vis spectra of H2T4 treated glass before dipping (black line) and after 15 minutes (green line) and 30 min (pink line) from dipping in (a) 1 μM, (b) 5 μM and (c) 10 μM $Zn(NO_3)_2$ solutions.

H_2T4 1μM in solution is not able to detect Zn^{2+} if the concentration is below 500 μM, the spectroscopic variations cannot be observed in less than 1 hour. As showed in, increasing ten times the Zn^{2+} concentration a weak hypochromic effect can be observed after 15 minutes (figure 60).

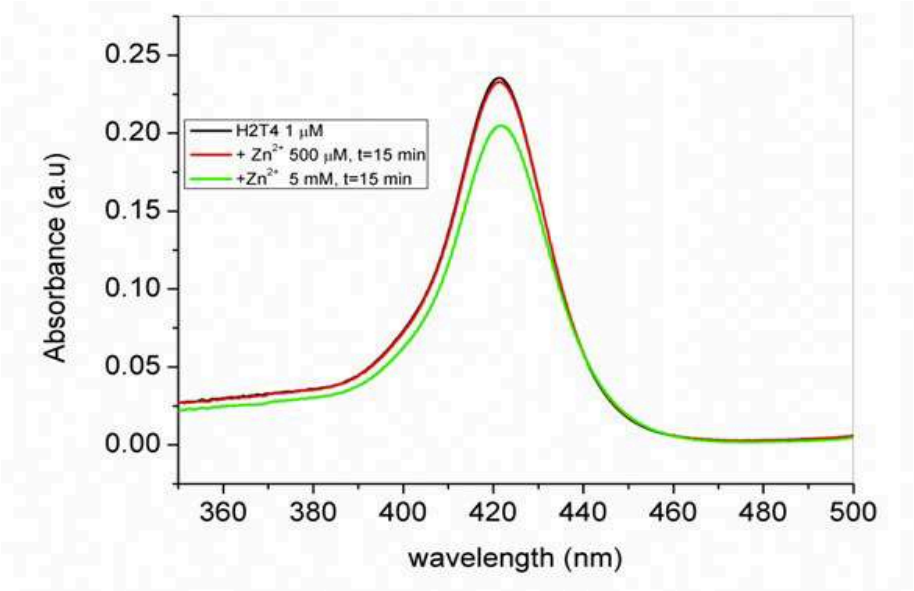

Figure 60: UV-Vis spectra of [H_2T4] 1μM (black line) in ultrapure water pH= 7 in presence of [Zn^{2+}] 500 μM (red line) or 5 mM (green line).

When porphyrin is deposited on the substrate, the metalation process is faster, and the sensitivity increases enormously.

H_2T4 deposited on glass is able to detect Zn^{2+} at 1 μM concentration in 15 minutes, while if 1 μM H_2T4 is dispersed in solution, the minimum quantity Zn^{2+} necessary to observe substantial spectroscopic variation in 15 minutes is not less than 5 mM.

The identification of Zn^{2+} using functionalized glass is easy and requires an analysis time less than 1 hour (15-30min). It is fundamental to underlying that, the functionalization of glass does not allow porphyrin dispersing in solution.

The metalation mechanism of porphyrin in solution was largely studied, as suggested by Eigen,[109] the process respect the following pathway: the metal proximity in the coordinative sphere of porphyrin cause a distortion of the ring with solvent exchange processes and deprotonation of the nitrogen atoms of the pyrrole till the formation of the metalloporphyrin. The metalation process is considered first order respect to the metal ion concentration; the distortion of the porpphyrin ring was widely demonstrated.

H_2T4 on glass has showed an enhanced sensitivity towards Zn^{2+} respect to the porphyrin solutions; suggesting a different kinetic. The porphyrin deposition, cause a ring distortion useful to accelerate the metalation process of the macrocicle. In particular the attached porphyrins show at least one of the nitrogen atoms of the pyrrole, making it more prompt for the metal chelation.

The distortion of the porphyrin on the glass is indicated by the shape of the Soret band that is broader and shifted respect to the Soret of the free porphyrin in solution; it is a consequence of the electrostatic interaction between the positive porphyrin and the negative surface of the substrate. The alteration of the ring geometry accelerates the detection of the Zn^{2+}.

Following the approach used for sensing of Zn^{2+}, we evaluate the H_2T4 capability to detect Pb^{2+} ions in solution.

The functionalized glass was dipped in $Pb(NO_3)_2$ solutions having concentration 1, 5 and 10 μM, UV-Vis spectra of deposited H2T4 show detectable hypochromic effect at 433 nm, immediately after dipping and for all the ion concentration (figure 61). After 15 minutes dipping, and at concentrations 5 and 10 μM the appearance of a new band at 500nm related to the Pb^{2+} complexation can be seen (figure 4 panels b and c).

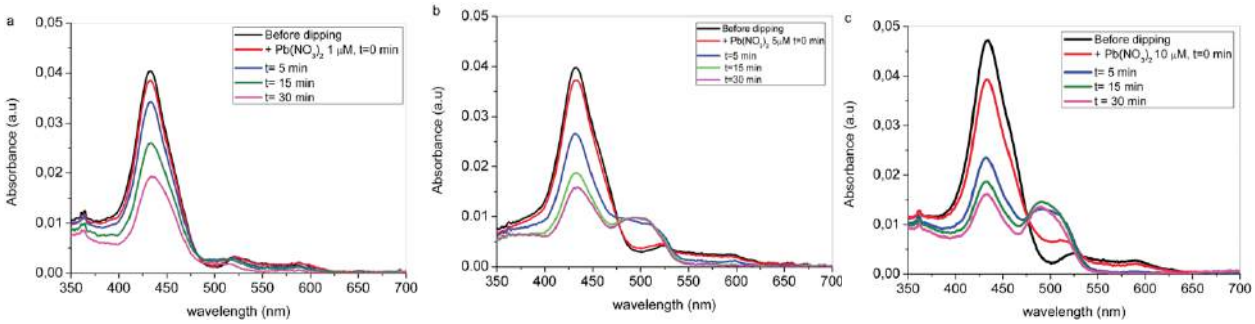

Figure 61: UV-Vis spectra of H_2T4 treated glass before dipping (black line) and after 0 minutes (red line), 5 min (blue line), 15 minutes (green line) and 30 min (pink line) from dipping in $Pb(NO_3)_2$ solutions (a) 1 μM, (b) 5 μM and (c) 10 μM.

At the 1mM Pb^{2+} concentration the band at 500 nm is not clearly detectable. While the Soret band splitting (in the component at 433nm and the new one at 500 nm), observed at higher concentrations, is subjected to variation in the relative intensities upon increasing the glass dipping time, the same evidence is observed in H_2T4 1 μM solution titrated with increasing amount of Pb^{2+} (figure 62).

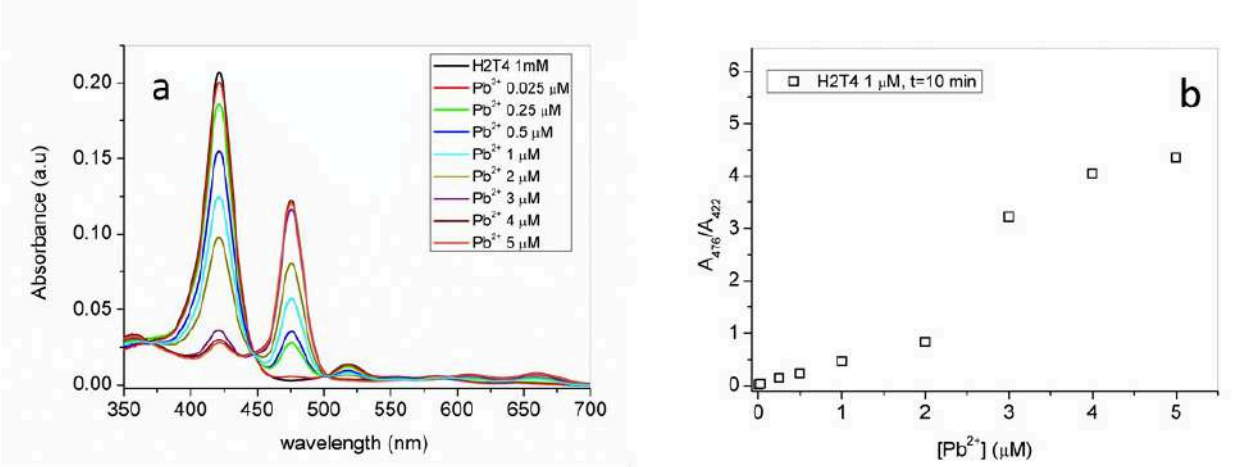

Figure 62: UV-Vis spectra of H_2T4 1 μM in water pH=7 (a) and related plot of A476/A422 ratio (b), upon increasing [Pb2+].

The here reported spectroscopic evidences clearly indicate that H_2T4 deposited on glass is able to separately detect, both Zn^{2+} and Pb^{2+} in water solutions.

Obviously natural water contains different metal ions contemporary dispersed; the challenge in metal ions detector device is that they must be able to identify the presence of coexisting metal ions in samples.

For the above, porphyrin functionalized glass was dipped in solutions containing constant Zn^{2+} and variable Pb^{2+} concentrations (figure 63).

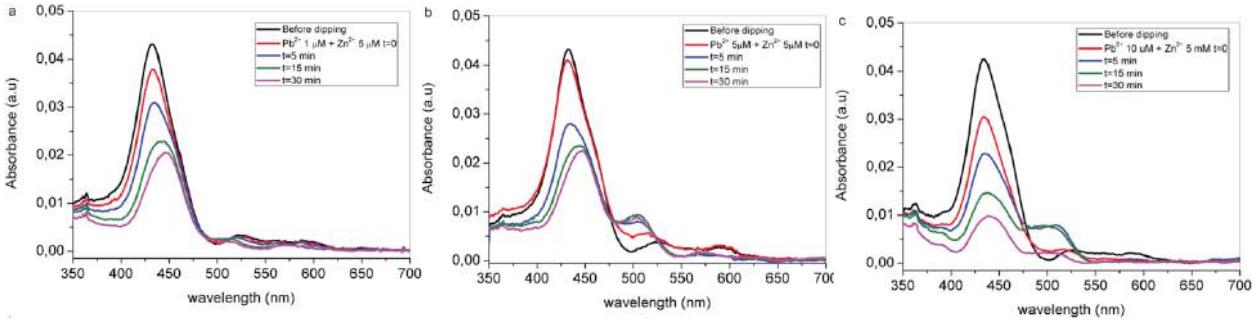

Figure 63: UV-Vis spectra of H_2T4 treated glass before dipping (black line) and after 0 minutes (red line), 5 min (blue line), 15 minutes (green line) and 30 min (pink line) from dipping in (a) 1 μM, (b) 5 μM and (c) 10 μM $Pb(NO_3)_2$ solutions containing $Zn(NO_3)_2$ 5 μM.

The contemporary presence of the two metal ions is evidenced by the increasing hypochromic effect observed in the Soret band; respect to what observed when only Zn or Pb ions are present alone in solution, in the case of their coexistence in the sample the hypocromic effect after only 15 minutes is more pronounced.

In the case of the contemporary presence of the two metal ions three main cases can be evaluated

1) the Pb^{2+}concentration is lower respect to the Zn^{2+}, together with the hypochromic effect, it is possible to observe a shift of the Soret band at 450 nm (indicating the formation of ZnT4) and the growth of the band at 500 nm (due to the formation of PbT4).

2) the Pb^{2+} concentration is equal to the Zn^{2+}, the Soret band is shifted at 450nm and the band at 500nm is well visible.

3) the Pb^{2+}concentration is higher respect to the Zn^{2+}, the decrease of the Soret band at 433 nm is more pronounced than in the previous cases and also the profile is different. Due to the high contribution of the band at 450 nm the peak at 433 nm shows a different shape associated with the presence of ZnT4.

The above resumed spectroscopic evidences are strictly related to the analysis time, in fact increasing the glass dipping time cause the lost of information.

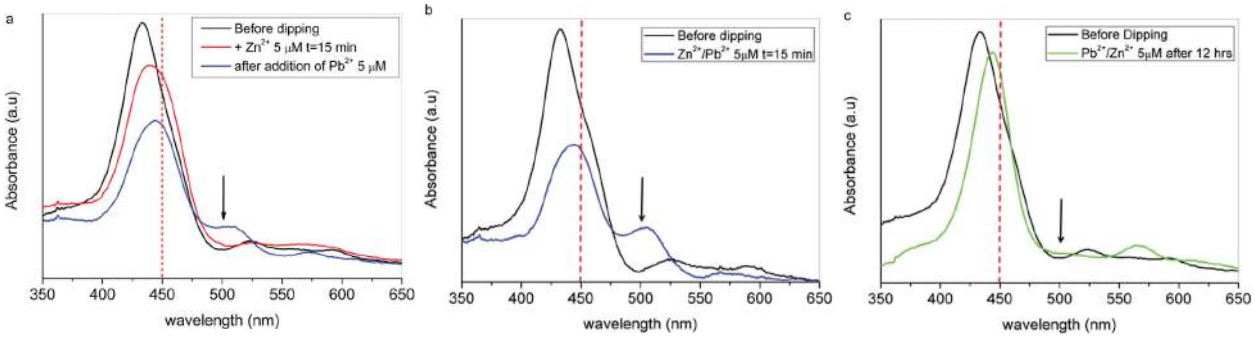

Figure 64: UV-Vis spectra of H_2T4 treated glass before (black line) and afterdipping in aqueous solutions containing [Zn^{2+}] = 5 μM and [Pb^{2+}] = 5 μM; (a) [Zn^{2+}] = 5 μM is added before [Pb^{2+}] = 5 μM; (b) [Zn^{2+}] = 5 μM and [Pb^{2+}] = 5 μM are added simultaneously; (c) UV-Vis spectra of H_2T4 treated glass after 12 hours dipping in aqueous solutions containing [Zn] = 5 μM and [Pb^{2+}] = 5 μM.

As showed in figure 64, after 12 hours dipping the only specie on the glass surface is the more stable ZnT4, even if the solution contains the same concentration of Zn^{2+} and Pb^{2+}, the band at 500 nm disappear during time.

The higher stability of ZnT4 respect to PbT4 can be explained as follow; Pb^{2+} has a higher radius respect to the Zn^{2+}, so Pb is able to assist the metal insertion of Zn inside the porphyrin core. Pb^{2+} in fact, form a sitting atop (SAT) intermediate with H_2T4, lowering the activation energy for the bind of the Zn^{2+}, the intermediate formation has the effect to decrease the activation energy for the formation of ZnT4.

At the same time the formation of the SAT PbT4 has the capability to lower the detection limit in for the Zn^{2+} in porphyrin solutions.

The here reported results show that the contemporary detection of Zn and Pb ions is possible in a consistent way, using a poprphyrin functionalized glass and a non-expensive and easy to use spectrophotometer, also the measurement is more reliable in an analysis time of 15-30 minutes.

4 *PORPHYRINS IN ENERGY STORAGE*

Nowadays, a technological society requires new and more efficient energy storage devices.

There are two fundamentals ways to store electrical energy; indirectly as in batteries, where potentially available chemical energy require Faradaic oxidation and reduction of the active reagents at the electrode surface; the second one is direct, a non-Faradaic energy storage in electrostatic way, like negative and positive electric charges on a plate of a capacitors.

In batteries, the chemical interconversions of the anode and cathode materials must to occur, despite the "change" can be conducted in a reversible thermodynamic way, the process involve very often irreversibility, thus the life of battery cells usually is restricted to one thousand to several thousand of charge and discharge cycles.

In capacitors, it is necessary only an excess and a deficiency of electron charges on the capacitor plates in the charge process and the opposite in the discharge process; chemical changes are not involved, the cyclability in terms of charge and discharge is almost unlimited.

The limit of capacitors is their small amount of charge storage; they have a low energy density; to go beyond this limit the study of capacitors with a high surface area like for example carbon powders has increasing widely in the last years.[110-113]

Also the film-state supercapacitors has an increased surface and they would combine the advantage of miniaturization and flexibility and could integrate with other organic optoelectronic devices, which would lead to the next-generation consumer electronic devices. However, the film-state supercapacitors that meet large capacitance, high energy density, and outstanding stability remain a substantial challenge.

Among the thin materials useful in supercapacitors field, transition metal oxides (TMO) are the most studied, because their crystal structure easily allows obtaining nanosheets using liquid phase exfoliation (LPE), for instance.

In the last years increasing attention was dedicated in studying manganese dioxide (MnO_2) nanosheets, not only because MnO_2 is a well-known functional transition metal oxide, with distinctive properties, but also of high abundance, low cost, and good environment compatibility. [114] Moreover it can be exfoliated, to undergo a two-dimensional nanomaterial having significantly different features from those found on the bulk counterparts.

2D nanomaterials have an intrinsic high surface area and flexibility, moreover some of them exhibit high mechanical strength, together with high electrical and thermal conductivities, and also high dielectrical constants can be observed. This is due to the two dimentions quantum confinement that leads to an important modification of the electronic structure wich induces novel physical phenomena.

Like other 2D materials, MnO_2 nanosheets are characterized by a thickness around nanometer or smaller scale with a lateral size ranging from submicrometers to micrometers.

The typical crystal structure of MnO_2 nanosheets shows three atomic layers, where two O sheets are above and below an Mn one. Each Mn coordinates six O atoms to form an edge-sharing MnO_6 octachedra.

The vacancies in Mn layer make MnO_2 nanosheets negatively charged, repulsive to each other. Moreover, the d-d transition of Mn ions in the MnO_6 octahedral structure results in a broad absorption spectrum starting from 200 ending at 600 nm with a large molar extinction coefficient (ε max = 9.6 Å$\sim$103 M^{-1} cm^{-1}) at 380 nm.[115]

The possibility of modifying MnO_2 nanomaterial's surfaces, together with the opportunity to design a nanocomposite with enhanced properties was the staring point to design a new system.

In this context, is well known that porphyrins are widely used for layered materials functionalization having many application from water purification to sensing, from organic solar cells to catalisys.[116-119]

In order to evaluate the possibility to non-covalently functionalize MnO_2 nanosheets with porphyrins many experiments was performed. A positively charged H_2T4 and a negatively charged H_2TPPS porphyrin where used in MnO2 nanosheet dispersions.

It was reported that one of the best solvents for the MnO_2 nanosheet preparation by LFP is N-Metil-2-pyrrolidone (NMP). The exfoliation yield using this solvent is relatively high, and also the obtained dispersions were stable for a long time. [114]

Thus, MnO_2 and the porphyrins were firstly dispersed in NMP. By comparing the UV-Vis spectra in water and in NMP no huge difference are observed in the absorption bands of these molecules, just a shift of the Soret band together with a weak hypochromic effect as shown in figure 65. This data confirm us that there are no porphyrins aggregation phenomena in NMP.

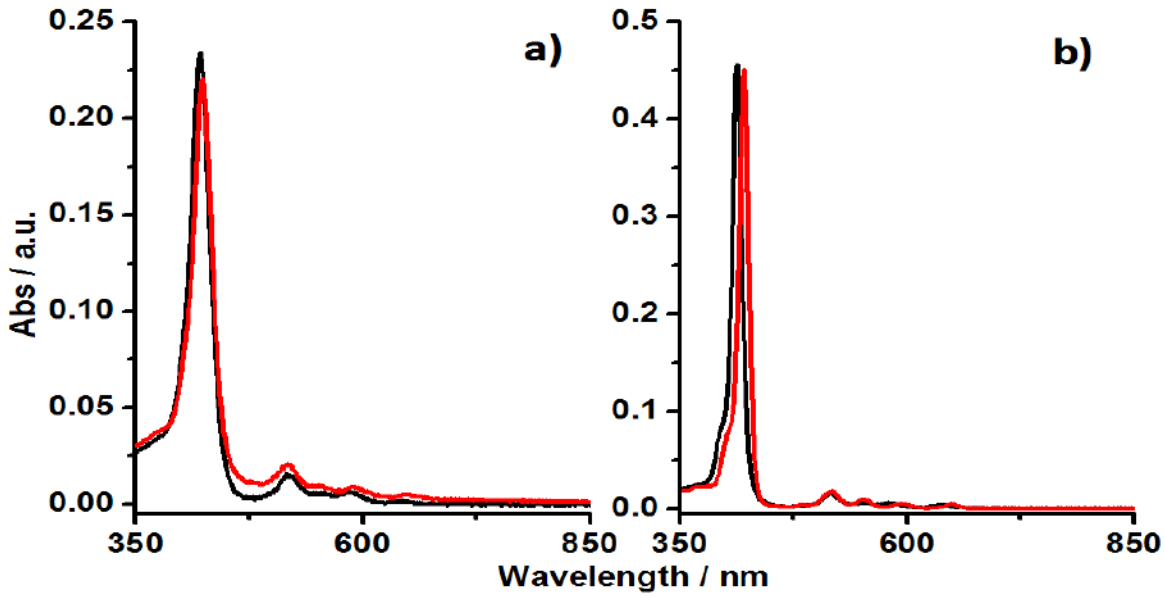

Figure 65: a) UV vis spectra of H_2T4 1mM in water (black), and in NMP (red); b) UV vis spectra of H_2TPPS 1mM in water (black), and in NMP (red).

Titrations of MnO_2 with increasing amount of porphyrins were performed and no evidences of interactions could be observed (figure 66). The plot of the absorbance value of the Soret band vs the concentration of the porphyrin clearly shows that the increase of the absorbance values follow a linear trend, confirming the absence of any interaction.

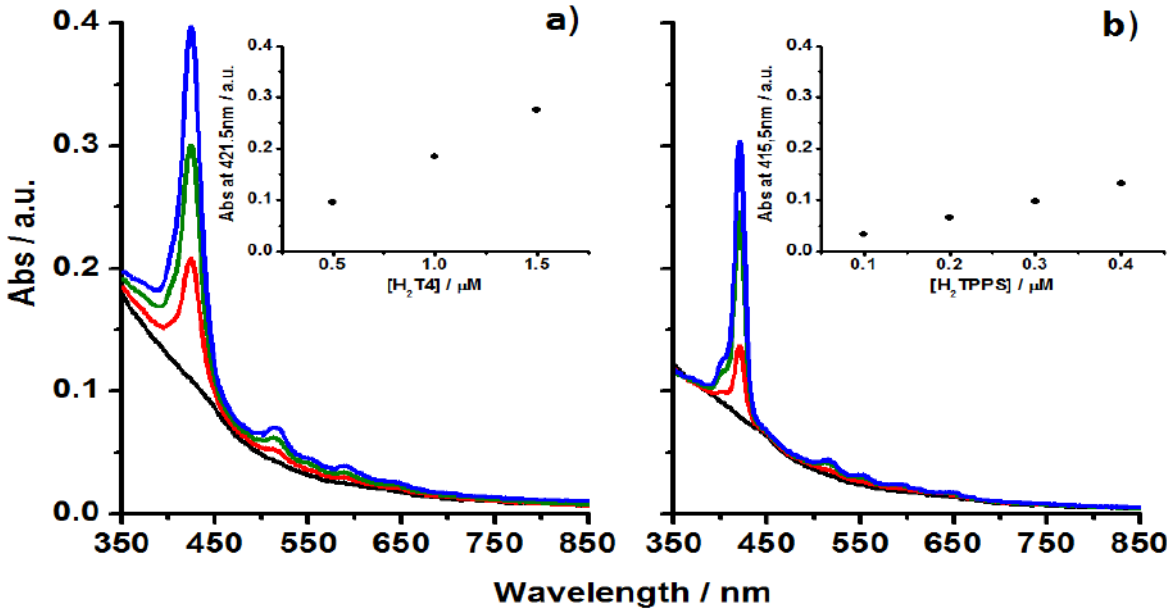

Figure 66: UV vis spectra of the titration of MnO_2 using increasing concentration of the porphyrin a) H_2T4 and b) H_2TPPS. The inset shows the Abs value of the Soret band in function of the porphyrin concentration.

To create the correct condition for the interaction to occur, different experimental parameters were changed: the ratio between the two components, the pH of the solution and, the temperature; these last one was changed to evaluate if the interaction is a kinetic guided process.

The absence of modifications in the UV spectra, demonstrates that there are no interactions in these working conditions. Even after stirring and sonication the solutions, no effect was observed.

The next step is to change drastically the working condition. We started from solid MnO_2 obtained by sedimentation from the NMP solution. The powder was dispersed in water and water solutions of porphyrins are added.

As, to the best of our knowledge, there are no literature data reports regarding the interactions between porphyrins and MnO_2; we follow the experimental procedure of Yin *et al.*.[116] This publication reports the non covalent functionalization of MoS_2 with 5,10,15,20-tetrakis(1-methyl-4-pyridinio)porphyrintetra(p -toluenesulfonate) (TMPyP).

We added 1.5 μM of porphyrin to 0.025mg/mL of MnO_2 in 4 mL of water. Then the solution was held for 2 hours in the dark under stirring.

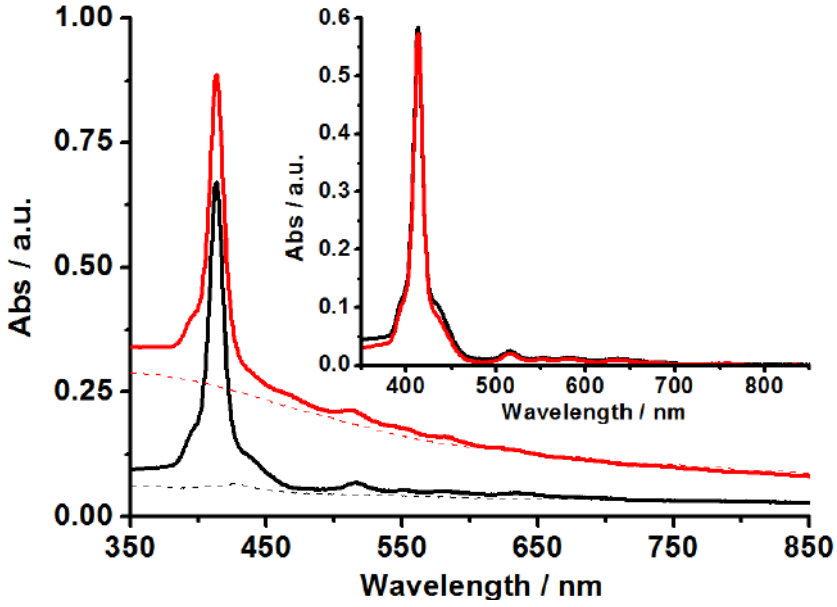

Figure 67: UV vis spectra of the solutions containing MnO_2 0.025mg/mL dashed lines and MnO_2 plus H_2TPPS 1.5mM continuous lines, before (black) and after (red) 2hrs stirring, The inset shows the UV vis spectra of H_2TPPS 1.5mM before (black) and after (red) 2hrs stirring.

After the 2 hours stirring, the UV-Vis spectrum was recorded. In the solution containing the mixture MnO_2 plus H_2TPPS no evidence of interaction could be observed (figure 67).

On the other hand, a huge hypochromic effect in the Soret band can be observed in the MnO_2 plus H_2T4 solution, demonstrating that porphyrin molecules interacted with MnO_2 nanosheets (figure 68).

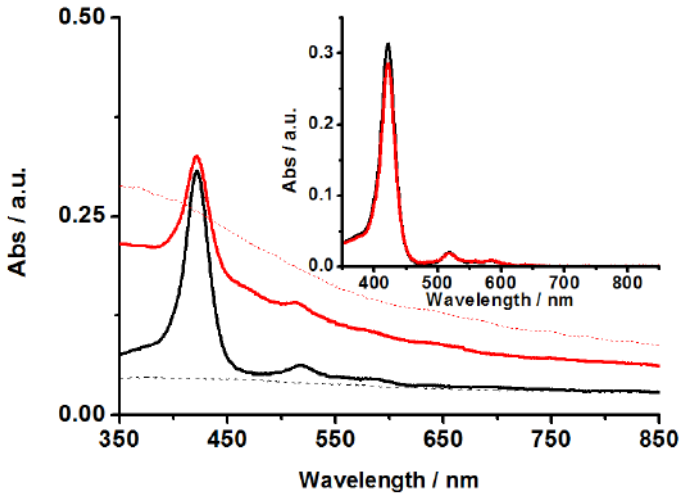

Figure 68: UV vis spectra of the solutions containing MnO_2 0.025mg/mL dashed lines and MnO_2 plus H_2T4 1.5mM continuous lines, before (black) the inset shows the UV vis spectra of H_2T4 1.5mM before (black) and after (red) 2hrs stirring.

Stirring disaggregates the MnO_2 sheets, thus exposing a higher active material surface area. This effect is confirmed by the increased absorbance in the UV-Vis spectra (figure 67 and 68 dashed red lines).

ζ potential measurements, showed in table 2, revealed that MnO_2 surface is negatively charged. Thus, MnO_2 nanosheets surface charge change to more positive values upon interaction with H_2T4 porphyrin.

Table 2: ζ potential measurements

	Dilution	ζ potential	STD
MnO_2	1:100	-39.9	2.78
	1:10	-43	3.4
	No dilution	-37.3	0.678
MnO_2+ H_2T4	1:100	-36	10.5
	1:10	-42.8	1.67
	No dilution	-26.9	0.803

The physic-chemical and structural characterization of the obtained functionalized material can be performed by XPS and Raman spectroscopy.

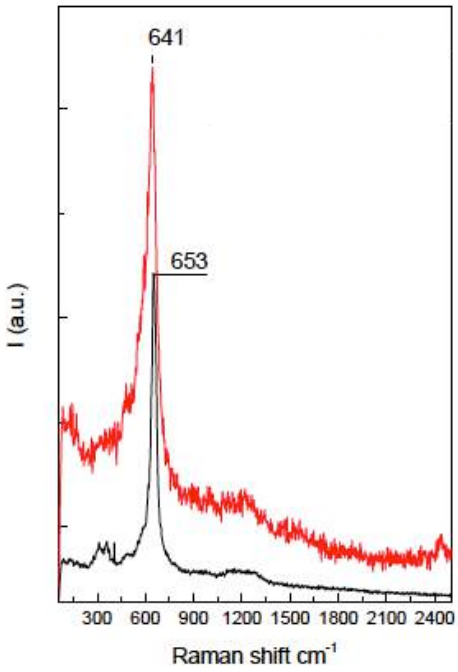

Figure 69: Raman spectra of MnO_2 (black) and MnO_2 plus H_2T4 (red).

The Raman spectra in figure 69 also suggest a modification of the MnO_2 surface, after the porphyrin interaction; the shift to lower frequencies of the band at 653 cm^{-1} confirms the higher defectivity of the material.

XPS measurements were carried out for further confirming the obtained results. XPS is a technique able to give information on the atomic composition of the surface, analyzing the atomic sensitivity factors of the elements; the group of Prof. Gulino performed for us XPS measurements.

In the figure 70, the overlap of the different binding energies related to C (figure 70a), Mn $2p_{3/2,½.}$ (figure 70b), O (figure 70c) and N (figure 70d). Despite no differences can be observed in the B.E. of the C, because of the huge amount of surfactant added in the synthesis of the MNO_2; the shifts observed in all the other spectra are a consequence of the interaction between the porphyrin and the MnO_2 nanosheet.

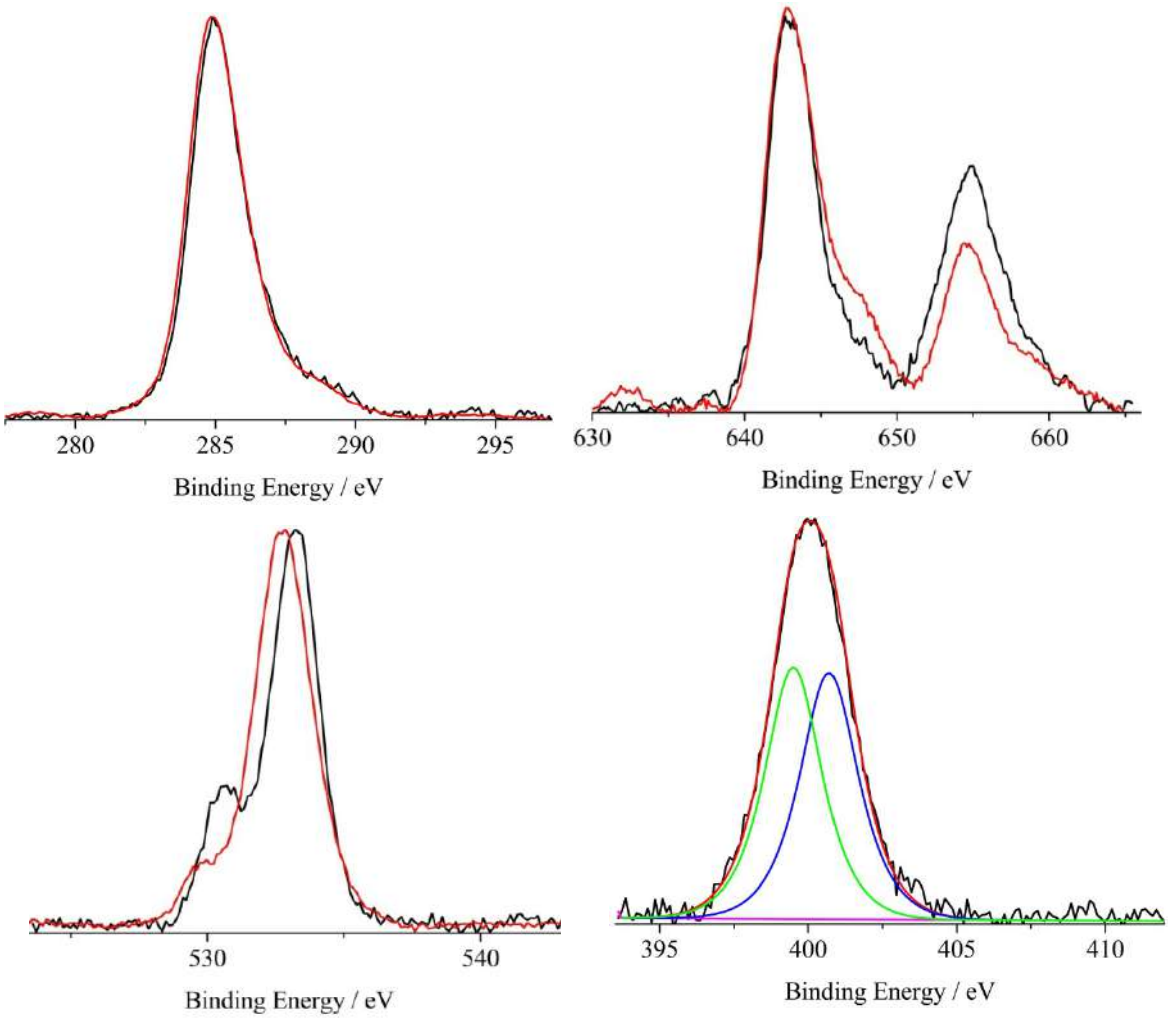

Figure 70: XPS Spectra

Electrochemical characterization was also conducted to evaluate if the interaction of porphyrin on MnO_2 surface can enhance the MnO_2 supercapacitor performance.

By using cyclic voltammetry it is possible to assess if the electronic conductivity of MnO_2 can be modified by the porphyrin.

Preliminary data has shown that there is an effect on the CV of MnO_2. When porphyrin is on the nanosheets the capacitance per gram is increased. In figure 71 the plot of the capacitance per gram (C_m) versus the scan rate shows that the C_m is higher in the sample MnO_2 plus $H2T_4$ (green dots) compared to the sample containing MnO_2 alone (black dots). For comparison purposes, the C_m was measured also for the porphyrin alone (red dots).

The increased capacitance observed in the MnO_2 system let us to think that the supramolecular functionalization can be used to increase the supercapacitor features of the nanosheets; further measurements must be done to ascertain the ciclability of the presented system.

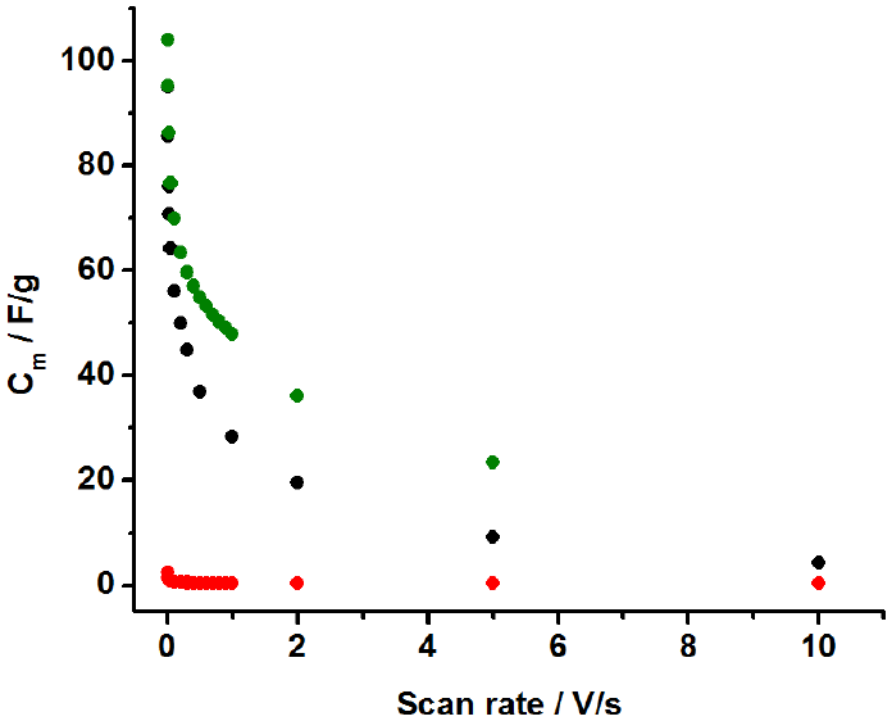

Figure 71: Plot of the values of C_m vs the scan rate obtained from the CV measurements of MnO_2 (black dots), H_2T4 (red dots) and a the MnO_2 functionalized with H_2T4 (green dots).

CONCLUSIONS

Porphyrins are a versatile class of molecules, they were chosen from Nature for many fundamentals applications, the deep knowledge of their characteristic is useful for emulate Nature and obtain device more compatible and efficient.

To study the aggregation pathway of porphyrin macromolecules in the presence of biocompatible polyelectrolytes or amino acids is a starting point for the design of new functional nanomaterials bio inspired. Moreover is an interesting approach to shield light in the mechanisms that are involved in the homochirality of life.

The knowledge of porphyrins features has allowed also, using them in different field such us sensing and energy storage.

The non covalent method here presented, allow for the synthesis of systems with the opportune characteristic in a easy and not time consuming way, avoiding to spent lot of time and money; this approach on the other side require a deep knowledge of the molecules behavior in the chosen condition, weak forces are very sensitive to small variations in the chemical physics conditions of the system. Working on supramolecular process require a very precise control of many parameter at the same time, any minimum variation can drive the system in unwanted routes.

REFERENCES

1. J.M. Lehn Supramolecula Chemistry: Concepts and perspectives, VCH Weinheim, **1995.**
2. D. Philip, J.F. Stoddart, *Angew. Chem. Int. Ed*. Engl. **1996**, 35, 1154-1196.
3.J.M Lehn *Angew Chem. Int. Ed.* **1988**, 27, 89-112
4. G. Vantomme, E.W. Meijer, *Science* **2019**, 363, 6434, 1396-1397.
5. F. Gasparrini, D. Misiti, C. Villani, *J. of Crhomatography A,* **2001**, 35-50.
6. I. S. Choi, N. Bowden and G. M. Whitesides, *Angew. Chem., Int. Ed.*, **1999**, 38, 3078.
7. J.M. Lehn, *Proc. Natl. Acad. Sci. U.S.A.,* **2002**, 99, 4763-4768.
8. J.-M. Lehn, *Angew. Chem., Int. Ed. Engl.*, **1990**, 29, 1304.
9. J.-M. Lehn, *Chem.–Eur. J.*, **2000**, 6, 2097.
10. G. M. Whitesides, J. P. Mathias, C. T. Seto, *Science*, **1991**, 254, 1312.
11. D. S. Lawrence, T. Jiang and M. Levett, *Chem. Rev.*, **1995**, 95, 2229.
12. D. Philp and J. F. Stoddart, *Angew. Chem., Int. Ed. Engl.*, **1996**, 35, 1154.
13. S. Leinninger, B. Olenyuk and P. J. Stang, Chem. Rev., **2000**, 100, 853;
14. S. R. Seidel and P. J. Stang, *Acc. Chem. Res.*, **2002**, 35, 972.
15. G. F. Swiegers and T. J. Malefetse, *Chem. Rev.*, **2000**, 100, 3483.
16. L. F. Lindoy and I. M. Atkinson, *RSC Cambridge*, 2000.
17. G. Oliviero, J. Amato, N. Borbone, S. D'Errico, A. Galeone, L. Mayol, et al., *Chem. Commun.,* **2010**, 46, 8971-8973.
18. E.M. Reyes-Reyes, Y. Teng, P.J. Bates, *Cancer Res.* **2010**, 70, 8617-8629.
19. V. D'Atri, G. Oliviero, J. Amato, N. Borbone, S. D'Errico, L. Mayol, et al., *Chem. Commun.*, **2012**, 48, 9516-9518.
20. V. D'Atri, N. Borbone, J. Amato, V. Gabelica, S. D'Errico, G. Piccialli, L. Mayol, G. Oliviero, *Biochimie*, **2014**, 99, 119-128.
21. R.A. Hegstrom D.K. Kondepudi, *Scient. American* **1990**, 108-115.
22. M. Liu, L. Zhang, T. Wang, *Chem. Rev.*, **2015**, 115, 7304-7397.
23. C. Blanco, M. Stich, D. Hochberg, *Chem. Phys. Lett.* **2011**, 505, 140-147.
24. F.C. Frank, *Biochimica et Biophysica Acta,* **1953**, 11, 459-463.
25. I. Gutman, *J. Sci. I. R. Iran,* **1995**, 6, 231-234.
26. S.F. Mason, Chemical Evolution, *Oxford University Press*, Oxford, **1991**.
27. R. Plasson, D.K. Kondepudi, H. Bersini, A. Commeyras, K. Asakura, *Chirality*, **2007**, 19

589.

28. C. Blanco, M. Stich, D. Hochberg, *Chem. Phys. Lett.*, **2011**, 505, 140-147
29. G. H. Wagnie`re, *Wiley-VCH*, **2007**.
30. P. L. Luisi, *Cambridge Univ. Press*, **2006**.
31. J.C. Chambron, F.R. Keene, *Wiley* **2017.**
32. F. Helmic, C.C. Lee, A.P.H.J. Schenning, E.W. Meijer, *J. Am. Chem. Soc.*, **2010**, 132, 16753-16755.
33. M.M. Green, N.C. Peterson, T. Sato, A. Teramoto, R. Cook, S. Lifson*Science*, **1995**, 268, 1860-1866.
34. J. J. Flores, W.A. Bonner, G.A. Massey, *J. Am. Chem. Soc.*, **1977**, 99, 3622–3625.
35. Bailey, A. Chrystomou, J.H. Hough, T.M. Gledhill, A. Mc Call, S. Clark, F. Menard, M. Tamura, *Science*, **1998**, 281, 672–674.
36. W.L. Noorduin, A.A. Bode, M. van der Meijden, H. MEEKES, A.F. van Etteger, W.J. van Enckevort, P.C. Christiansen, B. Kaptein, R.M Kellogg, T. Rasing, E.Vilieg, *Nat. Chem*, **2009**, 9, 729-732.
37. R. Berger, M. Quack, *ChemPhysChem*, **2001**, 1, 57–60.
38. D.K. Kondepudi, G.W Nelson, *Nature*, **1985**, 314, 438–441.
39. V. Aquilanti, G.S. Maciel, *Orig. Life Evol. Biosph.*, **2006**, 36, 435–441.
40. J.M. Ribò, J. Crusats, F. Sagues, J. Claret, R. Rubires, *Science*, **2001**, 292, 2063–2066.
41. A. D'Urso, R. Randazzo, L. Lo Faro, R. Purrello, *Angew. Chem. Int. Ed.*, **2010**, 49, 108–112.
42. C. Escudero, J. Crusats, I. Dìez-Pérez, Z. El-Hachemi, J.M. Ribò ,*Angew. Chem. Int. Ed.*, **2006**, 45, 8032–8035.
43. O. Arteaga, A. Canillas, J. Crusats, Z. El-Hachemi, J. Llorens, E. Sacristan, J.M. Ribó, *ChemPhysChem*, **2010**, 11, 3511–3516.
44. N. Micali, H. Engelkamp, P.G. van Rhee, P.C.M, Christianen, L. Monsù Scolaro, J.C. Maan, *Nat. Chem.*, **2012**, 4, 201-2017.
45. Gouterman, M. J. Mol. Spectroscopy, **1961**, 6, 138.
46. L.J. Prins, D.N. Reinhoudt, P. Timmerman, *Angew. Chem. Int. Ed.*, **2001**.40, 2382.
47. P. Rothemund, *J. Am. Chem. Soc.*, **1935**, 57, 2010.
48. G. Scheibe, *Angew. Chem.,* **1937**, 50, 51.
49. G. Scheibe, L.Kandler, H. Ecker, *Naturwissenschaften* **1937**, 25, 75.
50. G. Scheibe, *Angew. Chem.*, **1937**, 50, 212–219.

51. G. Scheibe, *Angew. Chem.*, **1936**, 49, 563.

52. E. E. Jelley, *Nature*, **1936**, 138, 1009 – 1010

53. I.E. Borissevitch, S.C. Gandini, *J. Photochem. Photobiol. B: Biol.,* **1998**, 43, 112.

54. R.F. Pasternack, E.J. Gibbs, A. Antebi, S. Bassner, L. Depoy, D.H. Turner, A. Williams, F. Laplace, M.H. Lansard, C. Merienne, M. Perrée-Fauvet, *J. Am. Chem. Soc.*, **1985**, 107, 8179.

55. P. Kubat, K. Lang, K. Prochazkovà, Jr.P. Anzenbacher, *Langmuir*, **2003**, 19, 422.

56. R. Giovannetti, L. Alibabaei, L. Petetta, *Journal of Photochemistry and Photobiology A: Chemistry*, **2010**, 211,108.

57. M. De Napoli, S. Nardis, R. Paolesse, M.G.H. Vicente, R. Lauceri, R. Purrello, *J. Am. Chem. Soc.*, **2004**, 126, 5934-5935.

58. C.M.A. Gangemi, R. Randazzo, M.E. Fragalà, G.A. Tomaselli, F.P. Ballistreri, A. Pappalardo, R.M. Toscano, G. Trusso Sfrazzetto, R. Purrello, A. D'Urso, *New J. Chem*., **2015**, 39, 6722-6725.

59. N. Micali, A. Romeo, R. Lauceri, R. Purrello, F. Mallamace, L. Monsu` Scolaro *J. Phys. Chem. B*, **2000**, 104, 9416-9420.

60. O. Ohmo, Y. Kaizu, H. Kobayashi, *J. Chem. Phys.*, **1993**, 99, 4128.

61. A.M. Van de Craats, J.M. Warman, *Adv. Mater.*, **2001**, 12, 130.

62. P. W. Bohn, *Annu. Rev. Phys. Chem.*, **1993**, 44, 37.

63. L. Augenstein, R. Mason, B. Rosenberg, *Academic Press: New York*, **1964**, 23-42.

64. E. G. McRae, M. Kasha, *J. Chem. Phys*. **1958**, 28, 721.

65. M. Kasha, H. R. Rawls and M. A. El Bayoumi, *Pure Appl. Chem.*, **1965**, *11*, 371.

66. R. Randazzo, A. Savoldelli, D.A. Cristaldi, A. Cunsolo, M. Gaeta, M.E. Fragalà, S. Nardis, A.D'Urso, R. Paolesse, R. Purrello, *J. Porphyrins and Phtalocyanines,* **2016**, 1272-1276.

67. A. Sorrenti, Z. El-Hachemi, O. Artega, A. Canillas, J. Crusats, J.M. Ribó, *Chem. Eur. J.* **2012**,18, 8820 – 8826.

68. N. Micali, V. Villari, M.A. Castriciano, A. Romeo, L. Monsù Scolaro, *J. Phys. Chem. B* **2006**, 110, 8289-8295.

69. N. Micali, F. Mallamace, A. Romeo, R. Purrello, L. Monsù Scolaro, *J. Phys. Chem. B*, **2000**, 104, 5897–5904

70. D.L Akins, H-R Zhu, C. Guo, *J Phys Chem*, **1996**, 100, 5420-5425.

71. A.S.R. Koti, J. Taneja, N. Periasamy, *Chem Phys Lett*, **2003**, 375, 171–176.

72. R. Rubires, F. Crusats, Z. El-Hachemi, T. Jaramillo, M. Lopez, E. Valls, J.A. Farrera, J.M. Ribo, *New J. Chem.*, **1999**, 189-198.

73. J.M. Ribó, J. Crusats, J.A. Farrera, M.L. Valero, *J. Chem. Soc. Chem. Commun.*, **1994**, 6, 681–682.

74. A. Romeo, M.A. Castriciano, I. Occhiuto, R. Zagami,R.F. Pasternack, L. Monsu Scolaro, *J. Am. Chem. Soc.* **2014**, 136, 40−43.

75. I.G. Occhiuto, R. Zagami, M. Trapani, L. Bolzonello, A. Romeo, M. A. Castriciano, E. Collinib, L. Monsu` Scolaro, *Chem. Commun.*, **2016**, 52, 11520-11523.

76. Z. El-Hachemi, C. Escudero, O. Arteaga, A. Canillas, J. Crusats, G. Mancini, R. Purrello, A. Sorrenti, A. D'Urso, J. M. Ribó, Chirality **2009**, 21, 408 – 412.

77. R. Lauceri, A. Raudino, L. Monsù Scolaro, N. Micali, R. Purrello, J. Am. Chem. Soc. **2002**, 124, 894 – 895.

78. J.M. Short, J.A. Berriman, C. Kübel, Z. El-Hachemi, J.V. Naubron, T.S. Balaban, *ChemPhysChem*, **2013**, 14, 3209–3214.

79. A. Romeo, M.A. Castriciano, R. Zagami, G. Pollicino, L.Monsù Scolaro, R.F. Pasternak, *Chem. Sci.*, **2017**, 8, 961–967.

80. M. Gaeta, R. Randazzo, D.A. Cristaldi, A. D'Urso, R. Purrello, M.E. Fragalà, *J. Porphyrins Phthalocyanines*, **2017**, 21, 427–430.

81. J.K.M. Sanders, N. Bampos, Z. Clyde-Watson, S.L. Darling, J.C. Hawley, H.J. Kim, C.C. Mak, S.J Webb, *The Porphyrin Handbook* , *Academic Press*, **2000**, 1–48.

82. L. Zhang, M Liu, *J. Phys. Chem. B*, **2009**, 113, 14015–14020.

83. R. Purrello, E. Bellacchio, S. Gurrieri, R. Lauceri, A. Raudino, L. Monsù Scolaro, A.M. Santoro, J. Phys. Chem. B, **1998**, 102, 8852–8857.

84. E. Bellacchio, R. Lauceri, S. Gurrieri, L. Monsù Scolaro, A. Romeo, R. Purrello, J. Am. Chem. Soc., **1998**, 120, 12353-12354.

85. M. Gaeta, D. Raciti, R. Randazzo, C.M.A. Gangemi, A. Raudino, A. D'Urso, M.E. Fragalà, R. Purrello, Angew Chem. Int. E.d, **2018**, 57, 10656-10660.

86. J. G. Nørby, P. Ottolenghi, J. Jensen, Anal. Biochem., **1980**, 102, 318–320.

87. Z. El Hachemi, C. Escudero, F. Acosta-Reyes, M.T. Casas, V. Altoe, S. Aloni, G. Oncinis, A. Sorrenti, J. Crusats, J.L. Campos, J.M. Ribó, *J. Mater. Chem. C*, **2013**, 1, 3337–3346.

88. G. Charalambidis, E. Georgilis, M.K. Panda, C.E. Anson, A.K. Powell, S. Doyle, D. Moss, T. Jochum, P.N. Horton, S.J. Coles, et al. *Nat. Commun.,* **2016**, 7, 12675.

89. V. Cantonetti, D Monti, M. Venanzi, C. Bombelli, F. Ceccacci, G. Mancini, *Tetrahedron Asymmetry*, **2004**, 15, 1969–1977.

90. D. Monti, V. Cantonetti, M. Venanzi, F. Ceccacci, C. Bombelli, G. Mancini, Chem. Commun. 2004, 8, 972–973.

91. H. Jintoku, S. Shimoda, M. Takafuji, T. Sagawa, H. Ihara, *Mol. Cryst. Liq. Cryst.*, **2011**, 539, 63–67.

92. W. Shu-Jun, R. Wen-Juan, Z. Xiao-Jing, L. Dai-Bing, Z. Zhi-Ang, *Chin. J. Chem.*, **2005**, 23, 44–49.

93. D. Monti, M. Venanzi, M. Stefanelli, A. Sorrenti, G. Mancini, C. Di Natale, R. Paolesse, *J. Am. Chem. Soc.*, **2007**, 129, 6688–6689.

94. H. Jintoku, T. Sagawa, M. Takafuji, H. Ihara, *Org. Biomol. Chem.*, **2009**, 7, 2430–2434.

95. Q. Wang, Y. Chen, P. Ma, J. Lu, X. Zhang, J. Jiang, *J. Mater. Chem.*, **2011**, 21, 8057–8065.

96. A. Rananaware, D.D. La, M. Al Kobaisi, R.S. Bhosale, S.V. Bhosale, *Chem. Commun.*, **2016**, 52,10253–10256.

97. Y. Uemori, H. Munakata, S. Kitazawa, S. Osada, H. Imai, *J. Porphyrins Phthalocyanines*, **2012**, 16, 1285–1292.

98. L. Zeng, Y. He, Z. Dai, J. Wang, Q. Cao, Y. Zhang, *Chem. Phys. Chem.*, **2009**, 10, 954–962.

99. N.C.Maiti, S. Mazumdar, N. Periasamy, *J. Phys. Chem. B*, **1998**, 102, 1528–1538.

100. S. Jiang, L. Zhang, M. Liu, *Chem. Commun.*, **2009**, 41, 6252–6254.

101. R. Rotomskis, R. Augulis, V. Snitka, R. Valiokas, B. Liedberg, *J. Phys. Chem. B*, **2004**,108, 2833-2838.

102. S.M. Vlaming, R. Augulis, M.C.A. Stuart, J. Knoester, P.H.M. van Loosdrecht, *J. Phys. Chem. B*, **2009**, 113, 2273–2283**.**

103. V. Snitka, M. Rackaitis, R. Rodaite, *Sensors and Actuators B*, **2005** 109, 159–166.

104. S. C. M. Gandini, E.L. Gelamo, R. Itri, M. Tabak, *Biophysical Journal,* **2003**, 85, 1259–1268.

105. Dubochet. J, *Angew. Chem. Int. Ed.*, **2018**, 57, 10842-10846

106. G. Ognibene, D. A. Cristaldi, R. Fiorenza, I. Blanco, G. Cicala, S. Scirè, M. E. Fragalà, *RSC Adv.*, **2016**, 6, 42778-42784

107. I. Oehme, O.S. Wolfbeis, *Mikrochim. Acta,* **1997**,126, 177-192.

108. E. S. Forzani, H. Zhang, W. Chen, N. Tao, *Environ. Sci. Technol.* **2005**, 39, 1257-1262.

109. G. Aragay, J. Pons, A. Merkoci, *Chem. Rev*. **2011**, 111, 3433–3458.

107. Y. Ding, W-H Zhu, Y. Xie, *Chem. Rev.*, **2017**, 117, 2203−2256.

108. C.M.A. Gangemi, G. Ognibene, R.Randazzo, A. D'Urso, R. Purrello, M.E. Fragalà, *New J. Chem*., **2018**, 42, 8717-8723.

109. K. Ishihara, S. Funahashi and M. Tanaka, *Inorg. Chem.*,**1983**, 22, 2564.

110. B.E. Conway Springer science plus Business media, LLC, **1999**

111. Y. Zhu, S. Murali, M.D. Stoller, K.J. Ganesh,W. Cai, P.J. Ferreira, A. Pirkle, R.M. Wallace, K.A. Cychosz, M. Thommes, D. Su, E.A. Stach, R.S. Ruoff, *Science,* **2011**,6037, 1537-1541.

112. P. Zhao, M. Yao, H. Ren, N. Wang, S. Komarneni, *Appl. Surface Science*, **2019**, 463, 931-938.

113. A. Borenstein, O. Hanna, R. Attias, S. Luski, T. Broussebc, D. Aurbach, *J. Mater. Chem. A*, **2017**, 5, 12653–12672

114. J. Coelho, B. Mendoza-Sánchez, H. Pettersson, A. Pokle, E. K McGuire, E. Long, L. McKeon, A.P. Bell, V. Nicolosi, *2D Mater.,* **2015**, 025005.

115. J. Chen, H. Meng, Y. Tian, R. Yang, D. Du, Z. Li, L. Qu and Y. Lin, *Nanoscale Horiz.*, **2018** DOI: 10.1039/C8NH00274F.

116. W. Yin, X. Dong, J. Yu, J. Pan, Z. Yao, Z. Gu, Y. Zhao *ACS Appl. Mater. Interfaces*, **2017**, 9, 21362−21370.

117. M. Zhao, Y. Wang, Q. Ma,Y. Huang, X. Zhang, J. Ping, Z. Zhang, Q. Lu, Y. Yu, H. Xu, Y. Zhao, H. Zhang, *ADV Mat*, **2015**, 45, 7372-7378.

118. A. Mahmood, J.Y. Hu, B. Xiao, A. Tang, X. Wang, E. Zhou, *J. Mater. Chem. A*, **2018**, 6, 16769-16797.

119. Ik Seon KwonIn Hye KwakHafiz Ghulam AbbasI.S. Kwon, I.H. Kwak, H.G. Abbas, H.W. Seo, J. Seo, K. Park, J. Park, H.S. Kang, *Nanoscale*, **2019**, 11, 3780-3785.